POWER EFFICIENT DESIGNS FOR 5G WIRELESS NETWORKS

by

Sharareh Kiani

A Thesis Submitted to the School of Graduate and Postdoctoral Studies in Partial Fulfillment of the Requirements for the Degree of

Doctor of Philosophy

in

ELECTRICAL AND COMPUTER ENGINEERING

The Faculty of Engineering and Applied Science

University of Ontario Institute of Technology
(Ontario Tech University)

Oshawa, Ontario, Canada

January 2021

THESIS EXAMINATION INFORMATION

Submitted by: **Sharareh Kiani**

Doctor of Philosophy in **Electrical and Computer Engineering**

Thesis Title: Power Efficient Designs for 5G Wireless Networks

An oral defense of this thesis took place on — in front of the following examining committee:

Examining Committee:

Chair of Examining Committee: Prof. Qusay Mahmoud

Research Supervisor: Prof. Shahram ShahbazPanahi

Research Co-supervisor: Prof. Min Dong

Examining Committee Member: Prof. Ying Wang

Examining Committee Member: Prof. Masoud Makrehchi

University Examiner: Prof. Ying Zhu

External Examiner: Prof. Robert Schober

The above committee determined that the thesis is acceptable in form and content and that a satisfactory knowledge of the field covered by the thesis was demonstrated by the candidate during an oral examination. A signed copy of the Certificate of Approval is available from the School of Graduate and Postdoctoral Studies.

ABSTRACT

In this dissertation, to step forward towards green communication, we study power-efficient solutions in three potential 5G wireless networks, namely an asynchronous multi-carrier two-way Amplify-and-Forward (AF) relay network, a multi-carrier two-way Filter-and-Forward (FF) network, and a massive Multiple Input Multiple Output (MIMO) network using the Non-Orthogonal Multiple Access (NOMA) scheme. In the first network, two transceivers using the Orthogonal Frequency Division Multiplexing (OFDM) scheme communicate through multiple relays in an asynchronous manner. As an attempt to design a simple solution, we assume the AF protocol at the relays. We jointly design the power allocation and distributed beamforming coefficients to minimize the total transmission power subject to sum-rate constraints. We propose an optimal semi-closed form solution to this problem and we show that at the optimum, the end-to-end channel has only one non-zero tap. To extend the first work to high data-rate scenarios, we consider a second relaying-based network which consists of two OFDM-based transceivers and multiple FF relays. We propose two approaches to tackle a total transmission power minimization problem: a gradient steepest descent-based technique, and a low-complexity method enforcing a frequency-flat Channel Impulse Response (CIR) response at the optimum. As the last network, we consider a massive MIMO-NOMA network with both co-located and distributed structures. We study the joint problem of power allocation and user clustering to minimize the total transmit power subject to QoS constraints. We propose a novel clustering algorithm which groups the correlated users into the same cluster and has an unique ability to automatically switch between using the spatial-domain-MIMO and the power-domain-NOMA. We show that our proposed method can substantially improve the feasibility probability and power consumption performance compared to existing methods.

Keywords: *Asynchronous Two-Way Relay Networks; Filter-and-Forward Relaying; Power Domain NOMA Massive MIMO; Channel Equalization; User Clustering*

DECLARATION

I, Sharareh Kiani, hereby declare that this thesis consists of original work of which I have authored. This is a true copy of the thesis, including any required final revisions, as accepted by my examiners

I authorize the University of Ontario Institute of Technology (Ontario Tech University) to lend this thesis to other institutions or individuals for the purpose of scholarly research. I further authorize University of Ontario Institute of Technology (Ontario Tech University) to reproduce this thesis by photocopying or by other means, in total or in part, at the request of other institutions or individuals for the purpose of scholarly research. I understand that my thesis will be made electronically available to the public.

ACKNOWLEDGEMENTS

First and foremost, praises and thanks to God, the Almighty, for His blessings bestowed on me.

I would like to express my deep and sincere gratitude to my supervisors Prof. Shahram ShahbazPanahi and Prof. Min Dong for giving me this great opportunity to carry out my research under their supervision, and for providing me their continuous guidance, support, patience, and immense knowledge. I would also like to thank Prof. Ali Grami for his valuable guidance and insightful comments.

Last but not least, my heartfelt gratitude to my husband Adel for his patience and wholehearted support, to my parents for their unconditional love, and to my friends for comforting me through thick and thin. The completion of this work would not have been possible without them.

STATEMENT OF CONTRIBUTIONS

Part of this dissertation described in Chapters 3 and 4 have been published as:

- [1] S. Kiani, S. Shahbazpanahi, M. Dong, G. Boudreau, "Power-optimal distributed beamforming for multi-carrier asynchronous bidirectional relay networks," IEEE Transactions on Signal and Information Processing over Networks, 2020
- [2] S. Kiani, S. Shahbazpanahi, M. Dong, and G. Boudreau, "Distributed equalization and power allocation for multi-carrier bidirectional filter-and-forward relay networks," 2020 IEEE International Conference on Acoustics, Speech and Signal Processing (ICASSP), Barcelona, Spain, 2020
- [3] S. Kiani, S. Shahbazpanahi, M. Dong, and G. Boudreau, "Joint power allocation and distributed beamforming design for multi-carrier Asynchronous two-way relay networks," 2019 IEEE 20th International Workshop on signal processing advances in wireless communications (SPAWC), Cannes, France, 2019

I hereby certify that I am the sole author of this thesis and that no part of this thesis has been published or submitted for publication. I have used standard referencing practices to acknowledge ideas, research techniques, or other materials that belong to others. Furthermore, I hereby certify that I am the sole source of the creative works and/or inventive knowledge described in this thesis.

Contents

List of Figures

Acronyms

CPU Central Processing Unit

AP Access Point

BS Base Station

MIMO Multiple Input Multiple Output

SNR Signal-to-Noise Ratio

SINR Signal-to-Interference-plus-Noise Ratio

ISI Inter-Symbol-Interference

AF Amplify-and-Forward

FF Filter-and-Forward

DF Decode-and-Forward

CF Compress-and-Forward

CP Cyclic Prefix

OFDM Orthogonal Frequency Division Multiplexing

QoS Quality of Service

FIR Finite Impulse Response

IIR Infinite Impulse Response

CIR Channel Impulse Response

CSI Channel State Information

NOMA Non-Orthogonal Multiple Access

OMA Orthogonal Multiple Access

LTE Long Term Evolution

TDD Time Division Duplexing

FDD Frequency Division Duplexing

SIC Successive Interference Cancellation

TWR Two-Way Relay

MABC Multiple-Access-Broadcast

SOCP Second Order Cone Programming

ZF Zero-Forcing

MRT Maximum Ratio Transmission

LoS Line-of-Sight

NLoS Non-Line-of-Sight

OP optimization Problem

DFT Discrete Fourier Transform

IDFT Inverse Discrete Fourier Transform

5**G** Next Generation

Chapter 1

Introduction

1.1 Overview

Over the past decade, engineers and researchers have forged a common consensus about the possible requirements for the Next Generation (5G) of cellular systems. As compared to the previous generations, 5G networks are required to support much higher data rates for applications such as high-definition video streaming, to provide massive connectivity especially for applications of machine-to-machine communication, and to promote more energy and power-efficient schemes [4]. These 5G de facto requirements for seamless connectivity and user experience call for enabling technologies that are able to evolve according to the ever-growing demands. Among the major technologies proposed to fulfill 5G requirements, cooperative relaying communication, massive Multiple Input Multiple Output (MIMO) technology, and Non-Orthogonal Multiple Access (NOMA) scheme are the techniques that are considered in this study.

Cooperative relaying has garnered considerable supports in the literature to enhance the energy efficiency, extend the network coverage, and obtain spatial diversity. The main idea is to form a virtual distributed multi-antenna system by utilizing multiple relay nodes to assist the communication between terminals. The relay nodes can collectively process their received signals and retransmit the processed signals to the destination(s). Of particular interest is two-way relaying, also known as bidirectional relaying, which provides higher spectral efficiency than one-way relaying. A common protocol for two-way relaying is a multiple-access-broadcast method in which all user pairs simultaneously send their signals

to the relay nodes in the multiple access phase, and then in the broadcast phase, the relays broadcast the processed version of their received signals toward the user pairs.

Massive MIMO technology is another important pillar of massive connectivity in 5G networks which enables high spectral efficiency as well as high spatial resolution for user multiplexing [4–6]. In massive MIMO networks, the number of antennas at the Base Station (BS) must be much larger than the number of users which are being served simultaneously. This massive number of antennas can be arranged in a *co-located* or *distributed* fashion in the network. The former architecture, the co-located massive MIMO, includes a single BS equipped with a large antenna array, whereas the latter setup, the distributed massive MIMO, consists of multiple distributed single-antenna Access Point (AP) nodes which are connected through a coordinating Central Processing Unit (CPU). Note that due to the diversity gain against the shadow fading, the distributed structure can potentially provide much better performance than the co-located setup [7–9].

Conventional wireless networks have been using Orthogonal Multiple Access (OMA) schemes to serve users by assigning an exclusive orthogonal resource block to each user in order to avoid inter-user interference. Although OMA can be implemented with simple receiver designs for a reasonable multiplexing gain, theoretically, it is an inadequate technique when there exists some interference or correlations among multiple users. More recently, the NOMA technology has been proposed which allocates non-orthogonal resources to control interferences. NOMA is considered as a spectrally efficient technique that reduces transmission latency and supports massive connectivity [10–12].

In this dissertation, to comply with the 5G requirements, we aim to design power-efficient solutions satisfying certain quality of service constraints on data rates or signal-to-interference-plus-noise ratios. In particular, we consider three scenarios in which the state-of-the-art 5G technologies are utilized to ensure seamless connectivity and high data-rate communication between users, while the transmission power is kept as minimum as possible. In the first two scenarios, we integrate a distributed cooperative relaying technology with an Orthogonal Frequency Division Multiplexing (OFDM) scheme in a form of two-way relaying networks, for which we design power-efficient solutions to fulfill 5G requirements. We envision a distributed relay-assisted Device-to-Device (D2D) communication setup where a

large number of relays can be deployed to enhance the spectral/energy efficiency. Note that such setups are not supported by the current Long Term Evolution (LTE) 4G networks. Lastly, in the third scenario, we consider a combination of the massive MIMO and NOMA technologies in a highly correlated environment. We design a power-efficient solution for both co-located and distributed massive MIMO networks.

In the remainder of this chapter, we first briefly overview the important technical terms which are frequently used in the forthcoming chapters. Afterward, we introduce our underlying motivations in conducting the presented research. We then present our objectives and research methodology that have been employed in our work. Finally, a summary of contributions and a list of publications are provided.

1.2 Terms and Definitions

1.2.1 Cooperative Relaying Communication

Cooperative relaying communication is defined as a class of techniques in which some nodes, commonly known as the relay nodes, have the ability to assist the communication between other nodes by performing different signal processing techniques on the received information and forward the processed signal to the desired receiver. Employing the relaying nodes in a distributed manner, cooperative relaying systems can increase the link reliability, spectral efficiency, transmission range, and capacity. Such techniques have been extensively studied in the literature and even implemented in 4G Long Term Evolution (LTE)-Advanced standard, where the low-power base stations assist the communication link between multiple users in a cooperative manner.

1.2.2 Synchronous and Asynchronous Networks

In the context of the cooperative relaying communication, a *synchronous* network is a network in which the symbol transmitted by each transceiver is received simultaneously at all relays, and also the signals transmitted by different relays arrive at the transceivers at the same time. To have a synchronous propagation environment, the delay spread, the

difference between the smallest propagation delay and the largest propagation delay, must be smaller than the transmitted symbol period length. In contrast, if the delay spread is larger than the symbol period length, then the network is called an *asynchronous* network. Due to the asynchronous nature of such networks, the transmitted symbols can interfere with each other causing Inter-Symbol-Interference (ISI). At high data rate regimes, the networks are often asynchronous, and thus, ISI cancellation techniques must be employed.

1.2.3 Two-Way versus One-Way Communication

Consider a communication link between two transceivers which are able to send or receive information. This communication link is called *one-way* (also known as unidirectional) link, if the communication occurs from the transmitter (source) node to the receiver (destination) node. That is, the signal can only be transmitted in one direction. In contrast, in *two-way* links (also known as bidirectional), both of the transceivers can mutually send and receive the information in both directions. Notice that the transceiver nodes establishing a two-way communication can have the either half-duplex or full-duplex capability. In this study, we consider relay networks consisting of two transceivers and multiple relays, where all the nodes are half-duplex.

1.2.4 Distributed Beamforming

Relaying networks have been exploited to increase the coverage and enhance data rates. In the multi-relay networks, the process of designing the relay weights is called beamforming (also called precoding). The beamforming process at the relays enables the network to fully exploit its potentials. Depending on design criteria, the beamforming optimization problem can be formulated by different optimization problems such as power minimization, rate maximization, or Signal-to-Interference-plus-Noise Ratio (SINR) maximization. The term *distributed beamforming* refers to any technique whereby multiple transmitting nodes cooperate with each other in order to improve the quality of the communication link at the receiver nodes. However, it should be pointed out that the improvement of energy efficiency comes at the price of the synchronization process needed between the cooperative nodes.

1.2.5 Relaying Protocols

There are several relaying protocols that define the function of any relay node in a relaying network. The most common of which are Amplify-and-Forward (AF), Decode-and-Forward (DF), Compress-and-Forward (CF), and Filter-and-Forward (FF) protocols. The simplest relaying protocol is the AF strategy whereby the received signal is amplified and transmitted towards the destination(s). The AF relaying protocol is of particular interest due to its simplicity, lower computational complexity, and lower implementation cost in comparison with other relaying methods [13–17]. However, it is well-known that AF relaying is not efficient in ISI-prone environments such as the frequency-selective channels. In our first work explained in Chapter 2, we consider the AF protocol at relay nodes.

The next common relaying protocols are DF and CF protocols. In the DF protocol, the relay first decodes the acquired signal, and then forwards the re-encoded message towards the destination. In the CF protocol, on the other hand, the relay first compresses the received message and then transmits the compressed version of the signal to the destination. The processing of the DF protocol is executed as a *hard* decision, and as a result, the achievable rates undergo some losses. Therefore, in some cases, the *soft* forwarded signal resulted from the CF-based relays is more desirable than the one from the DF-based relays. As compared to the AF protocol, both the DF and CF protocols come at much higher complexity cost, almost as high as a base station. Consequently, there is always a trade-off between the performance enhancement and the complexity cost when it comes to choosing either of these protocols.

For single-carrier transmissions, an Filter-and-Forward (FF) strategy has recently proposed in [18–21]. In this protocol, the received signal at the relay is directly filtered by a Finite Impulse Response (FIR) filter, and then the filtered signal is forwarded to the destination. While the FF protocol can be considered as an extension of the AF scheme, it can achieve much higher performance as compared to the AF protocol, and a lower computational complexity as compared to both DF or CF protocols. Furthermore, in the frequency-selective channels, the implementation of the FF protocol at the relay(s) provides a channel equalization approach to combat the ISI at the transceivers [20, 21].

1.2.6 Orthogonal Frequency Division Multiplexing

Multi-carrier modulation techniques have been used as an invaluable asset to combat ISI resulted from the frequency-selective channels at high data rate applications. The basic idea of a typical multi-carrier system is to divide the input data into multiple substreams, each of which is modulated over different orthogonal subcarrier frequencies. The symbol time of each substream is chosen to be much longer than the channel delay spread so that no ISI will be experienced in the substreams received at the receiver [22]. In other words, the substream bandwidth is designed to be much less than the coherence bandwidth of the channel so as to ensure a flat fading subchannel for each substream. One way to implement the multi-carrier modulation efficiently is through the OFDM scheme. One symbol of OFDM is formed by a block of the input data of size N. A cyclic prefix of the same length of (or larger than) the end-to-end CIR is added to each OFDM symbol. Therefore, the ISI resulted from the frequency-selectivity of the wideband channel can be completely eliminated from the received OFDM symbols at the receiver. However, the cost to pay is a reduction in data-rate because of the added overhead which in turn, calls for the extra power to send the cyclic prefix at the transmitter [22].

1.2.7 Massive Multi-Input Multi-Output Systems

Relying on transmitting and receiving data through multiple antennas, MIMO systems can increase data rates, improve reliability, enhance energy efficiency, and diminish interference. Massive MIMO is a state-of-the-art technology which employs hundreds of antennas to serve several terminals simultaneously in the same time-frequency resource block. Massive MIMO systems can obtain the same advantages of MIMO systems on a much greater scale [23]. Potentially, the massive MIMO technology can enhance the throughput and performance of the communication link by reducing the effects of noise, fast fading, and interference. Further, massive MIMO systems only rely on a simple yet phase-coherent signal processing, as well as some low complexity detection methods. The large-scale antenna array can only be used on the BS side, which gives the users the benefit of obtaining multiplexing gain through connecting to BS without undergoing the design complexity on their sides. Recently, the

distributed massive MIMO, in which the antennas are spread over an area as opposed to being co-located at the location of one BS, has gained a lot of attention [7–9, 24–26]. The distributed massive MIMO, also known as cell-free massive MIMO, can potentially provide a better coverage chance than the co-located massive MIMO due to its diversity gain against the shadow fading.

Massive MIMO requires full knowledge of the channel state information for both uplink and downlink directions to successfully be implemented. Conventionally, in the multi-user MIMO systems, the channel estimation task was accomplished by either using different times to send the pilot sequences, called Time Division Duplexing (TDD), or utilizing different frequencies, known as Frequency Division Duplexing (FDD). In other words, in the TDD mode, the channels can be estimated in the uplink transmissions, and later, the downlink channel matrix can be obtained from channel reciprocity, i.e., by using the transpose of the estimated uplink channels. On the other hand, by using different frequencies for uplink and downlink, FDD estimates the uplink channels at BS, and waits for the feedback from the users to estimate the downlink channels. However, the traditional FDD mode becomes impractical for massive MIMO systems, where a large number of antennas is used. As a result, the TDD mode can be used to help the channel estimation task in massive MIMO systems.

1.2.8 Non-Orthogonal Multiple Access Scheme

NOMA is a multiple access technique which allocates non-orthogonal resources to users in order to control the interferences. Multiplexing process in NOMA can be attained in either code-domain where sparse or non-orthogonal spreading sequences are used, or in power-domain where different power levels are used to distinguish the users. Power-domain NOMA, hereafter referred to as NOMA, is what commonly studied in literature and is also our focus. To exploit NOMA, the superposition coding at the transmitter and Successive Interference Cancellation (SIC) at the receiver must be employed. The key idea of performing SIC on a particular user is to decode the interfering signals from the *weaker users*, while successively subtracting the decoded interference signals from the received signal. To avoid prohibitive complexity of the SIC operation when the number of users is large, users are clustered into

smaller groups and NOMA is applied to each cluster [27–29]. Upon successful completion of SIC, part of the intra-cluster interference among users within each cluster can be removed.

1.3 Motivations

There is a unanimous consensus among scholars on the main requirements of 5G networks which include providing higher energy efficiency, enhancing spectral efficiency, and diminishing latency. However, accommodating ubiquitous coverage with high data rates demands a huge amount of power and energy especially in dense scenarios envisioned by the 5G network. Moreover, the ever-growing data traffic and seamless connectivity require technologies such as massive MIMO and cooperative relay communication which can render the energy consumption prohibitive. More importantly, energy consumptions and related carbon emissions as well as global air pollution have become a worldwide concern. As a result, developing *green* designs for the next generation of wireless networks has attracted a lot of interest among researchers [30–32]. In these studies, the authors are usually strive to satisfy the two contradictory requirements of minimizing the energy or power consumption while maintaining or increasing the network capacity or data rates. Motivated by the demands for green and power optimal designs, in this dissertation, we propose to minimize the total power consumption in three different 5G wireless network nominees while fulfilling some quality of service constraints on data rates or Signal-to-Interference-plus-Noise Ratio (SINR) values at user terminals. It is worth mentioning that all these 5G wireless network nominees has a distributed massive MIMO structure.

First Scenario: Power-Optimal Distributed Beamforming for Multi-Carrier Asynchronous Bidirectional Relay Networks

The majority of early results published on cooperative relaying networks assumed time synchronization at the symbol level for the relay nodes and at the transceivers [33–36]. This assumption is, however, unrealistic in real-world applications, where the relays are situated at different locations. As such, each relaying path can cause a propagation delay which is significantly different from that of the other relaying paths. Such a significant delay spread results in loss of synchronization and can lead to a multi-path end-to-end

channel at sufficiently high data rates. In such asynchronous relaying networks, the end-to-end channel between the transceivers is rendered frequency-selective, and thus, is prone to ISI. To overcome such ISI, different techniques such as post-channel and/or pre-channel equalization at the transceivers nodes [13, 16, 37–41], or equalization at the relays by using FF relaying strategy [20], or equalization at the transceivers and the relay nodes by using the single-carrier FF-based techniques [14, 18, 42] and multi-carrier methods [14, 43], can be employed. Aiming for a cost-effective design, we have considered an asynchronous two-way relaying network in which the burden of equalization is carried by the multi-carrier-based transceivers using the OFDM technique, while the relays are equipped with a simple AF relaying scheme. In this way, the OFDM-based transceivers can efficiently equalize the frequency-selective channel resulted from asynchronous transmissions, and thus, eliminate the ISI.

In the problem studied in Chapter 3, we consider the joint problem of power allocation and beamforming design for an asynchronous two-way relaying network consisting of multiple AF relay nodes and two OFDM-based transceivers. Such joint design of power allocation and beamforming weights has been investigated in the literature for asynchronous single-carrier and multi-carrier two-way relaying networks [16, 39, 44]. However, to the best of our knowledge, our work is the first attempt to solve the joint subcarrier power allocation and beamforming design by minimizing the total transmit power while satisfying some quality-of-service requirements on data rates for our considered network setup. Note that by using simplifying assumptions in our first work studied in Chapter 3, we are able to expand the results into a more complicated two-way relaying network which meets the fundamental requirements of 5G networks.

Second Scenario: Joint Power Allocation and Distributed Equalization Design for OFDM-Based Filter-and-Forward Two-Way Multi-Relay Networks

In the context of cooperative relaying networks, user-relays channels are often assumed to be frequency-flat. However, such a simplifying assumption can be unrealistic in high data-rate scenarios when the time-dispersive nature of multi-path channels results in frequency-selectivity. These frequency-selective channels lead to ISI at the receiver front-end of the users. To extend our study in the first scenario to broader applications, in the second

scenario, we assume frequency-selective channels between relays and the users. We are aware of only two approaches which deal with the frequency-selectivity of user-relays links in two-way relay networks. One approach is the single-carrier FF relaying scheme of [18–20], where the burden of the end-to-end channel equalization is on the shoulder of the relays. The proposed approaches in [18–20] are computationally prohibitive and may not always be feasible. The second approach is the multi-carrier technique of [43], where all relay and transceiver nodes use OFDM technology, thereby collectively equalizing the end-to-end channel. This approach is also computationally expensive and is highly susceptible to being trapped in a local minimum.

Due to the performance advantages of the FF relaying strategy, the integration of the FF relaying scheme in multi-carrier transmissions is particularly worthy of investigation. To the best of our knowledge, the problem of FF relaying in multi-carrier relaying networks has not been investigated before, with exception of [45, 46]. However, [45] and [46] have studied a three-node two-way relaying network which comprises of one single FF relay and two OFDM-based transceivers, and they have not considered a cooperative relaying network with multiple relays. In Chapter 4, we investigate the application of FF relaying in multi-carrier two-way relaying networks with multiple FF relay nodes. Therein, we consider the problem of joint power allocation and FIR filter coefficients design by formulating a total transmit power minimization problem subject to the quality of service constraints imposed on the data rates. To the best of our knowledge, prior to this work, the problem of FF relaying and power allocation in multi-carrier two-way relaying networks with multiple FF relay nodes has not been studied. Our proposed approach does not suffer from the shortcomings of both single-carrier schemes in [18–20] and the multi-carrier method in [43] as our method is always feasible and enjoy affordable computational complexity. It is worth mentioning that using time-domain filtering at the relays to tackle ISI only requires the optimization of a few filter taps at each relay, while the multi-carrier scheme of [43] asks for optimizing as many weights as the number of sub-carriers at each relay.

Third Scenario: Unsupervised User clustering and Power Allocation Design in NOMA-Aided Massive MIMO Networks

In the last scenario, we consider yet another distributed massive MIMO structure by

combining the massive MIMO and NOMA technologies, and we aim to design a power-efficient solution for the downlink transmission in such networks. Recently, the massive MIMO technology has been widely acclaimed for its ability to enhance spectral efficiency, improving energy efficiency, and enabling massive connectivity. Massive MIMO can exploit the spatial multiplexing gained from its massive number of serving antennas for serving a large number of users. However, massive MIMO systems notoriously suffer from the so-called pilot contamination effect [47]. Since the channel coherence time is limited, to estimate the uplink channels in a TDD mode, non-orthogonal pilot sequences must be used by users at different cells. This results in the pilot contamination issue. The most adverse effect of pilot contamination is on the ability of the BS to conduct coherent beamforming towards only one of the users with the shared pilot. It is shown in [48] that a NOMA scheme can be adopted to exploit the pilot contamination cleverly to diminish the pilot overheads. Moreover, in light of finite power and spectrum resources, NOMA is proven to be highly beneficial to support massive connectivity for 5G networks and beyond [10]. The potential benefits of NOMA encouraged us to study a NOMA-aided massive MIMO network as our third scenario.

The integration of NOMA into massive MIMO systems has attracted considerable attention in literature [49–53]. However, the joint problem of user clustering and power allocation in massive MIMO-NOMA systems has not been extensively studied in the literature. In Chapter 5, we investigate a joint user clustering and power allocation design in downlink transmissions of NOMA-aided massive MIMO networks. We aim to minimize the total transmit power while satisfying the required quality of service constraints on the received SINRs at each user. We develop a unified signal model and solution set which is applicable to both co-located and distributed massive MIMO scenarios. In particular, a fast and novel user clustering method based on machine learning algorithms is proposed. To the best of our knowledge, the joint problem of user clustering and power allocation design targeting the total transmit power minimization in downlink transmissions of NOMA-aided massive MIMO networks has not been investigated prior to this work.

1.4 Objective and Methodology

In this section, we overview the objectives and research methodologies which are pursued in the following chapters of the current dissertation.

1.4.1 Objective

In Chapter 3, we consider the problem of joint power allocation and distributed beamforming design for an *asynchronous* two-way multi-relay network, where two transceivers rely on the OFDM scheme to exchange information through multiple AF relay nodes. The network is assumed to be asynchronous in the sense that different relaying paths are subject to different propagation delays. This assumption renders the end-to-end channel between the two transceivers frequency selective. The impulse response of such a channel can be modeled as a finite impulse response system with multiple taps. We aim to find the optimal solution for the problem of the total transmission power minimization subject to two quality of service constraints on the transceivers rates in the aforementioned network.

In Chapter 4, we study a multi-carrier two-way relaying network consisting of two OFDM-based user transceivers and multiple FF relays. The FF relaying technique along with the multi-carrier scheme at the transceivers is utilized to suppress the ISI caused by the frequency-selectivity of the end-to-end channel. We aim to jointly optimize subcarrier power allocation at the transceivers and the FIR filters at the FF relays to minimize the total transmit power subject to two quality of service constraints measured by sum-rates at the transceivers.

In Chapter 5, we consider downlink transmissions in NOMA-aided massive MIMO networks in which a massive number of multiple access points simultaneously serve multiple users. The access points can be co-located at one location in a form of an antenna array at one single BS, or they can be distributed over an area in a form of multiple single-antenna BSs. Employing the NOMA scheme, the network groups the users into several clusters based on their channel characteristics. We aim to find a solution to the joint problem of the user clustering and power allocation designs by formulating a total transmit power minimization while SINRs at the user receiver sides are kept at some given thresholds.

1.4.2 Methodology

In this dissertation, we investigate three potential 5G network scenarios, each of which is discussed in detail in separate chapters. To approach each scenario, we adopt unique methods, a review of which is presented in this section.

First Scenario: Power-Optimal Distributed Beamforming for Multi-Carrier Asynchronous Bidirectional Relay Networks

In Chapter 3, we study a total power minimization problem in an *asynchronous* two-way multi-relay network with two OFDM-based transceivers and multiple AF relay nodes. We first model the system with the initial assumption that the relay-transceiver channels are frequency-flat while each relaying path is subject to a different propagation delay. The dissimilarity of propagation delays in the relaying paths leads to an asynchronous communication which renders the end-to-end channel between the two transceivers frequency-selective. Thus, we model the channel impulse response of the end-to-end channel as an FIR system with multiple taps. Assuming the relays' beamforming weights are frequency-independent, we show that our CIR model can reveal the contributions of different relays to each of the CIR taps. We then formulate the total transmit power minimization to jointly design the beamforming and power allocation coefficients. To approach this problem, for a fixed set of beamforming weights, we first use the Lagrange multipliers method to solve the optimization for the power coefficient values. Substituting the obtained power coefficients, we, then, reformulate the original optimization problem with respect to the beamforming weights. We show that at the optimum, the end-to-end channel must be frequency-flat, which means only one tap of the end-to-end CIR is non-zero. Using this result, we decompose the beamforming optimization into different subproblems each of which is defined for a separate tap of CIR. We devise a simple and fast semi-closed-form algorithm for the optimal solution of the total transmission power minimization subject to the transceivers rates constraints. Performing numerical analysis, we demonstrate that our proposed semi-closed form algorithm significantly outperforms the traditional best relay selection method. To further examine the performance of our proposed algorithm, we perform a complexity analysis, and a numerical examination to investigate the effects of band-limited filters at

the transceivers on our proposed solution.

Second Scenario: Joint Power Allocation and Distributed Equalization Design for OFDM-Based Filter-and-Forward Two-Way Multi-Relay Networks

In Chapter 4, we investigate a multi-carrier two-way relaying network consisting of two OFDM-based transceivers and multiple FF relays. We study the joint problem of subcarrier power allocation at the transceivers and the FIR filters at the FF relays to minimize the total transmit power subject to sum-rates constraints at the transceivers. We first model the signals and the end-to-end CIR for the multi-carrier two-way FF relaying network assuming that each relay-transceiver channel is frequency-selective. To approach the total transmit power minimization, we propose two approaches. The first approach is based on a gradient steepest descent technique where we transform the original optimization into an unconstrained minimization problem and use the quasi-Newton method to find a local minimum. In the second approach, we enforce a new constraint on the original optimization such that at the optimum, the frequency-selective end-to-end channel becomes frequency-flat. As a result, we are able to develop a semi-closed-form solution for the total transmit power minimization problem. Furthermore, we show that the second method can be used as an initial point for the gradient steepest descent technique. Aiming to evaluate the performance of the proposed methods with a benchmark, we obtain a lower bound for the minimum transmit power at the network. We show that the proposed techniques are within 3 dB of this lower bound. Through numerical results, we further show that our proposed methods outperform existing solutions for similar networks. Lastly, we perform a complexity analysis for our proposed semi-closed form solution to provide another means of evaluation.

Third Scenario: Unsupervised User clustering and Power Allocation Design in NOMA-Aided Massive MIMO Networks

In Chapter 5, we study downlink transmissions of NOMA-aided massive MIMO networks with multiple transmit antennas at BS(s) and multiple single-antenna users grouped into several NOMA clusters. The transmit antennas can be either co-located at one location, or be distributed over a serving area. To provide a power-efficient solution for the 5G

requirements, we aim to jointly design the user clustering and power allocation to minimize the total transmit power consumed in the network while certain SINR threshold levels are maintained. We first model the signals and system to obtain the pertinent expressions. We then show that the total transmit power minimization problem can be tackled separately for the user clustering and power allocation designs. We propose a modified unsupervised mean-shift clustering algorithm in which the correlation among users' channel vectors is utilized as a feature to group the users. Choosing such a criterion for clustering improves the poor performance of conventional massive MIMO systems in correlated propagation environments. Moreover, depending on the availability of enough spatial dimensions, the proposed clustering method is able to automatically switch between the two modes of NOMA-aided massive MIMO and the conventional massive MIMO. Substituting the clustering results into the original optimization problem, we can reformulate a linear programming optimization to obtain the power allocation coefficients. To evaluate the performance of the proposed algorithm, we consider two special case scenarios for co-located and distributed massive MIMO systems. Using numerical analysis, we examine and compare the performance of the proposed clustering and power allocation algorithm with the existing methods. We further provide a complexity analysis for our proposed clustering algorithm.

1.5 Summary of Contributions

The main contributions of the current dissertation are summarized as follows:

- We model and formulate a joint problem of power allocation and beamforming design for an asynchronous multi-carrier two-way relaying network consisting of multiple AF relays and two OFDM-based transceivers. We propose a fast and simple semi-closed form solution to this problem and we obtain jointly optimal power allocation and distributed beamforming weights. We show that at the optimum, the end-to-end channel must be frequency-flat, which means only one tap of the end-to-end channel impulse response is non-zero. As a result, our solution leads to a relay selection scheme, where only those relays which contribute to the optimal tap of the end-to-end channel impulse response can actively participate in the communication. We show

that our proposed algorithm can be implemented in a distributed manner. That is, the transceivers can solve the total transmission power minimization problem and broadcast only a few parameters to the relays. Then, each active relay can utilize these parameters along with its local Channel State Information (CSI) to calculate its beamforming weight. We further prove that the worst-case computational complexity of the proposed algorithm is linear in the number of the relays. Our simulation results demonstrate that the proposed semi-closed form algorithm significantly outperforms the traditional best relay selection method. In addition, we examine the effect of band-limiting transmit and receive filters on the proposed solution which can result in a performance loss in some applications. We show that this performance loss can be compensated by over-constraining the rates by the amount of the rate loss.

- We model and formulate a total transmit power minimization problem to jointly obtain the power allocation and FIR filter coefficients in a multi-carrier two-way relay network consisting of two OFDM-based transceivers and multiple FF relays. Prior to this work, the problem of FF relaying and power allocation in multi-carrier TWR networks with multiple FF relay nodes has not been studied. To tackle the formulated non-convex optimization, we propose two methods. In the first method, we develop a solution based on the gradient steepest descent technique. Since the performance of the first method is sensitive to the choice of the initial points, we propose the second method by restricting the feasible set of the original minimization to a set of points that result in a frequency-flat end-to-end channel impulse response. Under such constraint, we develop a semi-closed-form solution to the total transmit power minimization problem. Despite the loss of optimality arising from the aforementioned restriction, the second method brings forth a fast and simple solution which can also be used as an initial point for the first method. To evaluate the performance, we provide a complexity analysis for the second method. Furthermore, relaxing the original optimization problem, we obtain a lower bound which provides a benchmark for assessing the performances of our proposed methods. Our simulation results demonstrate that both proposed methods perform within 3 dB from this lower bound. Moreover, simulation studies are provided to evaluate the effects of changing design parameters on the performance

of the considered two-way relay network.

- We study the integration of a NOMA scheme into the downlink transmissions of massive MIMO networks with multiple single-antenna users and multiple access points while the users are grouped into several NOMA clusters. The access points can be either situated in a co-located manner at one location, or they can be distributed over a serving area. We formulate a total transmit power minimization problem subject to SINR constraints at the users to jointly design the user clustering and power allocation coefficients. This study is the first attempt which considers a joint problem of power allocation and user clustering design for minimizing the total transmit power in both co-located and distributed massive MIMO-NOMA networks. We present a three-step solution for the formulated minimization, where we first employ a machine-learning-based method to perform the NOMA user clustering task, then we design the beamforming weights, and lastly we solve a linear programming optimization solely for obtaining the power allocation coefficients. We propose a novel clustering algorithm based on the mean-shift algorithm, where we measure the correlation among users' channel vectors using the inner product operation to group the users in an unsupervised fashion. Clustering users based on their channel correlation features, our proposed method has the ability to automatically decide whether to group the users into NOMA clusters, or to serve the users by using the available degree of freedom provided by the spatial dimension in the massive MIMO system. As a result, our proposed method can improve an otherwise poor performance of conventional massive MIMO systems when the propagation environment is fairly correlated. We further provide a complexity analysis for our proposed clustering algorithm and show that the complexity of the proposed algorithm is linear with respect to the number of access points. We evaluate the performance of the proposed algorithm through numerical analysis for two case-studies, namely a co-located massive MIMO-NOMA network scenario and a distributed massive MIMO-NOMA network scenario. For each scenario, we examine and compare the performance of the proposed clustering and power allocation algorithm with the existing methods.

1.6 List of Publications

1. S. Kiani, S. Shahbazpanahi, M. Dong, and G. Boudreau, "Unsupervised user clustering and power allocation design in NOMA-aided massive MIMO networks," in preparation to be submitted.

2. S. Kiani, S. Shahbazpanahi, M. Dong, and G. Boudreau, "Joint power allocation and distributed equalization design for OFDM-based filter-and-forward two-way multi-relay networks," submitted to IEEE Transactions on Signal Processing, 2020.

3. S. Kiani, S. Shahbazpanahi, M. Dong, G. Boudreau, "Power-optimal distributed beamforming for multi-carrier asynchronous bidirectional relay networks," IEEE Transactions on Signal and Information Processing over Networks, 2020 [1].

4. S. Kiani, S. Shahbazpanahi, M. Dong, and G. Boudreau, "Distributed equalization and power allocation for multi-carrier bidirectional filter-and-forward relay networks," 2020 IEEE International Conference on Acoustics, Speech and Signal Processing (ICASSP), Barcelona, Spain, 2020 [2].

5. S. Kiani, S. Shahbazpanahi, M. Dong, and G. Boudreau, "Joint power allocation and distributed beamforming design for multi-carrier Asynchronous two-way relay Networks," 2019 IEEE 20th International Workshop on signal processing advances in wireless communications (SPAWC), Cannes, France, 2019 [3].

1.7 Outline of Dissertation

In this dissertation, we focus on designing power-efficient solutions for three potential types of 5G networks, namely asynchronous multi-carrier two-way AF relaying networks, multi-carrier two-way FF relaying networks, and NOMA-aided massive MIMO networks. The remainder of this dissertation is organized as follows: In Chapter 2, we provide three sections in which we conduct a survey on recent research results closely related to the design problems which we considered in each of the 5G network scenarios. In Chapter 3, we study

the joint design of power allocation and beamforming problem in an asynchronous multi-carrier two-way AF relaying network. We formulate a total transmit power minimization problem subject to sum rate constraints and propose a semi-closed form solution which provides the optimal power allocation and beamforming coefficients for the network. In Chapter 4, we present our proposed two solutions to the problem of power allocation and distributed equalization design in an OFDM-based two-way FF relaying network. We assess the performance of the proposed algorithms through numerical simulations and conducting complexity analysis. In Chapter 5, we discuss the joint problem of user clustering and power allocation in a NOMA-based massive MIMO network where we propose a novel user clustering algorithm and evaluate the performance of our proposed method through numerical simulations. We conclude the dissertation and discuss future work in Chapter 6. Finally, the appendices corresponding to Chapters 3, 4, and 5 are provided at the end of the dissertation.

1.8 Notations

In this dissertation, bold upper letters denote matrices and bold lower letters represent vectors. In addition, we use $(\cdot)^T$, $(\cdot)^H$, and $E\{\cdot\}$, to denote transposition, Hermitian transposition, and the expectation operator, respectively. We use $|\cdot|$ to represent the magnitude of a complex scalar or the cardinality of a set. $\mathbf{A} = \text{diag}(\mathbf{a})$ signifies a diagonal matrix whose diagonal entries are the elements of $\mathbf{a}$, while $\mathbf{A}(i,j)$ represents the (i,j)-the entry of matrix $\mathbf{A}$, and $\mathbf{a} \succeq 0$ indicates that all the elements of $\mathbf{a}$ are non-negative. The $N \times N$ identity matrix is denoted by $\mathbf{I}_N$. Similarly, $\mathbf{0}_{N\times M}$ stands for an $N \times M$ all-zero matrix, The principal eigenvalue and the normalized principal eigenvector of a matrix is represented as $\lambda_{\max}\{\cdot\}$ and $\mathcal{P}\{\cdot\}$, respectively.

Chapter 2

Literature Review

In this dissertation, we consider three scenarios, namely power-allocation distributed beamforming for multi-carrier asynchronous two-way relay networks, joint power allocation and distributed equalization design for OFDM-based FF two-way multi-relay networks, and unsupervised clustering and power allocation design in NOMA-aided massive MIMO networks. In this Chapter, we conduct a survey on the recent studies in the research areas associated with each of these scenarios. Accordingly, the literature review and discussions regarding the most similar publications related to each scenario are provided in three separate sections, respectively.

2.1 Two-Way Amplify-and-Forward Relaying

Cooperative relaying technology is considered as a promising energy-efficient candidate to provide spatial diversity and high throughput in next generation of wireless networks [54,55]. Two-Way Relay (TWR) networks are of growing interest because they are more spectrum-efficient than one-way relay networks, [55–61][1]. In a TWR strategy, two transceivers can simultaneously exchange information through one or more relay nodes. The most common protocol to establish a TWR network is the Multiple-Access-Broadcast (MABC) method [63]. In MABC, two phases are required to exchange two symbols between the two nodes: In the first phase, known as the multiple access (MA) phase, the two the transceivers

[1]Note that another important category in cooperative relaying communication is the multi-way relaying in which each user multicast its message towards a group of users [62]. However, this concept is beyond the scope of this dissertation.

simultaneously transmit the two information symbols they wish to exchange, toward the relay(s). In the second phase, called the broadcast (BC) phase, the signals received at the relay(s) are first processed and then, they are broadcasted back to the transceivers.

Among different relaying protocols, the AF relaying protocol is of particular interest due to its simplicity, lower computational complexity, and lower implementation costs [13, 14, 16, 17, 41]. It is well-known that AF relaying networks are not efficient in suppressing the ISI incurred by the frequency-selectivity of the end-to-end channel [20]. To overcome such ISI, different techniques can be adopted. One group of such techniques rely on post-channel equalization schemes [13], where the end-to-end channel is compensated for at the receiver front-end of the transceivers. The second group of ISI-suppression methods resorts to pre-channel (pre-coding) equalization techniques [37, 64], where the end-to-end channel is equalized at the transmitter front-end of the transceivers. Joint pre- and post-channel equalization approaches [16, 38–41] constitute yet another class of ISI-suppression methods, where both the transmitter and the receiver front-ends of the transceivers share the burden of the equalization of the end-to-end channel. In all these three groups of ISI-suppression techniques, the equalization is performed at the end nodes. One could also implement the task of equalization only at the relays by using the so-called FF relaying strategy which a single-carrier scheme [20].

2.1.1 Asynchronous TWR Networks

Early work on relay networks assumed time synchronization at the symbol level for the relay nodes and at the transceivers [33–36]. In a synchronous network, the symbol transmitted by each transceiver is received simultaneously at all relays, and also the signals transmitted by different relays arrive at the transceivers at the same time. However, this assumption is unrealistic in real-world applications, where the relays are situated at different locations. As such, each relaying path can cause a propagation delay which is significantly different from that of the other relaying paths. Such a significant delay spread results in an *asynchronous* behavior and can lead to a multi-path end-to-end channel at sufficiently high data rates. In such asynchronous networks, the end-to-end channel between the transceivers is rendered frequency-selective, and thus, is prone to ISI. Early investigations on TWR networks ignore

such a signal asynchronism, and thus, either model the end-to-end channel as a frequency-flat link or assume a single-subcarrier (narrowband) scenario [59, 65, 66].

2.1.2 Total Transmit Power Minimization

In an attempt to achieve the greenest design for cooperative TWR networks, the problem of total transmit power minimization has attracted considerable attention in the literature [17, 34,43,67–70]. Although these studies have a common goal of minimizing power consumption, they are different in their underlying network assumptions, design parameters, and problem constraints. For example, in [34], to design an optimally distributed beamforming in a single-carrier TWR network consisting of two users and multiple relays, a total transmit power minimization subject to the received Signal-to-Noise Ratio (SNR) values at users is considered. It is shown that under equal SNR constraints, the users collectively consume half of the total transmit power in the network. In [68] where the authors proposed an iterative algorithm to design the beamforming coefficients by minimizing the total transmit power subject to SINR constraints in a single-carrier TWR network with two single-antenna users and multiple multi-antenna AF relay nodes. The authors in [69] investigated the joint problem of power allocation and relay selection design for an OFDM-based TWR network. A graph-theoretical solution was proposed to minimize the transmit power consumed by the transmitters subject to the outage probability constraint. A closed-form solution for a relay selection design using a total power minimization subject to the received SNRs at the users was derived in [70].

In [43], a TWR network consisting of two transceivers and multiple relays is investigated. Assuming that all nodes employ OFDM schemes, the authors of [43] approach the problem of joint power allocation and beamforming design by formulating two separate problems: the minimization of the total consumed power subject to the data rate constraints, and the maximization of the sum-rate at the transceivers subject to a constraint on the total transmission power consumed throughout the TWR network. While a two-step iterative method is proposed for each problem, solving each problem calls for fixing either the beamforming weight vector or the transceivers' power allocation variables.

More recent publications on total transmit power minimization in TWR networks are discussed in [71–73]. The authors in [71] considered the optimal design of the decentralized beamforming for a single-carrier asynchronous TWR network, where the total power consumed in the network was minimized under data rate constraints at the transceivers. They proposed a semi-closed form solution in which at the optimum, the end-to-end impulse response of the channel becomes single-tap. In [72], a single-carrier asynchronous TWR network consisting of multiple multi-antenna relays and two transceivers was considered, where the relay beamforming matrices were assumed to be symmetric. To design power allocation coefficients and symmetric relay beamfornming matrices, the total power consumed in the network was minimized under the sum-rate constraints at the transceivers. Their results showed that to obtain the lowest power consumption under a fixed number of antennas in the network, the number of antennas per relay can be optimized. A joint problem of power allocation and beamforming matrices design in a TWR network formed by multiple transceiver pairs and multiple multi-antenna relays was studied in [73]. Assuming asymptotically orthogonal relay-transceiver channels, the authors proposed a computationally efficient solution which minimizes the total transmit power in the network while maintaining the SNR requirements at the transceivers.

2.1.3 Related Work Connected to Chapter 3

In Chapter 3, we consider the problem of joint power allocation and beamforming design for an asynchronous multi-carrier TWR network consisting of multiple AF relays and two OFDM-based transceivers. Aiming to satisfy Quality of Service (QoS) constraints, measured by transceivers' rates, we formulate a total transmission power minimization problem to obtain the jointly optimal power allocation and distributed beamforming weights. In our study, we consider the same network investigated in [16, 39] and thus, use the same data model originally presented in [16]. However, our work differs from [16, 39], as our design approach is to minimize the total power consumption subject to two QoS constraints on transceivers' data rates, while [16] relies on maximizing the smallest sub-carrier SNR under a total power constraint, and [39] resorts to a sum-rate maximization problem subject to a total power constraint. Nevertheless, similar to [16, 39], our solution boils down to a

relay selection scheme which renders the end-to-end channel frequency-flat. It is worth mentioning that the solutions provided by [16, 39] are not applicable to our problem, as the input to those solutions is a total power budget, while the inputs to our solution in this dissertation are two required data rates.

Our work in Chapter 3, is different from [43], as our approach does not assume any OFDM processing capability at the relays for the sake of relay simplicity, whereas [43] relies on OFDM schemes at the relays. Note that the study in [43] assumes that the transceiver-relay channels are frequency-selective, Such an assumption necessitates the employment of OFDM at the relay nodes to tackle the ISI incurred by these frequency-selective channels, while we herein model the transceiver-relay channels as frequency-flat links but with unequal propagation delays.

2.2 Two-Way Filter-and-Forward Relaying

It is a well-known fact that high data rate transmissions in frequency-selective channels cause ISI among transmitted symbols. In the context of TWR networks, different techniques have been proposed to tackle the ISI caused by the frequency-selectivity of the user-relay channels. On the one hand, in single-carrier transmissions, due to the ineffectiveness of the AF-based relaying techniques in suppressing the ISI, an FF strategy as an extension of AF strategy is proposed in [18–21]. In FF relaying, each relay is equipped with an FIR filter or an Infinite Impulse Response (IIR) filter, and the output of the filter is retransmitted to the user pairs. On the other hand, in multi-carrier transmissions, employing schemes such as OFDM at the user and/or relay nodes have been proved advantageous to cope with ISI. Using the OFDM systems at the nodes can transform an otherwise frequency-selective end-to-end channel into multiple frequency-flat sub-channels and thus remove the ISI from the received signals [39, 43, 45, 46, 74, 75].

2.2.1 Filter-and-Forward Relaying Scheme

For one-way relaying networks, the application of the FF relaying scheme on single-carrier transmissions have been studied in [18–20, 76]. In [18], the authors assume that the desti-

nation node uses an equalizer, while the relay nodes employ IIR filters. The FF relaying schemes are developed to maximize the SNR ratio at the destination node subject to a total relay power constraint. It is shown in [18] that the performance of IIR filters is comparable with the performance of FIR filters with a reasonable filter order. In [19], the FF design is investigated for one-way relaying networks where the relay nodes have multiple antennas, and the destination node uses a simple equalizer. The numerical results in [19] illustrate that for a fixed number of antennas for the relay nodes, a remarkable performance improvement can be achieved if the antennas are concentrated in a few relay nodes instead of spreading them over many relay nodes. In [20], assuming no equalization at the destination, the authors design the FF relays' FIR filters based on three different approaches: The first approach involves minimization of the total transmit power subject to SINR constraints; the second method maximizes of the destination's SINR subject to a total transmit power constraint, and the third approach deal with a maximization of the sum-rate subject to individual relay transmit power constraints. Recently, in [76], the authors study a filter design problem by maximizing SINR subject to a relay transmit power constraint in a single-carrier one way relaying network including an FF relay node, a source node, and a destination node.

For two-way relaying networks, the problem of FF relays' weight design with the assumption of frequency-selective relay-transceiver channels is studied in [21, 42, 45, 46]. The authors in [42] assume two cases in which transceivers are either equipped with a simple slicer or an equalizer where the relay nodes employ FIR or IIR filters. The optimal FF relays' filters are obtained for the case of transceivers with simple slicers by maximizing the minimum SINR subject to a constraint on the relay transmit power, and for the transceivers with equalizers, by minimizing the total relay transmit power subject to SINR constraints case, and for the latter case by minimizing the sum of mean-squared error at the transceivers. In [21], without assuming any equalizer at the transceivers, the authors propose two methods to design FF relays: one method relies on minimizing the total transmit power subject to SINR constraints and the second method maximizes the worst SINR subject to the relay transmit power requirements. It is shown that these problems can be written as the Second Order Cone Programming (SOCP), which can be solved using the standard convex optimization methods. The simulation results confirm that the FF relaying can dramatically

improve the performance as compared to AF relaying.

Both [21] and [42] investigate the problem of ISI cancellation over single-carrier transmissions in order to avoid the complexity involved in multi-carrier transmissions. However, multi-carrier schemes such as OFDM have been proved to be an efficient technique to remove ISI. Therefore, the integration of the FF relaying with OFDM systems seems an attractive proposition for investigation. To the best of our knowledge, the problem of FF relaying in multi-carrier schemes has not been investigated before with the exception of [45, 46]. The FF relay beamforming design for a single-input-single-output OFDM-based and a MIMO-OFDM-based one-way relaying network with one single FF relay node studied in [45] and [46], respectively. Authors in [45] consider the problem of FIR filter design for a transparent three-node full-duplex relaying network with single-input single-output OFDM transmission. Transparent operation means that, in the relaying network, the destination node is not aware of the relay node. Therefore, the relay node has only access to the CSI knowledge of the relay-source channel and not that of the relay-destination channel. This operation leads to an inexpensive implementation of the relaying network. A single FF relay is used to directly filter the incoming signals at the chip rate of the OFDM transmissions so as to remove the complexity of using OFDM processing at the relay. Three design criteria are considered in [45], namely minimizing the transmit power of the relay subject to SNR constraints per sub-carriers, maximizing the worst SNR per sub-carrier subject to transmit power constraints, and maximizing the throughput subject to the transmit power constraints. Using the convex relaxation and projected gradient method, the authors propose three algorithms as the solution to the three design criteria. In [46], the joint design of the FIR filter and MIMO decoder/encoder for a single-relay MIMO-OFDM network is considered. The authors of [46] rely on two design approaches, namely a weighted sum mean-square-error minimization technique and a sum-rate maximization method, which are equivalent to each other under certain conditions. It is shown that for a given MIMO design, the FIR filter design at the FF relay amounts to a quadratically-constraint optimization problem whose solution can be found by the conversion to a semi-definite programming problem. The numerical results demonstrate the effectiveness of the FF relaying compared to AF relaying for MIMO-OFDM systems.

2.2.2 Related Work Connected to Chapter 4

In Chapter 4, we study the problem of joint power allocation and FIR filter design for FF relays in a multi-carrier TWR network, where two OFDM-based transceivers communicate with each other through multiple relays employed FF relaying schemes. We formulate a total transmit power minimization problem subject to the quality of service constraints imposed on the transceivers' data rates. Motivated by the results in [39] and [16], we propose a semi-closed form solution which restricts the feasible set of the original minimization to a set of points that result in a frequency-flat end-to-end channel impulse response. To the best of our knowledge, prior to this work, the problem of FF relaying and power allocation in multi-carrier TWR networks with multiple FF relay nodes has not been studied.

The study in [20] does not address multi-carrier schemes and the investigation in [45] is not applicable to TWR networks with multiple relay nodes. Moreover, none of the previous work has considered the design approach investigated in this dissertation. To the best of our knowledge, this work is the first study that considers the application of filter-and-forward relaying in multi-carrier systems. We are aware of only two approaches which deal with frequency-selectivity of transceiver-relays links in two-way relay networks. One approach is the single-carrier filter-and-forward relaying scheme of [18–20], where the burden of the end-to-end channel equalization is on the shoulder of the relays. This approach is computationally prohibitive and may not always be feasible. The second approach is the multi-carrier technique of [43], where all relay and transceiver nodes use OFDM technology, thereby collectively equalizing the end-to-end channel. This approach is also computationally expensive and is highly susceptible to being trapped in local minimums. Our approaches do not suffer from these shortcomings as they are always feasible and enjoy affordable computational complexity, while outperforming both single-carrier schemes of [18–20] and the multi-carrier method of [43].

2.3 NOMA-Aided Massive MIMO Networks

NOMA has been considered as a spectrally efficient technique which reduces transmission latency and supports massive connectivity by allocating non-orthogonal resources to users

[10–12]. Multiplexing process in NOMA can be attained in either code-domain where sparse or non-orthogonal spreading sequences are used, or in power-domain where different power levels are assigned to users. To enable NOMA, the superposition coding at the transmitter and the SIC operation at the receiver must be employed. To avoid prohibitive complexity of the SIC operation when the number of users is large, users are clustered into smaller groups and NOMA is applied to each cluster [27–29]. Upon successful completion of SIC, part of the intra-cluster interference among users within each cluster can be removed. However, the inter-cluster interference among users of different clusters remains unresolved. One technique to mitigate such interference is to use multi-antenna-based techniques such as adopting zero-forcing (ZF) beamforming [77], or employing signal alignment schemes [78,79].

Massive MIMO technology is another important pillar of 5G networks to offer high spectral efficiency as well as high spatial resolution for user multiplexing [4–6]. In massive MIMO networks, a large number of antennas simultaneously serve at multiple users. This massive number of antennas can be arranged in the network in a *co-located* or *distributed* fashion. Due to the diversity gain against the shadow fading, the distributed structure can potentially provide much better performance than the co-located setup [7–9].

Recently, integration of NOMA schemes into massive MIMO networks has attracted considerable attention in the literature in the context of co-located massive MIMO [11, 49–51, 80], or distributed massive MIMO [81–85]. The integration of power domain NOMA in massive mmWave MIMO systems is studied in [11], where a BS with a large-scale antenna array is serving multiple users. The users are grouped into separate clusters using a random clustering scheme and SIC operations are used at users to mitigate the intra-cluster interference within each cluster. A design of precoding/detection matrices for a co-located MIMO-NOMA downlink scenario with perfect knowledge of CSI is considered in [49], where fixed power allocation coefficients and user-pairing schemes are exploited. Under the assumption of having a lower number of antennas at BS than the number of users, it is shown that MIMO-NOMA can outperform its counterpart, MIMO-OMA, particularly when users with fairly distinctive channels are paired together. In [50], authors performed a comparison between NOMA and OMA schemes based on outage sum-rates expressions in massive MIMO systems when limited feedback and imperfect CSI are considered. A beamforming

design problem for downlink transmissions from a multi-antenna BS to multiple single-antenna users under perfect CSI assumption is studied in [51], where the users rely on using NOMA principle to cancel the interference from other users whose instantaneous channels are relatively weaker. In addition, asymptotic and deterministic capacity expressions for mmWave MIMO-NOMA systems are derived in [80].

For distributed massive MIMO networks, the authors in [81] studied the application of NOMA on throughput improvement of the network. In another study in [82], the achievable sum-rate expressions are derived for cell-free massive MIMO-NOMA networks. It is shown that considering intra-cluster pilot contamination and imperfect SIC operations, NOMA schemes are unable to perform as efficient as OMA schemes. In [83], another achievable rate analysis in a cell-free NOMA-aided massive MIMO with spectrum sharing is investigated. In [84], the authors evaluated the performance of Zero-Forcing (ZF) and Maximum Ratio Transmission (MRT) precoders on a hybrid cell-free massive MIMO and NOMA network. It is shown that the massive MIMO-NOMA with ZF precoder always outperforms its OMA counterpart with MRT precoder. A closed-form expression for the bandwidth efficiency of a NOMA-based cell-fee massive MIMO is derived in [85].

Despite the established benefits of NOMA schemes to the conventional OMA methods, new studies have emerged that investigate the role of NOMA in massive MIMO systems [86–88]. An achievable rate analysis on a NOMA-based multi-user MIMO system is conducted in [86]. It is shown that NOMA can outperform the conventional multi-user beamforming when the path loss differences between the intra-cluster users are large enough. The authors in [87] compared the performance of a power-domain NOMA scheme with that of a co-located massive MIMO system in terms of sum-rates and achievable rate regions. They demonstrated that for i.i.d. Rayleigh fading channels, if the number of antennas in the BS is sufficiently high, the NOMA scheme always fails to compete with the performance of the massive MIMO system. In [88], an achievable rate performance comparison between a power-domain NOMA scheme and a co-located massive MIMO setup using ZF, in both line-of-sight and non-line-of-sight channels was carried out. It is proved analytically that in line-of-sight Rayleigh channels when the number of antennas is much greater than the number of serving users, the massive MIMO system outperforms the power-domain NOMA

scheme. However, it is demonstrated that in non-line-of-sight cases, the NOMA scheme can be a more suitable choice than the massive MIMO systems. Therefore, the authors in [88] proposed a hybrid NOMA approach which pairs the users based on the correlation between their channels. It is shown that the hybrid method can outperform the standalone massive MIMO scheme. In spite of the results yielded in [86–88], the authors had only considered a simple user pairing scheme which pairs a cell-edge user with a cell-center user, and only a co-located architecture for the massive MIMO system. As a result, to the best of our knowledge, the effects of a more advanced user clustering NOMA scheme on both co-located and distributed massive MIMO have remained uninvestigated.

The main goal of the study conducted in Chapter 5 of this dissertation, is to design the power allocation and user clustering coefficients for NOMA-aided massive MIMO networks in order to investigate the circumstances in which using NOMA can be beneficial to massive MIMO systems. As a result, in the following sections, we conduct a survey on the studies which consider the problem of power allocation and user clustering in massive MIMO-NOMA networks.

2.3.1 Power Allocation in Massive MIMO-NOMA Networks

Many power allocation schemes have been proposed in the literature for massive MIMO-NOMA systems in recent years [52, 89–91]. Employing massive MIMO systems revolves around accurate CSI estimations at the BS or APs [92–94]. However, assuming perfect knowledge of CSI is also a common practice in design stages of developing algorithms in virtue of providing insights on ultimate performance bounds. The imperfect CSI assumption can be considered at later stages such as the robust design stage. As a result, many studies on massive MIMO-NOMA networks have considered a perfect CSI assumption. For example, assuming perfect CSI, the authors in [52] investigated a total transmit power minimization problem subject to sum-rate constraints for designing power allocation coefficients and beamforming vectors in NOMA-aided multicast downlink transmissions, where two single-antenna users of weak and strong channel gains are clustered together to be served on each beam. The authors proposed an iterative algorithm to solve the problem, however, their method does not always converge to the optimal solution.

In [89], the authors assumed partial CSI feedback and a suboptimal random beamforming technique to design power allocation and user scheduling based on matching theory. The sum-rate maximization subject to quality of service requirements is considered for an overloaded scenario in which the number of radio frequency chains is much smaller than the number of users. Under the assumption of perfect knowledge of CSI, a joint power allocation and beamforming design for uplink transmissions in mmWave-NOMA was studied in [90], where a multi-antenna BS station serves two single-antenna users. The authors proposed a suboptimal solution for the problem of sum-rate maximization subject to minimal rate constraints at two users. The authors in [91] assumed perfect CSI to propose an iterative power allocation scheme which maximizes the achievable sum-rate under total transmit power constraints for mmWave MIMO-NOMA systems. By using NOMA, they employed a beam selection algorithm based on MIMO beamspace to support several users on a same beam.

Recently, the power allocation designs in energy/power-efficient MIMO-NOMA networks have gained an increasingly increasing popularity [95–98]. For instance, in [96], the authors propose a suboptimal power allocation solution to maximize the energy-efficiency of downlink transmissions for a MIMO-NOMA network in which two users are assigned to each sub-channel. In [97], a joint problem of power allocation and user scheduling was formulated to maximize the energy efficiency subject to QoS constraints at users in a millimeter wave MIMO-NOMA network. The authors in [98] studied the problem of power allocation and user scheduling in NOMA-based networks by formulating a total consumed power minimization under the sum-rate constraints.

2.3.2 User Clustering in Massive MIMO-NOMA Networks

Effective and efficient designs of user clustering schemes have become inevitable to properly exploit the potential of NOMA enabled massive MIMO networks [53, 99–101]. In [99], an iterative suboptimal solution to the joint problem of user clustering and resource allocation is proposed to maximize the sum of effective capacity in all users in downlink transmission of a co-located MIMO-NOMA network. The main idea of the proposed clustering algorithm is to cluster the users such that the intra-cluster users can be served on a same beam. A

cluster grouping algorithm and a max-min power allocation scheme for the downlink transmission of co-located MIMO-NOMA networks in millimeter-wave communications under a perfect CSI assumption were studied in [100]. Note that in millimeter-wave applications, the channels are sparse in angular domain and encompass both Line-of-Sight (LoS) and Non-Line-of-Sight (NLoS) paths. Considering the angle of arrival of the users, the clustering algorithm proposed in [100] exploits the fact that inter cluster interference can be diminished when the spatial direction distance grows large, and thus, allocates the users into a given number of clusters. Compared with a random cluster grouping, the authors showed that the proposed clustering method can enhance the sum-rate performance. Authors in [101] studied the power allocation and user clustering problem in millimeter-wave NOMA downlink transmissions by maximizing the sum-rate under the rate requirements and the total transmit power constraints. In particular, using Euclidean distance as a measure of channel correlation between the users and a multi-antenna BS, the authors proposed a machine-learning-based K-means algorithm to group those users which are physically close to each other into one cluster. It is demonstrated in [101] that the K-means based MIMO-NOMA system can improve the sum-rate performance compared to the MIMO-OMA system. In an attempt to consider the user clustering and power allocation design for uplink transmissions of massive MIMO-NOMA systems, the authors in [53] maximize the sum-rate subject to the received power constraints, and propose an optimal user clustering using extensive search.

2.3.3 Related Work Connected to Chapter 5

In Chapter 5, we study the integration of the NOMA scheme into the massive MIMO networks with both co-located and distributed structures. We aim to design the user clustering and power allocation coefficients to minimize the total transmit power consumed in the entire network while SINRs at the users are maintained at the required thresholds. We propose a machine-learning-based clustering algorithm which allocates the users into different clusters based on their channel characteristics. Our clustering algorithm can automatically decide on the best number of clusters in the network based on the available degree of freedom, and thus, it can be considered as a hybrid scheme.

Our study may seem closely related to the power allocation and user clustering problem

defined in [101]. However, the study in [101] is different from ours in three important aspects: Firstly, the authors in [101] studied a co-located massive MIMO-NOMA system in millimeter-wave applications while we have considered a massive MIMO-NOMA system for both co-located and distributed structures. Second, a sum-rate maximization under the rate requirements and the total transmit power constraints is considered in [101] in contrast to the problem of total power minimization subject to SINR constraints in our study. Lastly, although both studies considered a machine-learning-based approach for the user clustering problem, we have proposed a novel clustering algorithm which successfully overcomes the impediments of the clustering algorithm proposed in [101]. In other words, since the proposed clustering method in [101] is based on the K-means clustering concept, it suffers from two main problems: 1) the number of clusters must be given to the algorithm; 2) Due to the usage of Euclidean distance as the criterion to measure the correlations among users associated with the same cluster, the proposed clustering in [101] is prone to mistake in the presence of phase noises.

Chapter 3

Power-Optimal Distributed Beamforming

In this chapter, we focus on the problem of joint power allocation and beamforming design for an asynchronous half-duplex TWR network in an OFDM system, consisting of multiple AF relays and two OFDM-based transceivers. Aiming to satisfy QoS constraints, measured by transceivers' rates, we formulate a total transmission power minimization problem to obtain the jointly optimal power allocation and distributed beamforming weights. A semi-closed form solution is proposed for this problem. It is rigorously proven that this solution leads to a relay selection scheme, where only those relays which contribute to the optimal tap of the end-to-end channel impulse response can actively participate in the communication.

The remainder of this chapter is organized as follows: Section 3.1 presents our signal model and derived expressions for the average total transmission power and the sum-rates. Section 3.2 introduces the optimization problem and the corresponding semi-closed-form solution. In Section 3.4, we discuss the numerical results.

3.1 Preliminaries

Consider an asynchronous TWR network in an OFDM system which consists of two transceivers, denoted as TR_1 and TR_2, communicating through L AF relay nodes, as shown in Fig.3.1. All nodes are equipped with a single antenna. The beamforming weight of the l-th AF relay node is indicated by w_l, for $l = 1, 2, \ldots, L$. We assume no direct link exists between the

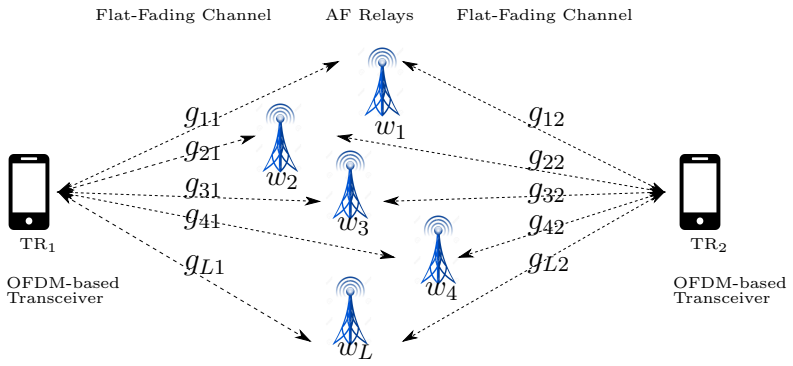

Figure 3.1: Two-way relay network setup with two OFDM-based transceivers and L AF relaying nodes.

two transceivers. A flat-fading channel is assumed between each transceiver and each relay node[1]. We further assume channel reciprocity, i.e., the channel coefficients representing the links between each transceiver and each relay in both directions are the same. The channel coefficient corresponding to the link between the l-th relay and TR_m is denoted by g_{lm}, for $m = 1, 2$. Each transceiver employs an OFDM scheme with N sub-carriers. To enable a bidirectional communication between the two transceivers, two time slots are needed. In the first time slot, TR_1 and TR_2 simultaneously transmit their OFDM symbols toward the relay nodes, while in the second time slot, each relay node amplifies and adjusts the phase of the signal that relays receives during the first time slot, and broadcasts the so-obtained signal to the two transceivers. We assume that each transceiver has the perfect knowledge of the CSI of all transceiver-relay links, whereas it is assumed that each relay knows the local CSI between the two transceivers and itself in order to calculate the beamforming weights accordingly.

We assume that each relaying path, connecting the two transceivers through one of the relays, is subject to a propagation delay which depends on the locations of that relay and the two end-nodes. This propagation delay can be different from the propagation delay of other relaying paths. This assumption leads to an asynchronous communication, which in turn causes a multi-path end-to-end channel, i.e., multiple copies of the signal transmitted

[1]Assuming frequency-flat relay-transceiver channels has a clear application in satellite communication where satellites act as simple amplify-and-forward relays with frequency-independent amplification factors and where the transceiver-satellite links are frequency-flat. One can also envision applications in wireless networks where two far part base stations rely on other base stations, which are in their line of sight, to act as relays, thereby enabling two-way communication between those two base stations.

by one of the transceivers will be received at the others transceivers at different times. This multi-path phenomenon renders the end-to-end channel frequency-selective, and therefore, causes ISI. Note that OFDM scheme is not employed at the AF relay nodes as to avoid processing complexity at the relay nodes[2].

3.1.1 Channel Model

The discrete-time equivalent end-to-end channel can be modeled as an FIR system with a maximum order of N_c. The value of N_c is determined via dividing the maximum propagation delay by the sampling period, T_s. Let w_l denote the complex beamforming weight of the l-th relay, while τ_l signifies the propagation delay of the l-th relaying path. Given the channel reciprocity, we express the n-th tap of the end-to-end discrete-time end-to-end CIR as[3]

$$h_{12}[n] = h_{21}[n] = h[n] = \sum_{l=1}^{L} w_l g_{l1} g_{l2} I_n(\tau_l), \quad \text{for } n = 0, 1, \ldots, N_c - 1 \tag{3.1}$$

where $I_n(\tau_l)$ is an indicator function whose value is equal to 1, when $\tau_l \in ((n-1)T_s, nT_s]$, and zero otherwise. It follows from (3.1) that each relay contributes to only one tap of the end-to-end CIR. That is, the l-th relay contributes to the n-th tap of $h[\cdot]$, if the propagation delay τ_l of the corresponding relaying path linking the two transceivers satisfies $(n-1)T_s < \tau_l \leq nT_s$, for $n = 0, 1, \ldots, N_c - 1$. Note that the channel model in (3.1) relies on the important assumption that the beamforming weights, i.e., w_l's, at the relay nodes are frequency-independent. Indeed, our approach does not assume frequency-dependent processing (for example, through OFDM processing) capability at the relays for the sake of relay simplicity. Assuming frequency-dependent beamforming weights requires the use of OFDM reception and transmission schemes at the relays, which results in relay complexity. Using (3.1), we introduce the end-to-end channel tap vector $\mathbf{h}$ as

$$\mathbf{h} = \mathbf{B}\mathbf{w}\,. \tag{3.2}$$

[2]The power allocation problem for an asynchronous TWR network where all the nodes including the relays adopt the OFDM technique is studied in [39]. It is assumed in [39] that the channels between each transceiver and each relay are frequency-selective, thereby causing ISI. To overcome this ISI necessitates the implementation of OFDM schemes at the relays.

[3]See Appendix A.1 for the detail derivation of this model.

Here, $\mathbf{w} = [w_1\ w_2\ \ldots\ w_L]^T$ denotes $L \times 1$ relay beamforming weight vector, and $\mathbf{h}$ is the channel vector, $\mathbf{h} \triangleq [h[0]\ h[1]\ \ldots\ h[N_c-1]\ \mathbf{0}_{1\times(N-N_c)}]^T$, which is padded with $N - N_c$ zeros assuming $N \geq N_c$. In (3.2), $\mathbf{B}$ is an $N \times L$ relay contribution matrix indicating the relationship between each tap of the end-to-end CIR and the relay weights which contribute (or subscribe) to that tap. From (3.1), for $n = 0, 1, \ldots, N-1$, and $l = 1, 2, \ldots, L$, the $(n+1, l)$-th entry of $\mathbf{B}$ is defined as

$$\mathbf{B}(n+1, l) \triangleq g_{l1} g_{l2} I_n(\tau_l). \tag{3.3}$$

From (3.3), it can be observed that each relay can contribute to only one tap of the end-to-end CIR $h[\cdot]$. Later, we will use the specific structure of matrix $\mathbf{B}$ to facilitate the derivation of the solution to the problem that we herein consider, namely the problem of joint sub-carrier power allocation and relay beamforming for two-way AF relay networks.

3.1.2 Signal Model

To combat the ISI incurred by the frequency-selective nature of the end-to-end channel, it is herein assumed that TR_1 and TR_2 communicate using an OFDM system. Fig. 3.2 shows the typical structure of an OFDM-based transceiver. In this figure, S/P and P/S signify the serial-to-parallel and the parallel-to-serial conversion blocks, respectively, the $N \times N$ matrices $\mathbf{F}$ and $\mathbf{F}^H$ stand for the Discrete Fourier Transform (DFT) and the Inverse Discrete Fourier Transform (IDFT) matrices, respectively, and $\mathbf{T}_{\mathrm{cp}}$ and $\mathbf{R}_{\mathrm{cp}}$ denote the Cyclic Prefix (CP) insertion and the CP deletion matrices, respectively. We assume the information symbols, $s_1[\cdot]$ and $s_2[\cdot]$, transmitted respectively by TR_1 and TR_2, have unit powers, i.e., $E\{|s_1[i]|^2\} = E\{|s_2[i]|^2\} = 1$, for $i = 1, 2, \ldots, N$.

At the output of the S/P conversion at TR_m, for $m \in \{1, 2\}$, the resultant $N \times 1$ signal vector is denoted as $\mathbf{s}_m \triangleq [s_m[1]\ s_m[2]\ \ldots\ s_m[N]]^T$. Let P_{im} indicate the transmission power allocated to the i-th sub-carrier at TR_m, for $m \in \{1, 2\}$ and $i \in \{1, ..., N\}$. The amplitude-adjusting matrix at TR_m is defined as $\mathbf{A}_m \triangleq \mathrm{diag}\{\sqrt{P_{im}}\}_{i=1}^N$. At the transmitter side, in order to retain the ability to remove ISI at the receiving side, a CP of length of N_{cp} is added to the output of the IDFT block (given by $\mathbf{F}^H \mathbf{A}_m \mathbf{s}_m$), where $N_{\mathrm{cp}} \geq N_c$. Specifically, define the CP insertion matrix as $\mathbf{T}_{\mathrm{cp}} \triangleq [\bar{\mathbf{I}}_N^T\ \ \mathbf{I}_N^T]^T$, where $\bar{\mathbf{I}}_N$ is the last N_{cp} rows of the

identity matrix $\mathbf{I}_N$. Hence, the output vector of the CP insertion operation is given by $\mathbf{T}_{\rm cp}\mathbf{F}^H\mathbf{A}_m\mathbf{s}_m$, for $m = 1, 2$. Let $M = N + N_{\rm cp}$ denote the final length of the OFDM symbol, given by $\mathbf{T}_{\rm cp}\mathbf{F}^H\mathbf{A}_m\mathbf{s}_m$, transmitted from TR_m toward the relay nodes. After applying the beamforming weights at the relays, the $M\times 1$ vector of the (time-domain) signals transmitted by the l-th relay is given as

$$\mathbf{x}_l = w_l \left(g_{l1}\mathbf{T}_{\rm cp}\mathbf{F}^H\mathbf{A}_1\mathbf{s}_1 + g_{l2}\mathbf{T}_{\rm cp}\mathbf{F}^H\mathbf{A}_2\mathbf{s}_2 + \boldsymbol{\eta}_l \right) \tag{3.4}$$

where $\boldsymbol{\eta}_l \triangleq [\eta_l(0)\ \eta_l(T_s)\ \ldots\ \eta_l((M-1)T_s)]^T$ is the equivalent received noise vector at the l-th relay, with $\eta_l(t)$ being the corresponding white Gaussian noise process, with zero mean and variance of σ^2. As seen from (3.4), the noise vector $\boldsymbol{\eta}_l$ is multiplied by the weight w_l and arrives at the transceivers. At the receiver side of TR_m, after S/P conversion process, the CP is removed from the received OFDM symbol by using the $N \times M$ CP deletion matrix, defined as $\mathbf{R}_{\rm cp} \triangleq [\mathbf{0}_{N\times N_{\rm cp}}\ \ \mathbf{I}_N]$. The $N \times 1$ received signals vector at the output of DFT block at TR_m, for $m = 1, 2$, can be written as

$$\mathbf{y}_m = \mathbf{A}_m\mathbf{H}_{mm}\mathbf{s}_m + \mathbf{A}_{\bar{m}}\mathbf{H}_{\bar{m}m}\mathbf{s}_{\bar{m}} + \mathbf{F}\mathbf{R}_{\rm cp}\mathbf{n}_m \tag{3.5}$$

where we define $\bar{m} = 2$, if $m = 1$, and $\bar{m} = 1$, if $m = 2$, $\mathbf{n}_m$ denotes the $M \times 1$ equivalent noise vector[4] received at TR_m, matrix $\mathbf{H}_{\bar{m}m} = \mathbf{H}_{m\bar{m}} \triangleq \mathrm{diag}\{\mathbf{F}\mathbf{h}\}$ is a diagonal matrix of the Fourier transform of the channel vector $\mathbf{h}$ defined in (3.2), $\mathbf{H}_{mm}$ is a diagonal matrix of the Fourier transform of the equivalent channel impulse from TR_m to the relays and from the relays back to TR_m, for $m \in \{1, 2\}$. As a result, the first term in (3.5) is known as the self-interference term at TR_m. Using the perfect knowledge of CSI, each transceiver can cancel its own self-interference term from the received signal $\mathbf{y}_m$. As a result, after the self-interference cancellation at TR_m, the resulting signal vector $\tilde{\mathbf{y}}_m$ can be expressed as

$$\tilde{\mathbf{y}}_m = \mathbf{y}_m - \mathbf{A}_m\mathbf{H}_{mm}\mathbf{s}_m = \mathbf{A}_{\bar{m}}\mathbf{H}_{\bar{m}m}\mathbf{s}_{\bar{m}} + \mathbf{F}\mathbf{R}_{\rm cp}\mathbf{n}_m\,, \qquad \text{for } m \in \{1, 2\}. \tag{3.6}$$

Total Average Transmit Power and Sum-rate Expressions: In this work, we consider the total transmission power minimization subject to the sum-rate constraints

[4]Note that this noise is the superposition of the receiver's measurement noise and the relay measurement noises after they are amplified at the relay and they are attenuated by the relay-transceiver channels. For further details on the noise modeling, please see [16].

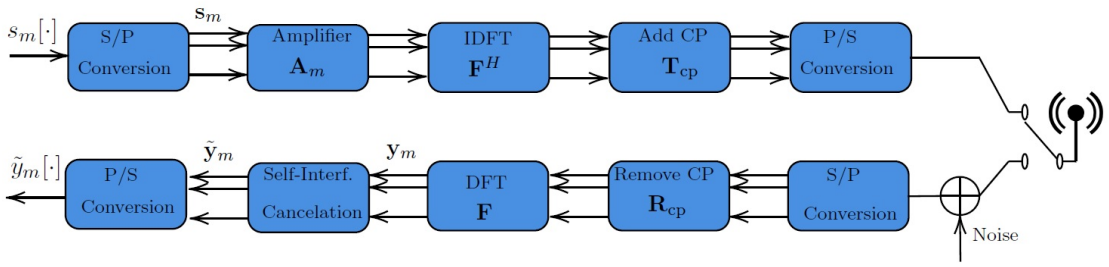

Figure 3.2: Block diagram of the OFDM-based transceiver TR_m, $m = 1, 2$.

at each transceiver over the considered TWR network. In this section, we present the expressions of the total transmission power and the sum-rate at each transceiver as derived in [16]. Let $\mathbf{p}_m = [P_{1m}\ P_{2m}\ \ldots\ P_{Nm}]^T$ be an $N \times 1$ vector of transmission powers over the OFDM sub-carriers at TR_m. The total average transmission power in the TWR network is the sum of the average transmit powers at both transceivers and the average transmission power of the L relay nodes. While the average transmission power at TR_m is equal to $\frac{\mathbf{1}^T\mathbf{p}_m}{N}$, for $m \in \{1, 2\}$, the average transmission power at the l-th relay, denoted by P_l, can be easily derived from (3.4) as

$$P_l = \frac{E\{\mathbf{x}_l^H \mathbf{x}_l\}}{M} = \frac{|w_l|^2}{N}\left(|g_{l1}|^2 \mathbf{1}^T\mathbf{p}_1 + |g_{l2}|^2 \mathbf{1}^T\mathbf{p}_2 + \sigma^2 N\right)$$

and then the total average transmission power over all relay nodes, denoted as P_{r}, can be written as

$$P_{\text{r}} = \frac{\mathbf{1}^T\mathbf{p}_1}{N}\mathbf{w}^H\mathbf{D}_1\mathbf{w} + \frac{\mathbf{1}^T\mathbf{p}_2}{N}\mathbf{w}^H\mathbf{D}_2\mathbf{w} + \sigma^2\mathbf{w}^H\mathbf{w} \tag{3.7}$$

where $\mathbf{D}_m$ is a diagonal matrix whose l-th diagonal element is given by $\mathbf{D}_m(l, l) = |g_{lm}|^2$, for $m \in \{1, 2\}$. Therefore, the expression for the total average transmission power over the TWR network is given by

$$P_T = \sum_{m=1}^{2} \frac{\mathbf{1}^T\mathbf{p}_m}{N}\left(1 + \mathbf{w}^H\mathbf{D}_m\mathbf{w}\right) + \sigma^2\mathbf{w}^H\mathbf{w}. \tag{3.8}$$

The achievable sum-rate over N sub-carriers at TR_m, for $m = 1, 2$, is given by

$$R_m(\mathbf{p}_{\bar{m}}, \mathbf{w}) = \sum_{i=1}^{N} 0.5 \log_2(1 + \text{SNR}_{im}), \tag{3.9}$$

where SNR_{im} denotes the received SNR over the i-th sub-carrier at TR_m. We now derive an expression for SNR_{im}, for $m = 1, 2$. Using (3.6), we obtain the average power of the signal component over the i-th sub-carrier, received at TR_m, denoted as P^s_{im}, as

$$P^s_{im} = NP_{i\bar{m}}|\mathbf{f}_i^H \mathbf{B}\mathbf{w}|^2 \tag{3.10}$$

where $\mathbf{f}_i = N^{-\frac{1}{2}}[1 \;\; \exp(\frac{j2\pi(i-1)}{N}) \;\; \ldots \;\; \exp(\frac{j2\pi(i-1)(N-1)}{N}]^T$ is the i-th Vandermonde column vector of the IDFT matrix $\mathbf{F}^H$. Likewise, the average power of the noise component received at TR_m over the i-th sub-carrier, denoted as P^n_{im}, can be obtained as [16]

$$P^n_{im} = \sigma^2(1 + \mathbf{w}^H \mathbf{D}_m \mathbf{w}). \tag{3.11}$$

From (3.10) and (3.11), SNR_{im} can be formulated, for $m = 1, 2$, as

$$\text{SNR}_{im} = \frac{NP_{i\bar{m}}|\mathbf{f}_i^H \mathbf{B}\mathbf{w}|^2}{\sigma^2(1 + \mathbf{w}^H \mathbf{D}_m \mathbf{w})}, \quad \text{for } i = 1, 2, \ldots, N. \tag{3.12}$$

Ultimately, inserting (3.12) into (3.9) yields the achievable sum-rate over N sub-carriers at TR_1 and TR_2, respectively.

3.2 Total Transmit Power Minimization

We aim to minimize the average total transmission power (given in (3.8)) consumed in the entire network, while the achievable transmission rates, given in (3.9) are satisfying the minimum rate requirements, i.e., $R_1(\mathbf{p}_2, \mathbf{w}) \geq r_1$ and $R_2(\mathbf{p}_1, \mathbf{w}) \geq r_2$, where r_1 and r_2 are the required threshold rate values at TR_1 and TR_2, respectively. This minimization problem is formulated as

$$\min_{\mathbf{w}} \min_{\substack{\mathbf{p}_1 \succeq 0 \\ \mathbf{p}_2 \succeq 0}} P_T, \qquad \text{s.t. } R_m(\mathbf{p}_{\bar{m}}, \mathbf{w}) \geq r_m, \qquad \text{for } m = 1, 2 \tag{3.13}$$

We now show that at the optimum, the inequality constraints in (3.13) are satisfied with equality, i.e., $R_1(\mathbf{p}_2, \mathbf{w}) = r_1$ and $R_2(\mathbf{p}_1, \mathbf{w}) = r_2$. To do so, let us assume that at the optimum, any of the two inequality constraints is satisfied with strict inequality, that is $R_1(\mathbf{p}_2, \mathbf{w}) > r_1$ and/or $R_2(\mathbf{p}_1, \mathbf{w}) > r_2$. We can reduce the value of one of the entries of the optimal power $\mathbf{p}_1$ and/or $\mathbf{p}_2$ such that $R_2(\mathbf{p}_1, \mathbf{w})$ and/or $R_1(\mathbf{p}_2, \mathbf{w})$ are still greater than

r_2 and r_1, respectively. However, these new values of $\mathbf{p}_1$ and/or $\mathbf{p}_2$ result in a lower value of the objective function, thereby, contradicting the optimality. Hence, the optimization problem (OP) in (3.13) can be rewritten as

$$\min_{\mathbf{w}} \min_{\substack{\mathbf{p}_1 \succeq 0 \\ \mathbf{p}_2 \succeq 0}} P_T, \text{ s.t. } R_m(\mathbf{p}_{\bar{m}}, \mathbf{w}) = r_m, \text{for } m = 1, 2 \tag{3.14}$$

Using (3.8) and (3.9), we can rewrite the OP (3.14) as

$$\begin{aligned} \min_{\mathbf{w}} \min_{\substack{\mathbf{p}_1 \succeq 0 \\ \mathbf{p}_2 \succeq 0}} & \sum_{m=1}^{2} \frac{\mathbf{1}^T \mathbf{p}_m}{N} \left(1 + \mathbf{w}^H \mathbf{D}_m \mathbf{w}\right) + \sigma^2 \mathbf{w}^H \mathbf{w} \\ \text{s.t.} & \sum_{i=1}^{N} 0.5 \log_2(1 + \text{SNR}_{im}) = r_m, \text{ for } m = 1, 2\,. \end{aligned} \tag{3.15}$$

To solve (3.15), we first consider the inner minimization in (3.15) and aim to find the optimal values of $\mathbf{p}_1$ and $\mathbf{p}_2$ for a fixed $\mathbf{w}$. We then tackle the outer minimization problem[5].

3.2.1 Power Allocation Problem

For any fixed $\mathbf{w}$, the inner minimization in (3.15) amounts to solving two separate OPs: one for obtaining $\mathbf{p}_1$, and one for obtaining $\mathbf{p}_2$. With the SNR expression in (3.12), the OP, which yields the optimal value of $\mathbf{p}_1$ for any fixed $\mathbf{w}$, is formulated as

$$\begin{aligned} \min_{\mathbf{p}_1 \succeq 0} \quad & \frac{\mathbf{1}^T \mathbf{p}_1}{N} \left(1 + \mathbf{w}^H \mathbf{D}_1 \mathbf{w}\right) \\ \text{s.t.} \quad & \sum_{i=1}^{N} 0.5 \log_2 \left(1 + \frac{N P_{i1} |\mathbf{f}_i^H \mathbf{B} \mathbf{w}|^2}{\sigma^2 (1 + \mathbf{w}^H \mathbf{D}_2 \mathbf{w})}\right) = r_2. \end{aligned} \tag{3.16}$$

By ignoring the inequality constraint $\mathbf{p}_1 \succeq 0$, the relaxed OP

$$\begin{aligned} \min_{\mathbf{p}_1} \quad & \frac{\mathbf{1}^T \mathbf{p}_1}{N} \left(1 + \mathbf{w}^H \mathbf{D}_1 \mathbf{w}\right) \\ \text{s.t.} \quad & \sum_{i=1}^{N} 0.5 \log_2 \left(1 + \frac{N P_{i1} |\mathbf{f}_i^H \mathbf{B} \mathbf{w}|^2}{\sigma^2 (1 + \mathbf{w}^H \mathbf{D}_2 \mathbf{w})}\right) = r_2. \end{aligned} \tag{3.17}$$

can be solved using the Lagrange multipliers method, for the minimization problem (3.17) has only one equality constraint. We will later show that ignoring $\mathbf{p}_1 \succeq 0$ will not cause

[5]Note that this approach does not cause any loss of optimality, see Page 133 of [102].

any loss of the optimality. To this end, the Lagrange function $\mathcal{L}(\mathbf{p}_1, \gamma)$ is defined as

$$\mathcal{L}(\mathbf{p}_1, \gamma) \triangleq \frac{\mathbf{1}^T \mathbf{p}_1}{N} \left(1 + \mathbf{w}^H \mathbf{D}_1 \mathbf{w}\right) + \gamma \left[r_2 - \sum_{i=1}^{N} 0.5 \log_2 (1 + \frac{N P_{i1} |\mathbf{f}_i^H \mathbf{B} \mathbf{w}|^2}{\sigma^2 (1 + \mathbf{w}^H \mathbf{D}_2 \mathbf{w})}) \right] \tag{3.18}$$

where γ is the Lagrange multiplier. Differentiating (3.18) with respect to P_{i1} and equating the derivative to zero yields the i-th sub-carrier power at TR_1, P_{i1}, as a function of γ, as

$$P_{i1} = \frac{\gamma N}{2 \ln 2 (1 + \mathbf{w}^H \mathbf{D}_1 \mathbf{w})} - \frac{1}{\beta_i(\mathbf{w})} \tag{3.19}$$

where we define $\beta_i(\mathbf{w}) \triangleq \dfrac{N |\mathbf{f}_i^H \mathbf{B} \mathbf{w}|^2}{\sigma^2 (1 + \mathbf{w}^H \mathbf{D}_2 \mathbf{w})}$. To find γ, we insert (3.19) back into the constraint in (3.16) and obtain (see Appendix A.2 for more details)

$$\gamma = \Gamma(\mathbf{w}) \left(\frac{2^{2 r_2}}{\prod_{i=1}^{N} |\mathbf{f}_i^H \mathbf{B} \mathbf{w}|^2} \right)^{\frac{1}{N}} \tag{3.20}$$

where the following definition is used: $\Gamma(\mathbf{w}) \triangleq \dfrac{2 \ln 2 (1 + \mathbf{w}^H \mathbf{D}_1 \mathbf{w})(1 + \mathbf{w}^H \mathbf{D}_2 \mathbf{w}) \sigma^2}{N^2}$. Therefore, the power P_{i1} on the i-th sub-carrier power at TR_1 can be obtained by inserting (3.20) into (3.19), and is thus given by (see Appendix A.3 for more details)

$$P_{i1} = \frac{\sigma^2 (1 + \mathbf{w}^H \mathbf{D}_2 \mathbf{w})}{N} \left(\frac{2^{\frac{2 r_2}{N}}}{\left[\prod_{i=1}^{N} |\mathbf{f}_i^H \mathbf{B} \mathbf{w}|^2 \right]^{\frac{1}{N}}} - \frac{1}{|\mathbf{f}_i^H \mathbf{B} \mathbf{w}|^2} \right). \tag{3.21}$$

To further simplify (3.21), we use the following lemma.

Lemma 3.2.1. *At the optimum of the minimization problem (3.14), the equality* $|\mathbf{f}_i^H \mathbf{B} \mathbf{w}| = |\mathbf{f}_j^H \mathbf{B} \mathbf{w}|$ *holds true for any* i *and* j.

Proof. See Appendix A.4. □

Lemma 3.2.1 implies that, the optimal beamforming weight vector $\mathbf{w}$ belongs to the set $\mathcal{W} \triangleq \{\mathbf{w} \big| \ |\mathbf{f}_i^H \mathbf{B} \mathbf{w}| = |\mathbf{f}_j^H \mathbf{B} \mathbf{w}|, \text{ for } i \neq j\}$. Therefore, without any loss of optimality, we can restrict the relay beamforming weights to the set $\mathcal{W}$. We can also use Lemma 3.2.1 to

write (3.21) as

$$P_{i1} = \frac{\alpha_2(\mathbf{w})}{N}\left(\frac{2^{\frac{2r_2}{N}}-1}{|\mathbf{f}_i^H\mathbf{B}\mathbf{w}|^2}\right) \tag{3.22}$$

where we define $\alpha_2(\mathbf{w}) \triangleq \sigma^2(1+\mathbf{w}^H\mathbf{D}_2\mathbf{w})$. Based on Lemma.3.2.1, at the optimum of the relaxed problem (3.17), the following equality holds true:

$$|\mathbf{f}_j^H\mathbf{B}\mathbf{w}|^2 = \frac{1}{N}\sum_{i=1}^{N}|\mathbf{f}_i^H\mathbf{B}\mathbf{w}|^2\,,\ \text{for}\ \ j\in\{1,2,\ldots,N\}. \tag{3.23}$$

Using Parseval's theorem [103], we can write

$$\sum_{i=1}^{N}\left|\mathbf{f}_i^H\mathbf{B}\mathbf{w}\right|^2 = \|\mathbf{B}\mathbf{w}\|^2. \tag{3.24}$$

Therefore, using (3.23) and (3.24), we further simplify (3.22) as

$$P_{i1} = \alpha_2(\mathbf{w})\left(\frac{2^{\frac{2r_2}{N}}-1}{\|\mathbf{B}\mathbf{w}\|^2}\right). \tag{3.25}$$

Similarly, the transmission power P_{i2} over the i-th sub-carrier at TR_2, can be obtained as

$$P_{i2} = \alpha_1(\mathbf{w})\left(\frac{2^{\frac{2r_1}{N}}-1}{\|\mathbf{B}\mathbf{w}\|^2}\right) \tag{3.26}$$

where $\alpha_1(\mathbf{w}) \triangleq \sigma^2(1+\mathbf{w}^H\mathbf{D}_1\mathbf{w})$. Note that since the rate thresholds r_1 and r_2 are positive values, the sub-carriers' powers are always positive, and therefore, the relaxations of $\mathbf{p}_1 \succeq 0$ and $\mathbf{p}_2 \succeq 0$ have not caused any loss of the optimality. Also, note that all sub-carriers at each transceiver receive the same level of power as P_{i1} and P_{i2} in (3.25) and (3.26) are independent of the sub-carrier index of i.

3.2.2 Distributed Beamforming Design

We now focus on the outer minimization in (3.15). To find the relay beamforming weight vector $\mathbf{w}$, we use (3.25) and (3.26) to write the sum of the transmission powers over sub-carriers at TR_m as

$$\mathbf{1}^T\mathbf{p}_m = N\alpha_{\bar{m}}(\mathbf{w})(2^{\frac{2r_{\bar{m}}}{N}}-1)(\|\mathbf{B}\mathbf{w}\|^2)^{-1} \tag{3.27}$$

Based on (3.27) the OP (3.15) can be expressed as

$$\min_{\mathbf{w}\in\mathcal{W}} \quad \frac{\sigma^2(1+\mathbf{w}^H\mathbf{D}_1\mathbf{w})(1+\mathbf{w}^H\mathbf{D}_2\mathbf{w})}{\|\mathbf{B}\mathbf{w}\|^2}(\beta_1+\beta_2)+\sigma^2\mathbf{w}^H\mathbf{w} \tag{3.28}$$

where $\beta_j \triangleq 2^{\frac{2r_j}{N}}-1$, for $j=1,2$. For any $\mathbf{w}\in\mathcal{W}$, it is proved in [16,39] that the end-to-end CIR $h[\cdot]$ will have only one non-zero tap. This in turn implies that at the optimum, the end-to-end channel is frequency-flat. This result amounts to a relay selection scheme in which the corresponding relays contributing to the zero taps of the end-to-end CIR will be switched off, and only those relays which contribute to that single non-zero tap should be turned on. From the specific structure of the matrix $\mathbf{B}$ in (3.3), we know that each relay can only contribute to one tap of the end-to-end CIR $h[\cdot]$. Let $\mathcal{U}_n$ denote the set of those values of $\mathbf{w}$ which result in $h[n]$ being non-zero, while all other taps are zero. That is

$$\mathcal{U}_n \triangleq \{\mathbf{w}|h[n]\neq 0, h[k]=0, \quad \text{for} \quad k\in\{0,1,\ldots,N-1\}\backslash\{n\}\}$$

If no relay contributes to the n-th tap of the end-to-end CIR $h[\cdot]$, $\mathcal{U}_n$ will be empty. In light of the fact that no relay can contribute to more than one tap of $h[\cdot]$, the sets of $\{\mathcal{U}_n\}_{n=0}^{N-1}$ are mutually exclusive, i.e., $\mathcal{U}_n\bigcap\mathcal{U}_{n'}=\emptyset$ for $n\neq n'$. Let $\mathcal{N}$ be the set of those values of n for which $\mathcal{U}_n$ is not empty, i.e., $\mathcal{N}=\{0\leq n\leq N-1|\,\mathcal{U}_n\neq\emptyset\}$. Then, the feasible set $\mathcal{W}$ of the beamforming weight vectors can be expressed as

$$\mathcal{W}=\bigcup_{n\in\mathcal{N}}\mathcal{U}_n. \tag{3.29}$$

It follows from (3.29) that the OP in (3.28) can be separately solved for each $n\in\mathcal{N}$. More specifically, using (3.29), we can rewrite the OP in (3.28) as

$$\min_{n\in\mathcal{N}}\min_{\mathbf{w}\in\mathcal{U}_n}\frac{\sigma^2(1+\mathbf{w}^H\mathbf{D}_1\mathbf{w})(1+\mathbf{w}^H\mathbf{D}_2\mathbf{w})}{\|\mathbf{B}\mathbf{w}\|^2}(\beta_1+\beta_2)+\sigma^2\mathbf{w}^H\mathbf{w}. \tag{3.30}$$

In other words, solving the OP in (3.28) amounts to first solving $|\mathcal{N}|$ subproblems. Each subproblem provides a beamforming weight vector $\mathbf{w}$. Then, the optimal beamforming weight vector is the one, among the solution to these subproblems, which leads to the smallest value of the total transmission power in the TWR network.

We now modify the vectors and matrices within the objective function in (3.30) such that this objective function can be rewritten in terms of the active relay nodes at the n-th tap of $h[\cdot]$, for $n \in \mathcal{N}$. Let $\mathbf{w}_n$ stand for the beamforming weight vector of those relays which contribute to the n-th tap of $h[\cdot]$. Furthermore, we define $\mathbf{b}_n$ as the $L_n \times 1$ vector of the non-zero elements of the $(n+1)$-th column of the matrix $\mathbf{B}^H$, where L_n denotes the number of relays which contribute to the n-th tap of $h[\cdot]$, for $n \in \mathcal{N}$. We can then write $\|\mathbf{B}\mathbf{w}\|^2 = \mathbf{w}^H\mathbf{B}^H\mathbf{B}\mathbf{w} = \mathbf{w}_n^H\mathbf{b}_n\mathbf{b}_n^H\mathbf{w}_n$. Also, let $\mathbf{D}_m^{(n)}$, for $m \in \{1,2\}$, be a diagonal matrix whose diagonal elements are the subset of the diagonal entries of $\mathbf{D}_m$ corresponding to the active relays at the n-th tap of the end-to-end CIR, for $n \in \mathcal{N}$. Defining the objective function in (3.30) as

$$f_n(\mathbf{w}_n) \triangleq \frac{\sigma^2(1+\mathbf{w}_n^H\mathbf{D}_1^{(n)}\mathbf{w}_n)(1+\mathbf{w}_n^H\mathbf{D}_2^{(n)}\mathbf{w}_n)}{\mathbf{w}_n^H\mathbf{b}_n\mathbf{b}_n^H\mathbf{w}_n}(\beta_1+\beta_2) + \sigma^2\mathbf{w}_n^H\mathbf{w}_n, \tag{3.31}$$

we can rewrite the minimization in (3.30) as

$$\min_{n\in\mathcal{N}} \min_{\mathbf{w}_n} \quad f_n(\mathbf{w}_n)\,. \tag{3.32}$$

Note that the inner minimization problem in (3.32) amounts to a total transmission power minimization problem for a subnetwork of those relays which are associated with $h[n]$, for $n \in \mathcal{N}$, see [17, 34]. For such a *synchronous* subnetwork, assuming that the selected relays are switched on and the rest of the relays switched off, the end-to-end CIR $h[\cdot]$ becomes *frequency-flat*. The inner minimization in (3.32) has a well-known semi-closed-form solution which is given in [17]. To present this semi-closed-form solution, we define the function $h_n(z)$, for $n \in \mathcal{N}$, as

$$h_n(z) \triangleq 1 - (\beta_1+\beta_2)\frac{z^{-2} - \lambda\mathbf{u}_n^H(z)\mathbf{D}_1^{(n)}\mathbf{u}_n(z)}{\lambda^2\mathbf{u}_n^H(z)(z\mathbf{D}_1^{(n)}+\mathbf{I}_{L_n})\mathbf{u}_n(z)}. \tag{3.33}$$

where we define

$$\mathbf{u}_n(z) \triangleq \Big((\beta_1+\beta_2)\mathbf{D}_2^{(n)} + \lambda(z\mathbf{D}_1^{(n)}+\mathbf{I}_{L_n})\Big)^{-1}\mathbf{b}_n \tag{3.34}$$

In (3.33), z belongs to the interval $\left(\frac{\beta_1+\beta_2}{\|\mathbf{g}_1^{(n)}\|^2}, +\infty\right)$, $\mathbf{g}_1^{(n)}$ is the $L_n \times 1$ vector defined as $\mathbf{g}_1^{(n)} \triangleq [g_{11}^{(n)} \quad g_{21}^{(n)} \quad \dots \quad g_{L_n1}^{(n)}]^T$, $g_{l1}^{(n)}$ denotes the channel coefficient between TR_1 and the

l-th relay which contributes to the n-th tap of $h[n]$, for $l \in \{1, \ldots, L_n\}$, and for any given parameter $z \in \left(\frac{\beta_1+\beta_2}{\|\mathbf{g}_1^{(n)}\|^2}, +\infty\right)$, the parameter λ is obtained as the provably unique positive solution [17] to the following non-linear equation:

$$\sum_{l=1}^{L_n} \frac{z|g_{l1}^{(n)} g_{l2}^{(n)}|^2}{(\beta_1+\beta_2)|g_{l2}^{(n)}|^2 + \lambda(z|g_{l1}^{(n)}|^2 + 1)} = 1 \tag{3.35}$$

where $g_{l2}^{(n)}$ is the channel coefficient between TR_2 and the l-th relay which contributes to the n-th tap of the end-to-end CIR, for $l \in \{1, \ldots, L_n\}$ and $n \in \mathcal{N}$. For any given $z \in \left(\frac{\beta_1+\beta_2}{\|\mathbf{g}_1^{(n)}\|^2}, +\infty\right)$, a simple Newton-Raphson method can be used to find λ as the unique solution of the equation in (3.35). In other words, the parameter λ is a function of the parameter z. For the so-obtained λ, the provably unique positive root of the function $h_n(z)$ defined in (3.33) can be calculated using a simple Newton-Raphson method. Let z_n denote the unique positive root of the function $h_n(z)$. Define λ_n as the value of λ obtained by solving (3.35) when z is replaced with z_n. Given the parameters z_n and λ_n, the optimal solution for the relay beamforming problem is given as

$$\mathbf{w}_n^{\mathrm{o}} = \sqrt{\frac{(\beta_1+\beta_2)}{k_n \lambda_n}} \mathbf{u}_n(z_n) \tag{3.36}$$

where $\mathbf{w}_n^{\mathrm{o}}$ denotes the optimal value of $\mathbf{w}_n$, while $\beta_m \triangleq (2^{\frac{2r_m}{N}} - 1)$, for $m \in \{1, 2\}$, and k_n is defined as

$$k_n = \mathbf{u}_n^H(z_n)(z_n \mathbf{D}_1^{(n)} + \mathbf{I}_{L_n})\mathbf{u}_n(z). \tag{3.37}$$

For the given set of optimal beamforming weight vectors, $\{\mathbf{w}_n^{\mathrm{o}}\}_{n\in\mathcal{N}}$, we can find the optimal tap of $h[\cdot]$, denoted as n_{opt}, which yields the minimum total transmission power. Indeed, from (3.32), the optimal tap n_{opt} can is given by

$$n_{\mathrm{opt}} = \arg \min_{n\in\mathcal{N}} f_n(\mathbf{w}_n^{\mathrm{o}}). \tag{3.38}$$

Note that for the optimal tap n_{opt}, the indices of the non-zero elements in the $(n_{\mathrm{opt}}+1)$-th row of $\mathbf{B}$ determine which relay nodes contribute to the optimal tap and thus must be activated. Let $\mathbf{w}_{\mathrm{opt}}$ denote the $L \times 1$ optimal beamforming weight vector for all relay nodes in the TWR network. We now explain how $\mathbf{w}_{\mathrm{opt}}$ can be constructed from $\mathbf{w}_{n_{\mathrm{opt}}}^{\mathrm{o}}$. For those

relay nodes which subscribe to the optimal tap n_{opt}, the corresponding entries in $\mathbf{w}_{\text{opt}}$ are equal to the corresponding entries in $\mathbf{w}^{\text{o}}_{n_{\text{opt}}}$. For those relay nodes which do not contribute the optimal tap n_{opt}, the corresponding entries in $\mathbf{w}_{\text{opt}}$ are zero. Given the optimal relay beamforming weight vector $\mathbf{w}_{\text{opt}}$, the optimal transmission power over the i-th sub-carrier in (3.25) at TR_m, denoted as P^{o}_{im} can be given as

$$P^{\text{o}}_{im} = \frac{\sigma^2 \beta_{\bar{m}} (\mathbf{w}^H_{\text{opt}} \mathbf{D}_{\bar{m}} \mathbf{w}_{\text{opt}} + 1)}{\|\mathbf{B}\mathbf{w}_{\text{opt}}\|^2} \tag{3.39}$$

As mentioned earlier, at the optimum, the power is equally distributed among all sub-carriers of each transceiver. Our proposed semi-closed-form solution to the total transmission power minimization in (3.14) for the OFDM-based asynchronous bidirectional relay network under the sum-rate constraints can be summarized as in Algorithm 1.

3.3 Remarks

The following remarks are in order.

Remark 1: We now show that the proposed scheme can be implemented in a distributed manner. As the two transceivers are assumed to have the global CSI knowledge, each transceiver can use (3.36)-(3.39) to obtain the design parameters. One of the two transceivers can then send three parameters, namely $\kappa_{n_{\text{opt}}}$, $z_{n_{\text{opt}}}$, and $\lambda_{n_{\text{opt}}}$ to all the active relays (i.e., those relays which contribute to the tap n_{opt} of the end-to-end CIR). Each of the $L_{n_{\text{opt}}}$ active relays can then use these three parameters along with its own local channel state information in (3.36) with $n = n_{\text{opt}}$, to obtain its own beamforming weight. To further clarify this point, note that in (3.36) with $n = n_{\text{opt}}$, the matrix $\mathbf{D}^{(n_{\text{opt}})}_m$, for $m = 1, 2$, is a diagonal matrix with its l-th diagonal entry being the amplitude squared of the channel coefficient between Transceiver m and the l-th relay which contributes to tap n_{opt} of the end-to-end CIR, for $l = 1, 2, \ldots, L_{n_{\text{opt}}}$. Also, the l-th entry of the vector $\mathbf{b}_{n_{\text{opt}}}$ is the product of the channel coefficients corresponding to the two links between the two transceivers and the l-th relay which contributes to tap n_{opt} of the end-to-end CIR, for $l = 1, 2, \ldots, L_{n_{\text{opt}}}$. As such, the l-th active relay can obtain its own beamforming vector using its own local CSI along with the three parameters $\kappa_{n_{\text{opt}}}$, $z_{n_{\text{opt}}}$, and $\lambda_{n_{\text{opt}}}$.

Algorithm 1 The proposed method

1. Define $\beta_1 \triangleq (2^{\frac{2r_1}{N}} - 1)$ and $\beta_2 \triangleq (2^{\frac{2r_2}{N}} - 1)$. Set $n = 0$.

2. If no relay contributes to the n-th tap of the end-to-end CIR (i.e., if the $(n+1)$-th row of the matrix $\mathbf{B}$ is zero), go to Step 9.

3. Let $\mathbf{b}_n$ denote $L_n \times 1$ vector of the non-zero entries of the $(n+1)$-th column of the $\mathbf{B}^H$, where L_n is the number of non-zero entries in the $(n+1)$-th column of $\mathbf{B}^H$. Also, for $m \in \{1, 2\}$, let $\mathbf{D}_m^{(n)}$ be an $L_n \times L_n$ diagonal matrix whose diagonal entries are a subset of the non-zero diagonal entries of $\mathbf{D}_m$ corresponding to those relays which contribute to the n-th tap of the end-to-end CIR. For $m \in \{1, 2\}$, let $g_{lm}^{(n)}$ signify the channel coefficient between TR_m and the l-th relay which contributes to the n-th tap of the end-to-end CIR, for $l \in \{1, \ldots, L_n\}$. Define the $L_n \times 1$ vector of all channel coefficients between TR_1 and those relays which subscribe to $h[n]$ as $\mathbf{g}_1^{(n)} \triangleq [g_{11}^{(n)} \;\; g_{21}^{(n)} \;\; \ldots \;\; g_{L_n 1}^{(n)}]^T$.

4. Define the function $h_n(z)$ as in (3.33), where for any $z \in \left(\frac{\beta_1+\beta_2}{\|\mathbf{g}_1^{(n)}\|^2}, +\infty\right)$, the parameter λ is obtained, using Newton-Raphson method, as the unique positive root of the non-linear equation in (3.35).

5. Use the Newton-Raphson method to obtain z_n as the unique positive root of $h_n(z)$ in the interval $\left(\frac{\beta_1+\beta_2}{\|\mathbf{g}_1^{(n)}\|^2}, +\infty\right)$.

6. Calculate k_n as in (3.37).

7. Obtain the value of the weight vector $\mathbf{w}_n^{\mathrm{o}}$ as in (3.36).

8. Use (3.31) to calculate $f_n(\mathbf{w}_n^{\mathrm{o}})$.

9. Set $n = n + 1$; if $n \leq N - 1$ go to Step 2; otherwise, go to the next step.

10. Find the optimal value of the end-to-end CIR tap, n_{opt} over all $n \in \mathcal{N}$, i.e., the value of n corresponding to the minimum value of $f_n(\mathbf{w}_n^{\mathrm{o}})$

$$n_{\mathrm{opt}} = \arg \min_{n \in \mathcal{N}} \; f_n(\mathbf{w}_n^{\mathrm{o}})$$

11. Denote the $L \times 1$ optimal beamforming weight vector with $\mathbf{w}_{\mathrm{opt}}$, where for those relay nodes which are associated with the optimal tap n_{opt} of the end-to-end CIR, the corresponding entries in $\mathbf{w}_{\mathrm{opt}}$ are equal to the corresponding entries in $\mathbf{w}_{n_{\mathrm{opt}}}^{\mathrm{o}}$, and the rest of the entries in $\mathbf{w}_{\mathrm{opt}}$ are zero, indicating those relay nodes which do not contribute the optimal tap n_{opt}.

12. For the optimal beamforming weight vector $\mathbf{w}_{\mathrm{opt}}$, calculate the i-th sub-carrier optimal transmission power at TR_1 and TR_2 as in (3.39).

Remark 2: To assess the computational complexity of our proposed power-optimal solution, we note that one first has to calculate the values of z_n and λ_n, for any $n \in \mathcal{N}$. For any n, the proposed technique involves obtaining z_n, as the unique positive root of (3.33) in the interval $\left(\frac{\beta_1+\beta_2}{\|\mathbf{g}_1^{(n)}\|^2}, +\infty\right)$, using a simple Newton-Raphson algorithm. In each iteration of this algorithm, one has to calculate λ as the unique positive root of (3.35) for any given value of z in the interval $\left(\frac{\beta_1+\beta_2}{\|\mathbf{g}_1^{(n)}\|^2}, +\infty\right)$, using a Newton-Raphson algorithm. The Newton-Raphson techniques converge very quickly [102] with the number of iterations in these two methods being insensitive to the problem under consideration [102]. Hence, the main computational burden of the proposed algorithm resides in evaluating the left-hand sides of (3.33) and (3.35). Since the size of $\mathbf{b}_n$ is $L_n \times 1$ and $\mathbf{D}_1^{(n)}$ and $\mathbf{D}_2^{(n)}$ are $L_n \times L_n$ diagonal matrices, the complexity of computing the quadratic terms in (3.33) is $\mathcal{O}(L_n)$. The computational complexity of calculating the left-hand side of (3.35) is also $\mathcal{O}(L_n)$. Thus, the computational complexity of obtaining z_n is $\mathcal{O}(L_n)$, so is the complexity of calculating λ_n. One can easily see that the computational complexity of calculating $\mathbf{w}_n^{\mathrm{o}}$ using (3.36) and (3.37) is also $\mathcal{O}(L_n)$. Consequently, for any value of $n \in \mathcal{N}$, evaluating the cost function $f_n(\mathbf{w}_n^{\mathrm{o}})$ in (3.31) has a computational complexity $\mathcal{O}(L_n)$. Therefore, the worst-case computational complexity of solving (3.38) is $\max_{n\in\mathcal{N}} \mathcal{O}(L_n)$. Since a maximum of L relays can contribute to tap n of the end-to-end CIR (i.e., $L_n \leq L$), we can conclude that the worst-case computational complexity of the proposed algorithm is $\mathcal{O}(L)$. It is worth noting that the maximum number of possible values of n, i.e., $|\mathcal{N}|$ is equal to the number of the relays L. In fact, when no two relays subscribe to the same tap, that is, when each relay is associated with a distinct tap of $h[\cdot]$, then the number of possible values of n, i.e., $|\mathcal{N}|$ is equal to L. If, on the other hand, all relays are associated with the same tap of $h[\cdot]$, then the number of possible values of n is equal to 1, as set $\mathcal{N}$ has only one element. As a result, number of points in the search space of the minimization problem (3.38) ranges from 1 to L.

Remark 3: Note that in this work, the underlying transmission is using a multi-carrier system, while the network studied in [44] is a single-carrier system. Because of this difference, the total power minimization in this work (i.e., (3.13)) requires the optimization of power allocation over $2N$ sub-carriers at the two transceivers, while the total power

minimization problem in [44] is carried out by directly optimizing the transmission powers at the two transceivers (in addition to relay beamforming weight vector). One would expect that the multi-carrier scheme considered here consumes less power, as compared with the single-carrier scheme in [44], due to the additional degrees of freedom offered by the multi-carrier scheme. Nevertheless, comparing the algorithm presented here with the technique derived in [44], one can observe that the optimized powers and the resulting techniques are identical (except for the use of DFT and IDFT in the multi-carrier scheme). Thus, both techniques consume the same amount of power for the same channel realizations and the same required rate thresholds. Indeed, the total power minimization problem for the single-carrier system of [44] is also simplified as the optimization problem (3.32). This is due to the fact that in both systems, *the end-to-end channel is active, meaning that the channel itself is subject to optimal design*[6]. Since in the multi-carrier scheme, the optimal end-to-end channel is frequency-flat, the power loading across subcarriers becomes uniform. In the single-carrier scheme, the optimal end-to-end channel is also frequency-flat. As such, in both systems, the power-optimal relay selection techniques lead to the selection of the same set of the relays, with beamforming weights that are identical in both approaches. *Note however that it was neither obvious nor straightforward to show the equivalence between the two systems.* We had to go through the power allocation optimization presented in this study to obtain this result, thereby showing that in multi-carrier systems the optimized end-to-end channel is indeed frequency-flat. Our analyses and derivations prove that OFDM may not be needed as a means to diagonalize (or equalize) the end-to-end channel. Nevertheless, legacy transceiver systems would still rely on OFDM signaling. Also, to allow the co-existence of this scheme with other OFDM based schemes, orthogonal frequency division multiple access (OFDMA) appears to be a reasonable solution, thereby justifying the use of OFDM in the considered communications scheme.

Remark 4: It is worth mentioning that the scenario of relay-assisted communication with frequency-selective relay-transceiver channels has already been studied in the multi-carrier scheme of [39] and in the single-carrier approach of [20, 21]. Considering a total

[6] Indeed, a relay channel belongs to the class of *active channels*, where the channel behavior can be adjusted for optimal performance. For more information on active channel design, we refer our reader to [104–106].

power minimization problem, the study in [39] led to a two-step iterative algorithm: in the first step, the target subcarrier sum-rates at the two transceivers are fixed, and then, the beamforming weight vectors and transceivers' transmit powers at each subcarrier are obtained in semi-closed forms. In the second step, the optimal values of the target subcarrier sum-rates at the two transceivers are obtained, using a water-filling type of solution, for the beamforming weight vectors and transceivers' transmit powers obtained in the first step. This two-step iterative technique is repeated until convergence is achieved. Unfortunately, this algorithm can quickly trap in a local minimum due to the water-filling nature of the second step. Indeed, those subcarriers which will be assigned zero powers in the water-filling step at any iteration, will not receive any power in the remaining iterations, thus trapping in a suboptimal solution which can be far from the optimal solution.

The investigation in [21] assumed a single-carrier distributed equalization scheme, where the burden of equalization of the end-to-end channel is shared among the relays. In this scheme, each relay employs an FIR filter, while the transceivers resort to a symbol-by-symbol detector, treating ISI as noise. The power minimization problem, in this case, leads to a solution which consists of a two-dimensional search over a grid that covers all possible values of transceiver powers and a second-order cone programming problem over each vertex of this grid. This solution is computationally expensive even for grids with moderate sizes and suffers from the finite resolution of the grid. More importantly, this solution assumes a fixed delay for the end-to-end channel, which appears to be suboptimal [18, 42].

Remark 5: In [38], the problem of jointly optimal design of linear pre-, post-channel equalizers and relay beamforming has been studied using minimization of the total mean squared error (MSE) under a total power budget constraint. This study rigorously proves that the total MSE is minimized when 1) the end to end channel has only one non-zero tap and 2) the pre-channel equalizers (i.e., pre-coding matrices) used at the transmitter front-end of the two transceivers are unitary. The latter condition implies that the single-carrier scheme of [13] (with the identity matrix used as pre-coding matrices) and multi-carrier schemes (with IDFT matrix employed as pre-coding matrices) are two optimal solutions to the power-constrained total MSE minimization approach. In this chapter, considering a multi-carrier scheme (with IDFT and DFT matrices acting as pre- and post-channel

linear block equalizers), we used a different design approach, namely rate-constrained total power minimization technique, to design a two-way relay network. Note however that the results of [38] cannot be used in this study for two reasons: 1) we are herein interested in rate-constrained total power minimization, while the results of [38] hold true for power-constrained total MSE minimization. 2) Here, we are not interested in the design of pre- and post-channel linear block equalizers as they are fixed, rather we are looking for optimal relay beamforming weight and subcarrier power allocation at the two transceivers, while the goal in [38] is the design of jointly optimal linear pre-, post-channel equalizers and relay beamforming weights. Interestingly, the two approaches lead to the same result: the end-to-end channel must has only one non-zero tap. However, in this study, the optimal non-zero tap depends on the minimum required rates, while in [38], the optimal non-zero tap is a function of the total power budget. It is also worth mentioning that the study in [37] assumes linear pre-channel linear block equalizers without any post-channel equalizer and aims to design the power allocation of the two transceiver and relay beamforming weights using a power-constrained total MSE minimization – which is different from our approach in this work. The end result in [37] is a single-carrier, while our scheme here is a multi-carrier technique. Interestingly, the optimal end-to-end channel in [37] is also single-tap, but the power allocation and beamforming weights of [37] is different from what we derived in this chapter.

3.4 Numerical Results

In this section, the performance of the proposed algorithm is numerically evaluated for an asynchronous TWR network. We consider a TWR network consisting of two fixed transceivers which employ the OFDM scheme with N sub-carriers and communicate through L relay nodes. The two transceivers are assumed to be 2 km apart and are fixed at the Cartesian coordinates of $(-1000, 0)$ m and $(1000, 0)$ m. The L relay nodes are randomly distributed, according to a uniform distribution, over a rectangular area of 1 km $\times$ 1 km centered around the middle point, $(0, 0)$ m. The propagation delay τ_l, of the l-th relaying path connecting the two transceivers through the l-th relay is calculated according to the distance of the l-th relay node from each of the transceivers, for $l = 1, \ldots, L$. We assume flat-

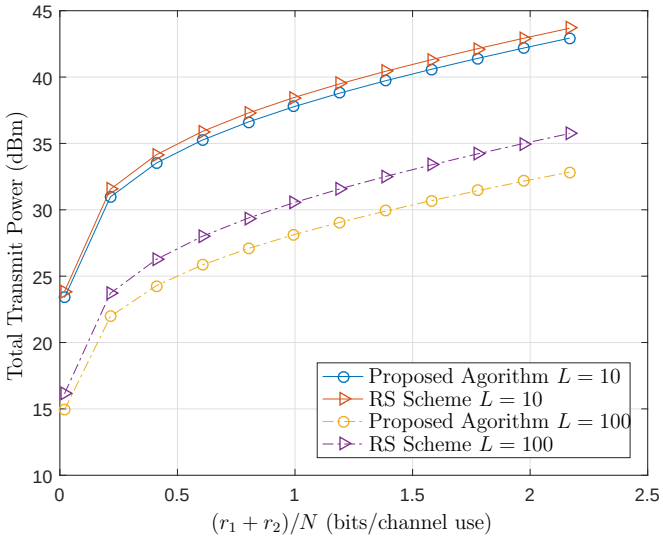

Figure 3.3: The power consumption performance using $N = 1024$.

fading channels between each relay and each transceiver. To model the large scale fading, we adopt the LTE standard with the path loss factor of 3.8 and the shadowing standard deviation of 8 dB. The shadowing is assumed to be independent and identically distributed (i.i.d.) among the nodes. The small-scale Rayleigh fading coefficients are modeled as i.i.d. complex circularly symmetric Gaussian random variables with zero mean and unit-variance. The received noise at the relays and at the transceivers are modeled as zero-mean white Gaussian random variables with variance $\sigma^2 = -174 + 10\log(B) = -104$ dBm, which corresponds to the noise level for 10 MHz transmission bandwidth. The transmission carrier frequency is set to 2.3 GHz. An equal rate threshold is considered at the two transceivers, $r_1 = r_2 = r$.

In Fig. 3.3, the performance of our proposed algorithm is compared with the performance of a simple relay selection (RS) scheme. The RS scheme opts for the best relaying path which results in the minimum transmission power among all relaying paths. On the other hand, in the proposed algorithm, at the optimum, a subset of relays contributing to the optimal tap of the end-to-end CIR is chosen, effectively forming a synchronous relay sub-network, and the rest of the relays will not participate in signal relaying. Fig. 3.3 demonstrates the optimal total transmission power averaged over 100 realizations of the relay locations versus the sum-rate thresholds, with $N = 1024$ sub-carriers. Two TWR networks with $L = 10$ and 100 relay nodes are considered for each method. It can be

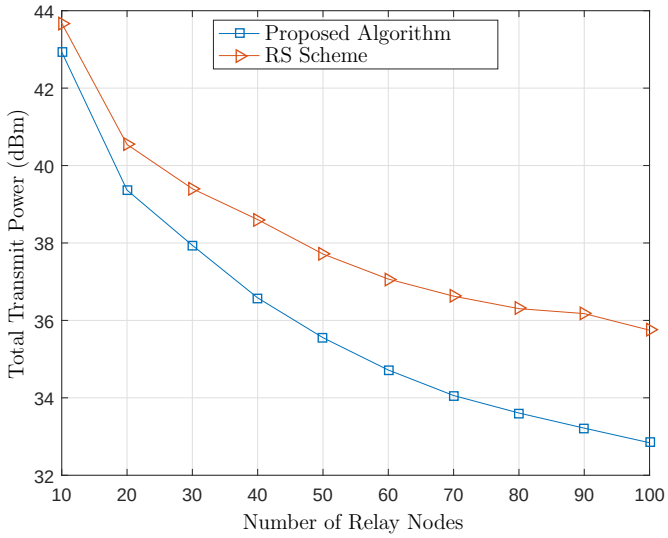

Figure 3.4: The effect of using different number of relay nodes on power consumption

seen from Fig. 3.3 that for the same number of relay nodes, $L = 10$ or 100, our proposed algorithm outperforms the RS scheme in terms of the minimum total transmission power consumed over the network. Furthermore, it follows from Fig. 3.3 that the higher the number of the relay nodes is, the more power saving our algorithm offers, as compared with the RS scheme. For example, at the sum-rate of $(r_1 + r_2)/N = 1$ (bit/channel use), for $L = 10$ relay nodes, the minimum total transmission power obtained by the RS scheme and our proposed algorithm are about 38.5 dBm and 37.8 dBm, respectively, which amounts to about 0.7 dB power saving by our algorithm. However, for $L = 100$ relay nodes, and at the same sum-rate, the minimum total transmission power achieved by the RS scheme and our proposed algorithm are respectively about 30.5 dBm and 28.1 dBm, and thus the power saving of our algorithm is increased to 2.4 dB. This observation can be explained by the fact that the proposed method benefits from spatial diversity of the relays. Moreover, at the optimum, all those relays which contribute to the optimal tap of the end-to-end CIR will be engaged in information exchange between the transceivers, as opposed to the RS scheme, where only one relay (which leads to the minimum transmission power among all relays) is involved in the communication between the transceivers. As a result, the more relay nodes exist in the effective synchronous relay sub-network, the higher degree of diversities can be achieved.

Fig. 3.4 illustrates the relationship between the total transmission power and the num-

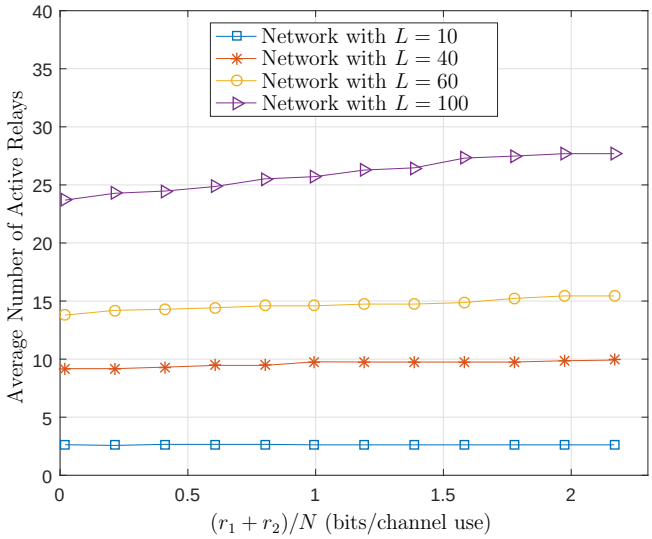

Figure 3.5: A comparison between the number of available relays and the averaged number of active relays versus the sum-rate thresholds.

ber of the relay nodes under the proposed algorithm and the RS scheme. Transceivers use $N = 1024$ sub-carriers, and the equal rate threshold at TR_1 and TR_2 is $r = r_1 = r_2 = 1100$ bits per OFDM symbol. It can be seen from Fig. 3.4 that by increasing the number of relays, our proposed algorithm increasingly outperforms the RS scheme. For example, increasing the number of relays from $L = 50$ to $L = 100$ will increase the power consumption gap between our proposed algorithm and the RS scheme from 2.1 dB and 2.9 dB. Fig. 3.4 can provide insights into the application of the large-scale relay networks, where a large number of relay nodes is used in a distributed fashion. Note that for a TWR network with L relay nodes, typically only a small portion of the relay nodes contributing to the optimal tap of the end-to-end CIR takes part in the communication between the transceivers. To elucidate the aforementioned point, in Fig. 3.5, we compare the average number of active relays in the TWR network versus the sum-rate thresholds for $L = 10, 40, 60$, and 100 relay nodes. As shown in Fig. 3.5, the average number of relay nodes which contribute to the optimal tap of the end-to-end CIR, over all relay location realizations, is much less than the total number the relay nodes, L in the network. In fact, Fig. 3.5 reveals that on average, about 25% to 28% of the relay nodes are active, regardless of the actual number of relay nodes in the network. Moreover, the average number of active relays for a fixed L does not vary considerably with different sum-rate thresholds. For instance, for the TWR network with

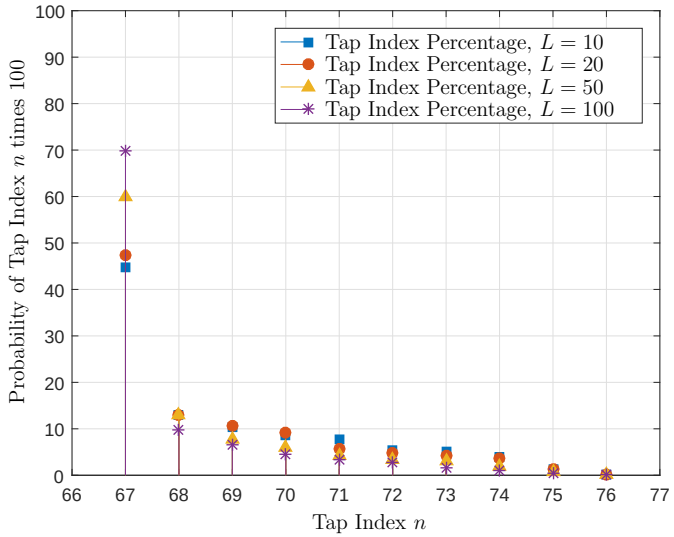

Figure 3.6: Percentage of the scenarios where the n-th channel tap is selected at $r_1 = r_2 = 1100$ bits.

$L = 60$, on average, only 14 to 15 relay nodes actively participate in the data transmission between TR_1 and TR_2, and this average number will approximately remain the same for all sum-rate threshold values considered.

Fig. 3.6 depicts the percentage of the scenarios when the n-th tap of the end-to-end CIR is selected among 1000 realizations. The distribution is plotted for the TWR network with $L = 10,\ 20,\ 50$ and 100 relay nodes. The rate threshold is $r_1 = r_2 = 1100$ bits per OFDM symbol. Note that those relays which contribute to the 67-th tap of the end-to-end CIR, cause the shortest relaying delay between the transceivers. In contrast, those relays which contribute to the last tap of the end-to-end CIR are the farthest away from the transceivers. It can be seen from Fig. 3.6 that the 67-th tap of the end-to-end CIR has the highest chance to be the optimal tap. This result substantiates the intuitive judgement that the shortest relaying path has the highest chance of being selected among all other relaying paths. Moreover, as shown in Fig. 3.6, by increasing the number of relays, the chance of the 67-th tap being selected will increase. One reason for this phenomenon is because of the channel hardening effect as the number of relay nodes increases. However, for the TWR networks with a smaller number of relay nodes such as $L = 10$ and $L = 20$, the overall percentage of times when the end-to-end CIR taps other than Tap 67 are selected, outweighs the percentage of times when the shortest path, i.e., the 67-th tap, is selected.

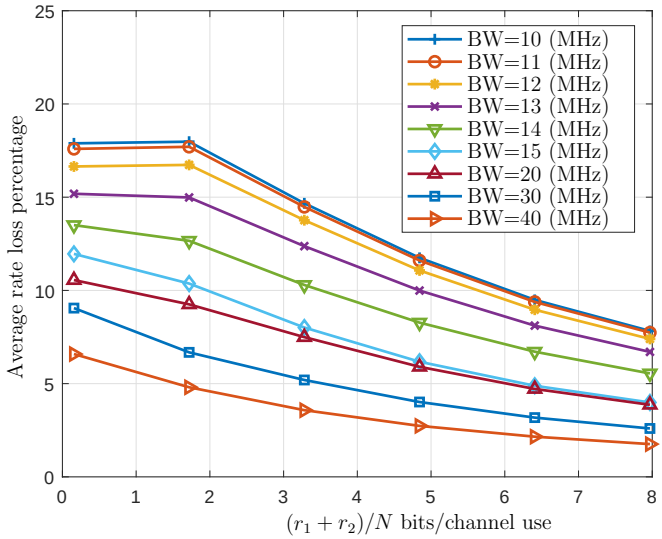

Figure 3.7: Average rate loss for different values of system bandwidth versus $(r_1 + r2)/N$ for $N = 128$.

For example, in the case of $L = 10$, the chance of the 67-th tap index being selected is only 44%, while the overall chance of the other taps being chosen is 56%. This means that, counter to the intuition that the relays closest to the LoS should always be selected, for sparse TWR networks, with a relatively small number of relay nodes, the chance that such relays would be optimal is less than 50%.

In our last experiment, we examine the effect of band-limiting transmit and receive filters on the proposed solution. In our model derivation, we assumed that those filters have infinite bandwidths. While such an assumption often appears in the literature, we understand that finite-bandwidth transmit and receive filters would lead to Gibbs phenomena, which could result in relays having minor effects on taps other than the main tap they are contributing to. We now show through numerical simulations how this phenomenon affects the performance of the proposed method. Fig. 3.7 shows the percentage of the average rate loss for different bandwidths of the system (dictated by the bandlimiting filters) for $L = 20$ and $N = 128$ and based on a communication bandwidth of 10 MHz. As can be seen from this figure with 10% guard band (bandwidth of 11 MHz), the loss is only 8% at high rate rates. As the system bandwidth is further increased, this loss is further reduced. In an ideal situation, where the bandwidth of the system is infinity, this loss is 0, as shown by our analytical derivation in this study. The highest value of rate loss percentage is about

17% for a system bandwidth of 11-12 MHz. Such a performance loss can be compensated for, in the proposed method, by over-constraining the rates by the amount of rate loss. Our numerical experiments show that with 10% guard band, such over-constraining would result in 0.56 dB to 1.86 dB increase in total power consumption for the range of sum-rates shown in Fig. 3.7 . This is a price that has to be paid in order to take advantage of the computational simplicity of the proposed solution.

Chapter 4

Joint Power Allocation and Distributed Equalization Design

In this chapter, we consider the problem of joint power allocation and FIR filter design for FF relays in a multi-carrier two-way relay network, where two OFDM-based transceivers communicate with each other through multiple relays employed FF relaying schemes. We formulate a total transmit power minimization problem subject to the quality of service constraints imposed on the transceivers' data rates. Such an objective ensures a power-efficient network in which for any required data rates, the lowest possible power is consumed in the whole network. We propose two methods to tackle the non-convex optimization of FF relaying design and power allocation for the aforementioned total transmit power minimization problem. To evaluate the performance of this method, we have made a complexity analysis for the second method. Furthermore, relaxing the original optimization problem, we obtain a lower bound which provides a benchmark for assessing the performances of our proposed methods.

The rest of this chapter is organized as follows, System description, channel model and signal model are provided in Section 4.1. In Section 4.2, we define the optimization problem and develop the derivation of a semi-closed-form technique for this problem. Some important remarks are provided in Section 4.3. In Section 4.4, the numerical results are presented to conclude the chapter.

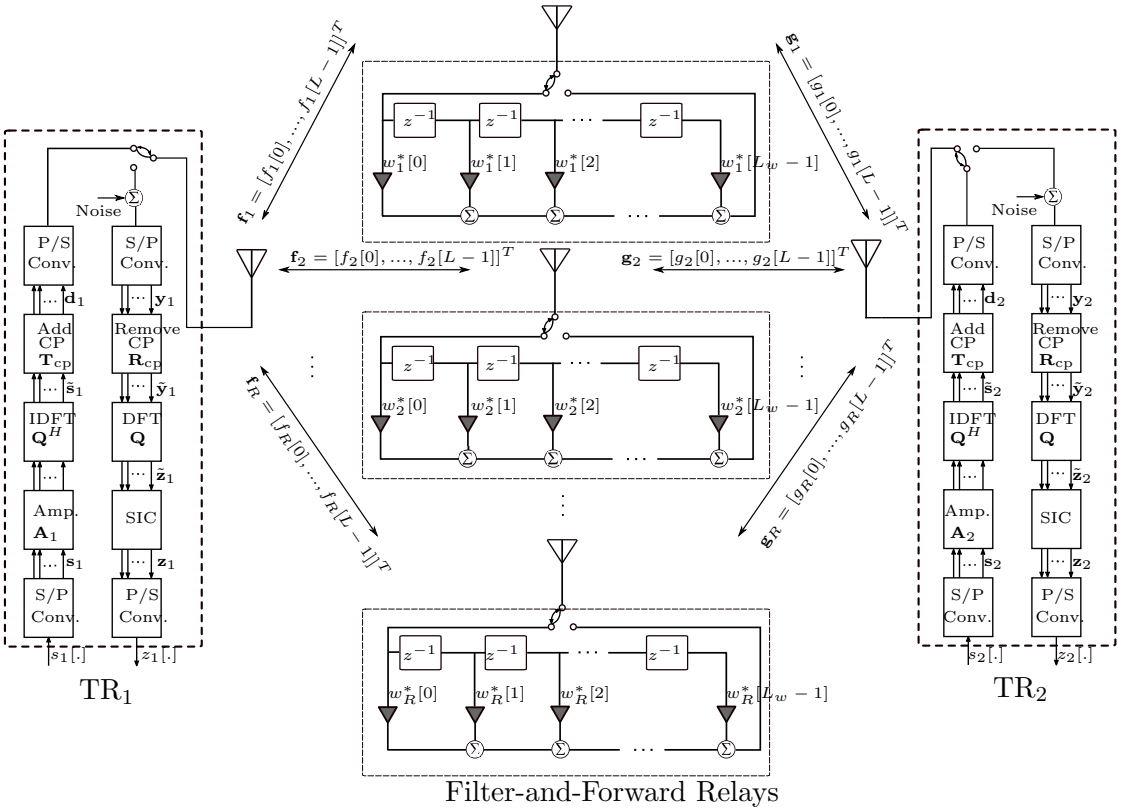

Figure 4.1: Illustration of the OFDM-based two-way FF relaying network with frequency-selective channels.

4.1 Preliminaries

We consider a TWR network which consists of two OFDM-based transceivers, denoted as TR_1 and TR_2, and R relay nodes, as shown in Fig.4.1. Each relay is equipped with an FIR filter, thereby implementing a FF relaying protocol in the TWR network. The information exchange between the transceivers is carried out in two time slots. In the first time slot, both transceivers transmit their information symbols towards the relay nodes. In the second time slot, the relay nodes simultaneously broadcast filtered versions of their received signals to the transceivers. We assume that the channel between each relay and each transceiver is *frequency-selective*. As a result, at high data rates, the transmission is likely to suffer from ISI. To suppress ISI, the system uses OFDM technology at the transceivers and FF relaying strategy at the relays, thereby performing equalization in a distributed manner. Perfect knowledge of the CSI is assumed at all nodes. We assume channel reciprocity between the relays and the transceivers. That is, the CIR for the link from any transceiver to any relay

is the same as the CIR for the link from the same relay to the same transceiver.

4.1.1 Channel Model

The impulse response of the frequency-selective channel between TR_1 (TR_2) and each relay can be modeled as a tapped delay line with L taps. Each of these channels has a few zero taps due to the delay of the signal propagation along the shortest path between the corresponding end nodes. For each transceiver-relay link, the number of these zero taps depends on the distance between the relay and the transceiver. In other words, these preceding zero taps account for the minimum delay required for the wave to travel between the transceiver and the relay. Let L_0 denote the smallest possible number of such zero taps among all relay-transceiver channel impulse responses.

Let $f_r[l]$ ($g_r[l]$) denote the l-th tap[1] of the impulse response $f_r[\cdot]$ ($g_r[\cdot]$) of the frequency-selective channel between the r-th relay and TR_1 (TR_2), where $l = 0, 1, \ldots, L-1$, while $\mathbf{f}_r \triangleq [f_r[0] \quad f_r[1] \quad \ldots \quad f_r[L-1]]^T$ ($\mathbf{g}_r \triangleq [g_r[0] \quad g_r[1] \quad \ldots. \quad g_r[L-1]]^T$) represents the vector of CIR taps for the link between the r-th relay and TR_1 (TR_2). We use $w_r[n]$ to signify the n-th tap of the FIR filter employed at the r-th relay, for $n = 0, 1, \ldots, L_w - 1$, where L_w is the maximum length of the FIR filter at the relay nodes. We define $\mathbf{w}_r \triangleq [w_r[0] \ w_r[1] \ \ldots \ w_r[L_w - 1]]^T$ as the $L_w \times 1$ vector of the filter coefficients at the r-th relay. Using the assumption of the channel reciprocity between each relay and each transceiver, we can now model the n-th tap of the end-to-end CIR, denoted as $h[\cdot]$, as follows

$$h[n] = \sum_{r=1}^{R} f_r[n] \star w_r^*[n] \star g_r[n], \qquad \text{for } n = 0, 1, ..., L_h - 1 \tag{4.1}$$

where $\star$ stands for the discrete-time linear convolution, and $L_h - 1$ is the index of the last non-zero tap[2] of the end-to-end CIR of $h[\cdot]$ with $L_h = 2L + L_w - 2$. Based on earlier discussions, the first L_0 taps of the end-to-end CIR are zero. We define

$$\tilde{h}_r[n] \triangleq f_r[n] \star g_r[n], \text{ for } n = 0, 1, \ldots, L_{\tilde{h}} - 1, r = 1, \ldots, R \tag{4.2}$$

[1]Note that some taps can have zero values.

[2]Note that as we assumed the first L_0 taps of $h[\cdot]$ are zero, the delay spread of $h[\cdot]$ will be equal to $L_h - L_0$.

where $L_{\tilde{h}} \triangleq 2L-1$. Based on (4.1) and (4.2), the n-th tap of the end-to-end CIR corresponding to the r-th relaying path, $h_r[n]$, can be expressed as

$$h_r[n] \triangleq \tilde{h}_r[n] \star w_r^*[n] \quad \text{for } n = 0, 1, ..., L_h - 1. \tag{4.3}$$

We can rewrite the linear convolution in (4.3) in vector form as

$$\mathbf{h}_r(\mathbf{w}_r) = \mathbf{B}_r \mathbf{w}_r^* \tag{4.4}$$

where the $L_h \times 1$ vector of the end-to-end CIR for the r-th relay can be defined as $\mathbf{h}_r(\mathbf{w}_r) \triangleq [h_r[0] \;\; h_r[1] \;\; \dots \;\; h_r[L_h-1]]^T$, and matrix $\mathbf{B}_r \in \mathbb{C}^{L_h \times L_w}$ has a Toeplitz structure with the first column and the first row given by vectors $[\tilde{h}_r[0] \;\; \tilde{h}_r[1] \;\; \cdots \;\; \tilde{h}_r[L_{\tilde{h}}-1] \;\; \mathbf{0}_{1\times(L_h-L_{\tilde{h}})}]^T$ and $[\tilde{h}_r[0] \;\; \mathbf{0}_{1\times(L_w-1)}]^T$, respectively.

Using (4.1) and (4.4), we represent the vector of the end-to-end CIR as

$$\mathbf{h}(\mathbf{w}) = \mathbf{B}\mathbf{w}^* \tag{4.5}$$

where $\mathbf{h}(\mathbf{w}) \triangleq [h[0] \;\; h[1] \;\; \dots \;\; h[L_h-1]]^T$, $\mathbf{B} \triangleq [\mathbf{B}_1 \;\; \mathbf{B}_2 \;\; \dots \;\; \mathbf{B}_R] \in \mathbb{C}^{L_h \times RL_w}$, and $\mathbf{w} \triangleq [\mathbf{w}_1^T \;\; \mathbf{w}_2^T \;\; \dots \;\; \mathbf{w}_R^T]^T \in \mathbb{C}^{RL_w \times 1}$. The channel model in (4.5) shows a linear relationship between the end-to-end CIR and FIR filter coefficients at the relays. It is worth mentioning that as the first L_0 taps of $\mathbf{h}(\mathbf{w})$ are zero, the first L_0 rows of $\mathbf{B}$ are zero.

4.1.2 Signal Model

The structure of an OFDM-based transceiver with N sub-carriers is shown in Fig. 4.1. The serial-to-parallel and the parallel-to-serial conversion blocks are denoted as S/P and P/S, respectively, the $N \times N$ DFT matrix and the inverse DFT (IDFT) matrix are represented by $\mathbf{Q}$ and $\mathbf{Q}^H$, respectively, and the CP insertion and the CP deletion matrices are signified by $\mathbf{T}_{\text{cp}}$ and $\mathbf{R}_{\text{cp}}$, respectively. We assume that the information symbols $s_1[\cdot]$ and $s_2[\cdot]$, which are transmitted respectively by TR_1 and TR_2, have unit power over each sub-carrier, i.e., $E\{|s_1[i]|^2\} = E\{|s_2[i]|^2\} = 1$, for $i \in \{1, \dots, N\}$. With P_{ij} denoting the transmit power which is allocated to the i-th sub-carrier at TR_j, $j \in \{1, 2\}$ and $i \in \{1, \dots, N\}$, the power-adjusting matrix at the j-th transceiver is defined as $\mathbf{A}_j \triangleq \text{diag}\{\sqrt{P_{ij}}\}_{i=1}^N$ for $j = 1, 2$. At

the output of the S/P converter on the transmitter side of TR_j, the obtained $N \times 1$ vector is denoted as $\mathbf{s}_j = [s_j[1] \;\; s_j[2] \;\; \ldots \;\; s_j[N]]^T$, for $j \in \{1, 2\}$. After power amplification, the resultant signal vector at the output of IDFT block, $\tilde{\mathbf{s}}_j$, is given as

$$\tilde{\mathbf{s}}_j = [\tilde{s}_j[1] \;\; \tilde{s}_j[2] \;\; \ldots \;\; \tilde{s}_j[N]]^T \triangleq \mathbf{Q}^H \mathbf{A}_j \mathbf{s}_j, \qquad \text{for} \qquad j \in \{1, 2\}. \tag{4.6}$$

In order to remove the inter-block-interference caused by the frequency-selectivity of the end-to-end channel at the receiving sides, a cyclic prefix of length L_{cp} is added to the output signal of the IDFT block, $\tilde{\mathbf{s}}_j$. Therefore, the cyclic prefix insertion matrix is defined as $\mathbf{T}_{\mathrm{cp}} \triangleq [\bar{\mathbf{I}}_N^T \;\; \mathbf{I}_N^T]^T$, where $\bar{\mathbf{I}}_N$ is defined as the last L_{cp} rows of the identity matrix $\mathbf{I}_N$. Note that the length L_{cp} of this cyclic prefix L_{cp} must be equal or greater than the delay spread of the end-to-end CIR $h[\cdot]$. The value of delay spread is equal to $L_h - L_0$ at the worst case.[3] The OFDM signal vector at the input of the P/S conversion is given as $\mathbf{d}_j = [\tilde{s}_j[N - L_{\mathrm{cp}} + 1] \;\; \ldots \;\; \tilde{s}_j[N] \;\; \tilde{s}_j[1] \;\; \tilde{s}_j[2] \;\; \ldots \;\; \tilde{s}_j[N]]^T$. At TR_j, the signal stream, which is composed of the concatenation of the serial version of $\mathbf{d}_j$'s, is denoted as $d_j[\cdot]$. At time n, the signal received at the r-th relay, $x_r[n]$, is given by

$$x_r[n] = \sum_{l=0}^{L-1} f_r[l] d_1[n-l] + \sum_{l=0}^{L-1} g_r[l] d_2[n-l] + \nu_r[n] \tag{4.7}$$

where $\nu_r[n]$ is the additive zero-mean white complex Gaussian noise with unit variance at the r-th relay at time n. At the r-th relay, the received signal $x_r[\cdot]$ is first filtered at the OFDM transmission chip rate, and then, is forwarded to the transceivers. After applying the FIR filtering, the signal $t_r[n]$ transmitted by the r-th relay at time n is given by

$$t_r[n] = \sum_{l=0}^{L_w-1} w_r^*[l] x_r[n-l]. \tag{4.8}$$

At the receiver side, at time n, the signal received by TR_1 and TR_2 can be expressed as

$$y_1[n] = \sum_{r=1}^{R} \sum_{l=0}^{L-1} f_r[l] t_r[n-l] + \zeta_1[n] \tag{4.9}$$

[3]Indeed, the delay spread is dictated not only by the length L_w of the FIR filters, but also by the values of the relays' FIR filter taps. These taps can be chosen such that the delay spread of the end-to-end CIR is smaller than $L_h - L_0$. In fact, in one of our proposed designs for the relays' FIR filters, this delay spread will be much smaller than $L_h - L_0$.

$$y_2[n] = \sum_{r=1}^{R} \sum_{l=0}^{L-1} g_r[l] t_r[n-l] + \zeta_2[n] \tag{4.10}$$

where $\zeta_j[\cdot]$ is the zero-mean, unit-variance Gaussian noise received at TR_j at time n, for $j = 1, 2$. The equivalent noise received at TR_1 and TR_2, denoted as $\eta_1[n]$ and $\eta_2[n]$, respectively, can be written as

$$\eta_1[n] \triangleq \sum_{r=1}^{R} \sum_{l=0}^{L-1} \sum_{l'=0}^{L_w-1} f_r[l] w_r^*[l'] \nu_r[n-l'-l] + \zeta_1[n] \tag{4.11}$$

$$\eta_2[n] \triangleq \sum_{r=1}^{R} \sum_{l=0}^{L-1} \sum_{l'=0}^{L_w-1} g_r[l] w_r^*[l'] \nu_r[n-l'-l] + \zeta_2[n]. \tag{4.12}$$

Let $\mathbf{y}_j \triangleq [y_j[0] \;\; y_j[1] \;\; \ldots \;\; y_j[M-1]]^T$ denote the $M \times 1$ received signal vector at TR_j, where $M \triangleq L_{\mathrm{cp}} + N$. The $N \times M$ cyclic prefix deletion matrix $\mathbf{R}_{\mathrm{cp}} \triangleq [\mathbf{0}_{N \times L_{\mathrm{cp}}} \;\; \mathbf{I}_N]$ removes the cyclic prefix from $\mathbf{y}_j$, and yields the $N \times 1$ vector $\tilde{\mathbf{y}}_j$ at TR_j, for $j = 1, 2$. At the output of the DFT block, the $N \times 1$ vectors $\tilde{\mathbf{z}}_1$ and $\tilde{\mathbf{z}}_2$ at TR_1 and TR_2 are respectively given as

$$\tilde{\mathbf{z}}_1 = \mathbf{A}_1 \mathbf{H}_{11}(\mathbf{w}) \mathbf{s}_1 + \mathbf{A}_2 \mathbf{H}_{21}(\mathbf{w}) \mathbf{s}_2 + \mathbf{Q} \mathbf{R}_{\mathrm{cp}} \boldsymbol{\eta_1} \tag{4.13}$$

$$\tilde{\mathbf{z}}_2 = \mathbf{A}_2 \mathbf{H}_{22}(\mathbf{w}) \mathbf{s}_2 + \mathbf{A}_1 \mathbf{H}_{12}(\mathbf{w}) \mathbf{s}_1 + \mathbf{Q} \mathbf{R}_{\mathrm{cp}} \boldsymbol{\eta_2} \tag{4.14}$$

where $\boldsymbol{\eta}_j \triangleq [\eta_j[0] \;\; \eta_j[2] \;\; \ldots \;\; \eta_j[M-1]]^T$ is defined as the equivalent $M \times 1$ noise vector received at TR_j, the (m,n)-th element of the DFT matrix is defined as $\mathbf{Q}(m,n) \triangleq N^{-\frac{1}{2}} \exp(\frac{-j2\pi(m-1)(n-1)}{N})$, and $\mathbf{H}_{12}(\mathbf{w}) = \mathbf{H}_{21}(\mathbf{w}) \triangleq N^{\frac{1}{2}} \mathrm{diag}\{\mathbf{Q}\bar{\mathbf{h}}(\mathbf{w})\}$, where $\bar{\mathbf{h}}(\mathbf{w})$ is the $N \times 1$ zero-padded version end-to-end CIR vector defined as $\bar{\mathbf{h}}(\mathbf{w}) \triangleq \left[\mathbf{h}^T(\mathbf{w}) \;\; \mathbf{0}_{1 \times N - L_h}\right]^T$. Also, for $j = 1, 2$, we define $\mathbf{H}_{jj}(\mathbf{w}) \triangleq N^{\frac{1}{2}} \mathrm{diag}\{\mathbf{Q}\tilde{\mathbf{h}}_{jj}(\mathbf{w})\}$, and $\tilde{\mathbf{h}}_{jj}(\mathbf{w})$ is an $N \times 1$ vector of the CIR corresponding to the link from TR_j to the relays and back to TR_j. Note that to ensure that inter-block interference exist only between two adjacent blocks, we must choose the number of sub-carriers N larger that the delay spread of all CIRs. Note that the diagonal matrices of $\mathbf{H}_{ij}(\mathbf{w})$, for $i, j \in \{1, 2\}$, are used in (4.13) and (4.14) due to the fact that the OFDM scheme at the transceivers equalizes the end-to-end channel. Indeed, the diagonal entries of $\mathbf{H}_{12}(\mathbf{w})(\mathbf{H}_{21}(\mathbf{w}))$ are the frequency response of the end-to-end CIR at multiple integers of $\frac{1}{N}$. The first terms in the right hand side of (4.13) and (4.14) are the self-interference terms received at TR_1 and TR_2, respectively. Having the perfect

knowledge of CSI, the transceivers remove their own self-interference term from the received signal, once they both compute the relay FIR filters. As a result, at the output of the self-interference cancellation block, the so-obtained $N \times 1$ signal vector $\mathbf{z}_1$ ($\mathbf{z}_2$) at TR_1 (TR_2) can be expressed as

$$\mathbf{z}_1 = \mathbf{A}_2\mathbf{H}_{21}(\mathbf{w})\mathbf{s}_2 + \mathbf{Q}\mathbf{R}_{\mathrm{cp}}\boldsymbol{\eta}_1 \tag{4.15}$$

$$\mathbf{z}_2 = \mathbf{A}_1\mathbf{H}_{12}(\mathbf{w})\mathbf{s}_1 + \mathbf{Q}\mathbf{R}_{\mathrm{cp}}\boldsymbol{\eta}_2 \tag{4.16}$$

The self-interference-free data models in (4.15) and (4.16) can now be used to derive the expression of the SNR at the two transceivers.

4.1.3 Total Transmit Power Expression

The objective of this work is to minimize the total transmit power subject to QoS constraints on the transceivers' rates in the system described in the previous section. Aiming to solve this minimization problem, we need to express the total transmit power and the transceivers' achievable sum-rate in terms of the design parameters. The total transmit power is equal to the average transmit power over all the OFDM sub-carriers at both transceivers plus the total average transmit power at the relays. Let $\mathbf{p}_j = [P_{1j} \;\; P_{2j} \;\; \ldots \;\; P_{Nj}]^T$ denote the $N \times 1$ transmit power vector allocated to the N sub-carriers at TR_j, for $j = \{1, 2\}$. Using (4.8), we can express the total average transmit power at the relays as[4]

$$P_r = \mathbf{w}^H(P_1\mathbf{D}_1 + P_2\mathbf{D}_2 + \mathbf{I}_{RL_w})\mathbf{w} \tag{4.17}$$

where $\mathbf{I}_{RL_w}$ is the $RL_w \times RL_w$ identity matrix, $P_j \triangleq \frac{\mathbf{1}^T\mathbf{p}_j}{N}$ denotes the average transmit power at TR_j, for $j \in \{1, 2\}$, and matrix $\mathbf{D}_j \in \mathbb{C}^{RL_w \times RL_w}$ is defined, for $j \in \{1, 2\}$, as

$$\mathbf{D}_j \triangleq \boldsymbol{\Pi}^H\left[\sum_{r=1}^{R}(\mathbf{I}_{L_w} \otimes \mathrm{diag}\{\mathbf{e}_{R,r}\})\mathbf{K}_j\mathbf{K}_j^H(\mathbf{I}_{L_w} \otimes \mathrm{diag}\{\mathbf{e}_{R,r}\})^H\right]\boldsymbol{\Pi}. \tag{4.18}$$

Here, $\mathbf{e}_{R,r}$ is the r-th column of the identity matrix $\mathbf{I}_R$, the $(RL_w) \times (L + L_w - 1)$ matrix $\mathbf{K}_j$ is defined as $\mathbf{K}_j \triangleq [\tilde{\mathbf{K}}_{j,0}^T \;\; \tilde{\mathbf{K}}_{j,1}^T \;\; \ldots \;\; \tilde{\mathbf{K}}_{j,L_w-1}^T]^T$, for $j = 1, 2$, where the following definitions

[4]Considering the FF relaying scheme shown in Fig. 4.1, the authors of [21] derive the expression of the average total transmit power at the relays in terms of $\mathbf{w}$ and the total transceivers' transmit powers P_1 and P_2. The expression in (4.17) is straightforwardly obtained from [21] using the definition of $\mathbf{w}$ in this study.

are used $\tilde{\mathbf{K}}_{j,l} \triangleq [\mathbf{0}_{R\times l} \quad \mathbf{F}_j \quad \mathbf{0}_{R\times(L_w-1-l)}]$, for $l = 0, ..., L_w - 1$, $\mathbf{F}_1 \triangleq [\mathbf{f}_1 \ \mathbf{f}_2 \ \dots \ \mathbf{f}_R]^T$, $\mathbf{F}_2 \triangleq [\mathbf{g}_1 \ \mathbf{g}_2 \ \dots \ \mathbf{g}_R]^T$. Also the $RL_w \times RL_w$ permutation matrix $\mathbf{\Pi}$ is defined as

$$\mathbf{\Pi} \triangleq [\mathbf{\Pi}_1^T \ \mathbf{\Pi}_2^T \ \dots \ \mathbf{\Pi}_{L_w}^T]^T. \tag{4.19}$$

Here, $\mathbf{\Pi}_l \triangleq \mathbf{I}_R \otimes \mathbf{e}_{L_w,l}^T$, where $\otimes$ denotes the Kronecker product operation, and $\mathbf{e}_{L_w,l}$ is the l-th columns of the identity matrix $\mathbf{I}_{L_w}$. Using (4.17), we express the total transmit power in the TWR network as

$$P_T(\mathbf{p}_1, \mathbf{p}_2, \mathbf{w}) = \sum_{j=1}^{2} \frac{\mathbf{1}^T \mathbf{p}_j}{N} \delta_j(\mathbf{w}) + \mathbf{w}^H \mathbf{w} \tag{4.20}$$

where we define $\delta_j(\mathbf{w}) \triangleq 1 + \mathbf{w}^H \mathbf{D}_j \mathbf{w}$. The total transmit power expressed in (4.20) serves as the objective function is our design optimization.

4.1.4 Sum-Rate Expressions

The achievable sum-rate over N sub-carriers at TR_1 and TR_2, respectively denoted as $R_1(\mathbf{p}_2, \mathbf{w})$ and $R_2(\mathbf{p}_1, \mathbf{w})$, can be given by[5]

$$R_j(\mathbf{p}_{\bar{j}}, \mathbf{w}) = \sum_{i=1}^{N} \log_2(1 + \mathrm{SNR}_{ij}) \tag{4.21}$$

where $\bar{j} = 2$ when $j = 1$, and $\bar{j} = 1$ when $j = 2$. and SNR_{ij} signifies the SNRs over the i-th sub-carrier received at TR_j, for $j = 1, 2$, and $i = 1, 2, \dots, N$. Let P_{ij}^{s} denote the average power of the signal component received at TR_j, over the i-th sub-carrier, for $j = 1, 2$, and $i = 1, 2, \dots, N$. At TR_1, using (4.15), we obtain P_{i1}^{s} as

$$\begin{aligned} P_{i1}^{\mathrm{s}} &= E\left\{ |[\mathbf{A}_2]_{ii} \, [\mathrm{diag}\{N^{\frac{1}{2}} \mathbf{Q}\bar{\mathbf{h}}(\mathbf{w})\}]_{ii} \, s_2[i]|^2 \right\} \\ &= N P_{i2} E\left\{ |s_2[i]|^2 \right\} \bar{\mathbf{h}}^H(\mathbf{w}) \mathbf{q}_i \mathbf{q}_i^H \bar{\mathbf{h}}(\mathbf{w}) \\ &= N P_{i2} \left| \mathbf{q}_i^H \bar{\mathbf{h}}(\mathbf{w}) \right|^2 \end{aligned} \tag{4.22}$$

where $\mathbf{q}_i = N^{-\frac{1}{2}}[1 \ \exp(\frac{j2\pi(i-1)}{N}) \ \dots \ \exp(\frac{j2\pi(i-1)(N-1)}{N})]^T$ is the i-th column of the IDFT matrix $\mathbf{Q}^H$, and the operator $[\cdot]_{ii}$ stands for the i-th diagonal entry of a matrix. Similarly,

[5]Note that in (4.21), we have ignored the pre-log factor needed to normalize the rate by the number of channel uses.

at TR_2, P_{i2}^{s} is given as

$$P_{i2}^{\mathrm{s}} = P_{i1} N |\mathbf{q}_i^H \bar{\mathbf{h}}(\mathbf{w})|^2. \tag{4.23}$$

Note that $N|\mathbf{q}_i^H \bar{\mathbf{h}}(\mathbf{w})|^2$ is the magnitude response of the end-to-end CIR at the i-th subcarrier. Let P_j^{n} denote the average noise power measured at TR_j's receiver, for $j = 1, 2$. It is derived as [21]

$$P_j^{\mathrm{n}} = \mathbf{w}^H \mathbf{D}_j \mathbf{w} + 1 = \delta_j(\mathbf{w}) \qquad \text{for } \; j = 1, 2. \tag{4.24}$$

Note that CP removal and DFT processing will not affect P_j^{n}, hence, we can use (4.24) as the expression for the received noise power at TR_j for the i-th sub-carrier, for all i. Using (4.22)-(4.24), we can write the SNR expressions, SNR_{i1} and SNR_{i2}, at the ith subcarrier of TR_1 and TR_2, respectively as

$$\mathrm{SNR}_{ij} = \frac{N P_{i\bar{j}} |\mathbf{q}_i^H \bar{\mathbf{h}}(\mathbf{w})|^2}{\delta_j(\mathbf{w})} \qquad \text{for } \; j = 1, 2. \tag{4.25}$$

4.2 Optimization Problem

We consider the joint optimization of power allocation and FF relays' FIR filter design over a TWR network with a pair of transceivers and multiple FF relay nodes. Our goal is to minimize the total transmit power in (4.20) while maintaining the QoS, in terms of the rates $R_1(\mathbf{p}_2, \mathbf{w})$ and $R_2(\mathbf{p}_1, \mathbf{w})$, above r_1 and r_2 at TR_1 and TR_2, respectively. This joint optimization problem is formulated as

$$\begin{aligned} \min_{\mathbf{w}} \min_{\substack{\mathbf{p}_1 \succeq 0 \\ \mathbf{p}_2 \succeq 0}} \quad & \sum_{j=1}^{2} \frac{\mathbf{1}^T \mathbf{p}_j}{N} \delta_j(\mathbf{w}) + \mathbf{w}^H \mathbf{w} \\ \text{subject to} \quad & \sum_{i=1}^{N} \log_2(1 + \mathrm{SNR}_{ij}) \geq r_j, \text{ for } j = 1, 2 \end{aligned} \tag{4.26}$$

Without loss of optimality, the equality constraints in (4.26) can be replaced with the equality[6]. As a result, the optimization problem in (4.26) can be written as

$$\begin{aligned} \min_{\mathbf{w}} \min_{\substack{\mathbf{p}_1 \succeq 0 \\ \mathbf{p}_2 \succeq 0}} \quad & \sum_{j=1}^{2} \frac{\mathbf{1}^T \mathbf{p}_j}{N} \delta_j(\mathbf{w}) + \mathbf{w}^H \mathbf{w} \\ \text{subject to} \quad & \sum_{i=1}^{N} \log_2(1 + \mathrm{SNR}_{ij}) = r_j, \quad \text{for } j = 1, 2 \end{aligned} \tag{4.27}$$

In the next subsection, we first present a gradient steepest descent based solution to (4.27), which can be used to obtain at least a locally optimal point. The performance of such a method, however, depends on the initial point. As such, in the following subsection, we present a computationally efficient method to obtain a reasonably good initial point for a gradient steepest descent based solution (such as the quasi-Newton algorithm). The latter method is also introduced as yet another suboptimal solution to the problem at hand.

4.2.1 Gradient Steepest Descent Based Method

To develop a gradient steepest descent based technique to tackle (4.27), we first solve the inner minimization for any given $\mathbf{w}$, thereby obtaining a cost function which depends only on $\mathbf{w}$, and then minimize this cost function to obtain a locally optimal value for $\mathbf{w}$ by way of gradient steepest descent approach. For any given $\mathbf{w}$, the inner minimization in (4.27) can be decomposed into the following two optimization problems:

$$\min_{\mathbf{p}_j \succeq 0} \frac{\mathbf{1}^T \mathbf{p}_j}{N} \delta_j(\mathbf{w}), \qquad \text{s.t.} \quad \sum_{i=1}^{N} \log_2\left(1 + \frac{N P_{ij} |\mathbf{q}_i^H \bar{\mathbf{h}}(\mathbf{w})|^2}{\delta_{\bar{j}}(\mathbf{w})}\right) = r_{\bar{j}} \tag{4.28}$$

for $j = 1, 2$, where $\bar{j} = 2$ when $j = 1$, and $\bar{j} = 1$ when $j = 2$. It can be shown that a water-filling solution can be used to express the optimal value of P_{ij} in terms of $\mathbf{w}$, denoted as $P_{ij}^{\mathrm{o}}(\mathbf{w})$, as [7]

[6]The reason is that if $R_1(\mathbf{p}_2, \mathbf{w}) > r_1$ and/or $R_2(\mathbf{p}_1, \mathbf{w}) > r_2$, one can decrease one of the entries of the optimal power vectors of $\mathbf{p}_1$ and/or $\mathbf{p}_2$ such that the inequalities still hold true. This, however, means that the new power vectors have smaller sum of entries compared to the original optimal power vectors, and thus, result in a smaller objective function, which is a contradiction.

[7]See Appendix B.1 for the derivation of (4.29).

$$P_{ij}^{\mathrm{o}}(\mathbf{w}) = \left[\frac{N\gamma_j(\mathbf{w})}{(\ln 2)\delta_j(\mathbf{w})} - \frac{\delta_{\bar{j}}(\mathbf{w})}{N|\mathbf{q}_i^H\bar{\mathbf{h}}(\mathbf{w})|^2}\right]^+ \tag{4.29}$$

where $\gamma_j(\mathbf{w})$ is the Lagrange multiplier for the minimization in (4.28) and is obtained, for any given $\mathbf{w}$, as the solution to the following equation for z:

$$\sum_{i=1}^{N}\log_2\left(1+\left[\frac{N^2|\mathbf{q}_i^H\bar{\mathbf{h}}(\mathbf{w})|^2 z}{\ln 2\delta_j(\mathbf{w})\delta_{\bar{j}}(\mathbf{w})}-1\right]^+\right) = r_{\bar{j}} \tag{4.30}$$

where we define $[x]^+ = \max(x, 0)$. For given $\mathbf{w}$, we now define the optimal value of $\mathbf{p}_j$ as $\mathbf{p}_j^{\mathrm{o}}(\mathbf{w}) \triangleq [P_{1j}^{\mathrm{o}}(\mathbf{w}) \quad P_{2j}^{\mathrm{o}}(\mathbf{w}) \quad \ldots \quad P_{Nj}^{\mathrm{o}}(\mathbf{w})]^T$, for $j = 1, 2$, and then write the optimization problem (4.27) as

$$\min_{\mathbf{w}} \quad \frac{\mathbf{1}^T\mathbf{p}_1^{\mathrm{o}}(\mathbf{w})\delta_1(\mathbf{w}) + \mathbf{1}^T\mathbf{p}_2^{\mathrm{o}}(\mathbf{w})\delta_2(\mathbf{w})}{N} + \mathbf{w}^H\mathbf{w} \tag{4.31}$$

which is an unconstrained minimization problem and can be solved using a gradient steepest descent technique such as quasi-Newton method. Note that for any given $\mathbf{w}$, the parameter $\gamma_j(\mathbf{w})$, and thus, $\mathbf{p}_1^{\mathrm{o}}(\mathbf{w})$ and $\mathbf{p}_2^{\mathrm{o}}(\mathbf{w})$ cannot be calculated in closed-form. Instead, rather they can be obtained only numerically. As such, the gradient of the cost function in (4.31) is not analytically available and has to be calculated numerically at each iteration using difference equations. The quasi-Newton method performs a cubic line search procedure by approximating the cost function at each iteration using a quadratic cost function with a positive semi-definite kernel (Hessian) matrix. At each iteration, the Hessian matrix can be updated using the so-called BFGS method ([1],[5],[8], and [9]).

It is worth mentioning that the quasi-Newton method is guaranteed to converge to a local minimum, and the global optimality cannot be claimed. Naturally, the quality of this local minimum depends on the initial point. In the next subsection, we propose a technique that can not only yield a reasonably good initial point for the quasi-Newton method but also can provide yet another method to tackle the problem at hand.

4.2.2 Frequency-Flat CIR Method

Since an explicit solution to the optimization problem in (4.27) may not be attainable, in

this section, we propose a suboptimal solution to (4.27), which can also serve as an initial point for the quasi-Newton based solution proposed in the previous section. Here, we restrict the solution to (4.27) to a set of points which will ensure that the end-to-end CIR has a *frequency-flat amplitude response*. This assumption, inspired by the results of [16] and [39], will ensure loss of optimality, notwithstanding, it will lead to a fast and simple suboptimal solution for the problem at hand[8]. Enforcing a frequency-flat *amplitude response* for the end-to-end channel amounts to adding, to (4.27), the constraints i.e., $|\mathbf{q}_i^H\bar{\mathbf{h}}(\mathbf{w})| = |\mathbf{q}_j^H\bar{\mathbf{h}}(\mathbf{w})|$, where $\mathbf{q}_i^H\bar{\mathbf{h}}(\mathbf{w})$ is the frequency response of the i-th sub-channel. That is, we write

$$\begin{aligned}
&\min_{\mathbf{w}} \min_{\substack{\mathbf{p}_1\succeq 0\\ \mathbf{p}_2\succeq 0}} \sum_{j=1}^{2} \frac{\mathbf{1}^T\mathbf{p}_j}{N}\delta_j(\mathbf{w}) + \mathbf{w}^H\mathbf{w} \\
&\text{subject to } \sum_{i=1}^{N} \log_2(1+\mathrm{SNR}_{ij}) = r_j \quad \text{for} \quad j=1,2 \\
&\qquad |\mathbf{q}_i^H\bar{\mathbf{h}}(\mathbf{w})| = |\mathbf{q}_k^H\bar{\mathbf{h}}(\mathbf{w})|, \text{ for } i\neq k,\ i,k=1,\ldots,N. \qquad (4.32)
\end{aligned}$$

Considering the inner minimization (which is not affected by adding the new constraints), we can still use the solution in (4.29) for $P_{ij}^{\mathrm{o}}(\mathbf{w})$. It can be easily seen that for any given $\mathbf{w}$ which ensures a frequency-flat amplitude response for the end-to-end CIR, the optimal value of $P_{ij}^{\mathrm{o}}(\mathbf{w})$ in (4.29) is the same for any subcarrier index i, and thus, from (4.30), we can obtain $\gamma_j(\mathbf{w})$ as

$$\gamma_j(\mathbf{w}) = \frac{\ln 2\delta_1(\mathbf{w})\delta_2(\mathbf{w})}{N^2}\left(\frac{2^{r_{\bar{j}}}}{\prod_{i=1}^{N}|\mathbf{q}_i^H\bar{\mathbf{h}}(\mathbf{w})|^2}\right)^{\frac{1}{N}}. \qquad (4.33)$$

Inserting (4.33) back into (4.29) yields the allocated power at the i-th sub-carrier at TR_1 as

$$P_{ij}^{\mathrm{o}}(\mathbf{w}) = \frac{\delta_{\bar{j}}(\mathbf{w})}{N}\left(\frac{2^{\frac{r_{\bar{j}}}{N}}}{\left[\prod_{i=1}^{N}|\mathbf{q}_i^H\bar{\mathbf{h}}(\mathbf{w})|^2\right]^{\frac{1}{N}}} - \frac{1}{|\mathbf{q}_i^H\bar{\mathbf{h}}(\mathbf{w})|^2}\right). \qquad (4.34)$$

Since at the optimum, we design the end-to-end channel such that $|\mathbf{q}_i^H\bar{\mathbf{h}}(\mathbf{w})| = |\mathbf{q}_k^H\bar{\mathbf{h}}(\mathbf{w})|$

[8]Both approaches in [16] and [39] are developed for the TWR networks, where the transceiver-relay channels are frequency-flat, yet, the end-to-end channel is frequency-selective due to differences in the delays of propagation between each transceiver and different relays. It is rigorously proved there that at the optimum, the end-to-end channel between the transceivers becomes frequency-flat.

for any $i \neq k$, the i-th sub-carrier power in (4.34) can be simplified as

$$\begin{aligned} P_{ij}^{\mathrm{o}}(\mathbf{w}) &= \frac{\delta_{\bar{j}}(\mathbf{w})}{N}\left(\frac{2^{\frac{r_{\bar{j}}}{N}}-1}{|\mathbf{q}_i^H\bar{\mathbf{h}}(\mathbf{w})|^2}\right) \\ &\overset{a}{=}\delta_{\bar{j}}(\mathbf{w})\left(\frac{2^{\frac{r_{\bar{j}}}{N}}-1}{\sum_{i=1}^{N}|\mathbf{q}_i^H\bar{\mathbf{h}}(\mathbf{w})|^2}\right) \overset{b}{=} \delta_{\bar{j}}(\mathbf{w})\left(\frac{2^{\frac{r_{\bar{j}}}{N}}-1}{\parallel \mathbf{B}^*\mathbf{w} \parallel^2}\right) \end{aligned} \tag{4.35}$$

where equality (a) holds true because $|\mathbf{q}_k^H\bar{\mathbf{h}}(\mathbf{w})|^2 = \frac{1}{N}\sum_{i=1}^{N}|\mathbf{q}_i^H\bar{\mathbf{h}}(\mathbf{w})|^2$ for any $k \in \{1,2,\ldots,N\}$, and equality (b) is ensured by using the Parseval theorem as we can write $\sum_{i=1}^{N}\left|\mathbf{q}_i^H\bar{\mathbf{h}}(\mathbf{w})\right|^2 = \|\bar{\mathbf{h}}(\mathbf{w})\|^2 = \|\mathbf{h}(\mathbf{w})\|^2 = \|\mathbf{B}\mathbf{w}^*\|^2 = \|\mathbf{B}^*\mathbf{w}\|^2$. It can be seen from (4.35) that at the optimum, power is equally allocated to all sub-carriers, and the sub-carriers' powers are always positive. Plugging (4.35) back into (4.32), we can express the outer minimization over $\mathbf{w}$ as

$$\begin{aligned} \min_{\mathbf{w}}\ & \frac{\delta_1(\mathbf{w})\delta_2(\mathbf{w})}{\parallel \mathbf{B}^*\mathbf{w} \parallel^2}(\beta_1+\beta_2) + \mathbf{w}^H\mathbf{w} \\ \text{s.t.}\ & |\mathbf{q}_i^H\bar{\mathbf{h}}(\mathbf{w})| = |\mathbf{q}_k^H\bar{\mathbf{h}}(\mathbf{w})|,\ \text{for}\ \ i,k = 1,\ldots,N. \end{aligned} \tag{4.36}$$

where $\beta_j \triangleq 2^{\frac{r_j}{N}} - 1$ for $j = 1, 2$. The constraint on (4.36) suggests that at the optimum, the frequency-flat end-to-end CIR vector, $\mathbf{h} = \mathbf{B}\mathbf{w}^*$, has only one non-zero entry, which is here referred to as the optimal tap of the end-to-end CIR. Equivalently, we can rewrite the minimization in (4.36) as

$$\begin{aligned} \min_{\mathbf{w}}\quad & \frac{\delta_1(\mathbf{w})\delta_2(\mathbf{w})}{\parallel \mathbf{B}^*\mathbf{w} \parallel^2}(\beta_1+\beta_2) + \mathbf{w}^H\mathbf{w}. \\ \text{subject to}\quad & \mathbf{B}\mathbf{w}^*\ \text{ having only one non-zero entry.} \end{aligned} \tag{4.37}$$

To deal with the constraint in (4.37), let us define $\mathcal{N} \triangleq \{0 \leq n \leq L_h - 1|$ the $(n+1)$th row of $\mathbf{B}^*$ is not zero$\}$, and $L_{\mathrm{nz}} \triangleq |\mathcal{N}|$ is the number of non-zero rows of $\mathbf{B}^*$. Now for any $n \in \mathcal{N}$, let $\mathbf{B}_{-n} \in \mathbb{C}^{(L_{\mathrm{nz}}-1)\times RL_w}$ symbolize matrix $\mathbf{B}^*$ after all its zero rows[9], as well as its $(n+1)$-th row (which is non-zero) is removed. Due to its block Toeplitz structure, $\mathbf{B}$ is of rank L_{nz}, and hence, $\mathbf{B}_{-n}$ is of rank $L_{\mathrm{nz}} - 1$. Therefore, constraining $\mathbf{B}\mathbf{w}^*$ to have only one non-zero entry is equivalent to the following condition:

$$\mathbf{B}_{-n}\mathbf{w} = \mathbf{0}, \quad \text{for some } n \in \mathcal{N}. \tag{4.38}$$

[9]The reason to remove all the zero rows is that if the $(n+1)$-th row of $\mathbf{B}^*$ is zero for any $n \in \{0,1,...,L_h-1\}$, then the n-th tap of the end-to-end CIR will be zero too, and therefore, this tap cannot be the non-zero optimal tap.

Since the rank of $\mathbf{B}_{-n}$ is $L_{\text{nz}}-1$, the condition in (4.38) is equivalent to imposing a total number of $L_{\text{nz}}-1$ linear constraints on $\mathbf{w}$ in (4.37), for some $n \in \mathcal{N}$. In order to be able to enforce these $L_{\text{nz}}-1$ constraints, sufficient degrees of freedom must be available for the TWR network design. As such, the length of $\mathbf{w}$, i.e. RL_w, must be greater than $L_{\text{nz}}-1$. In other words, matrix $\mathbf{B}_{-n}$ must have more columns than rows. Equivalently, this means that the number of the relay nodes, R, in the network and/or the length of the FIR filter, L_w, at each relay node must be chosen such that the following condition holds true

$$RL_w \geq \ L_{\text{nz}}-1. \tag{4.39}$$

In the extreme scenario[10], where $L_{\text{nz}} = L_h - L_0 = 2L + L_w - 2 - L_0$, the condition $L_w(R-1) \geq 2L - L_0 - 2$ must be satisfied.

To satisfy the condition in (4.39), one can either employ a sufficient number of relay nodes, which entails more hardware complexities in the TWR network, or increase the length of the FIR filter at the existing relay nodes, which demands more processing complexity. For any $n \in \mathcal{N}$, the condition $\mathbf{B}_{-n}\mathbf{w} = \mathbf{0}$ implies that $L_{\text{nz}}-1$ entries of $\mathbf{w}$ can be expressed in terms of the remaining $RL_w - L_{\text{nz}} + 1$ entries. Therefore, for any given $\mathbf{B}_{-n}$, there exists a matrix $\mathbf{C}_n \in \mathbb{C}^{RL_w \times (RL_w - L_{\text{nz}}+1)}$ such that

$$\mathbf{w} = \mathbf{C}_n \bar{\mathbf{w}}. \tag{4.40}$$

where $\bar{\mathbf{w}}$ is an $(RL_w - L_{\text{nz}} + 1) \times 1$ vector containing a subset of entries of $\mathbf{w}$. For the derivation of $\mathbf{C}_n$, see Appendix B.2.

We now focus on solving (4.37) based on (4.40). To do so, we can solve (4.37) for different non-zero tap indices of the end-to-end CIR, $n \in \mathcal{N}$. The optimal tap is the value of n results in the minimum total transmit power, and the optimal weight vector is the corresponding vector, which leads to that minimum total transmit power. Let $\mathcal{B}_n$ denote the set of those non-zero weight vectors $\mathbf{w}$ which cause only the n-th tap of the end-to-end channel to be non-zero while the rest of the taps are zero. Note that for different values of $n \in \mathcal{N}$, the sets $\{\mathcal{B}_n\}_{n\in\mathcal{N}}$ are mutually exclusive, i.e., $\mathcal{B}_n \cap \mathcal{B}_{n'} = \emptyset$, for $n \neq n'$. The

[10]The extreme scenario is when there is no zero rows in $\mathbf{B}$, other than the first L_0 rows, and thus, the rank of $\mathbf{B}$ is equal to $L_h - L_0$.

condition that $\mathbf{Bw}^*$ must have only one non-zero entry is equivalent to $\mathbf{w} \in \bigcup_{n\in\mathcal{N}} \mathcal{B}_n$, as $\{\mathcal{B}_n\}_{n\in\mathcal{N}}$ partitions the feasible set of the optimization problem (4.37). As a result, the minimization problem in (4.37) can be rewritten as

$$\min_{n\in\mathcal{N}} \min_{\mathbf{w}\in\mathcal{B}_n} \quad \frac{\delta_1(\mathbf{w})\delta_2(\mathbf{w})}{\|\mathbf{B}^*\mathbf{w}\|}(\beta_1+\beta_2) + \mathbf{w}^H\mathbf{w}. \tag{4.41}$$

We now focus on the inner minimization in (4.41) for a given $n \in \mathcal{N}$. The optimal weight vector in (4.41) corresponds to the weight vector which leads to the smallest total transmit power among all values of n. The constraint $\mathbf{w} \in \mathcal{B}_n$ in the inner minimization in (4.41) can be eliminated by substituting $\mathbf{w}$ in the cost function with (4.40). Also, defining $\mathbf{b}_n^H$ as the $(n+1)$-th row of $\mathbf{B}^*$, for $n \in \mathcal{N}$ and using the fact that the constraint $\mathbf{w} \in \mathcal{B}_n$ implies that only the $(n+1)$-th entry of $\mathbf{B}^*\mathbf{w}$ is nonzero, we can write $\|\mathbf{B}^*\mathbf{w}\|^2 = \|\mathbf{b}_n^H\mathbf{w}\|^2$. Consequently, the inner minimization in (4.41) can be transformed into an *unconstrained* optimization problem as

$$\min_{\bar{\mathbf{w}}} \quad \frac{\bar{\delta}_{1,n}(\bar{\mathbf{w}})\bar{\delta}_{2,n}(\bar{\mathbf{w}})}{\| \bar{\mathbf{b}}_n^H\bar{\mathbf{w}} \|^2}(\beta_1+\beta_2) + \bar{\mathbf{w}}^H\bar{\mathbf{C}}_n\bar{\mathbf{w}} \tag{4.42}$$

where $\bar{\delta}_{j,n}(\bar{\mathbf{w}}) \triangleq (1 + \bar{\mathbf{w}}^H\bar{\mathbf{D}}_{j,n}\bar{\mathbf{w}})$, for $j \in \{1,2\}$; matrix $\bar{\mathbf{D}}_{j,n} \in \mathbb{C}^{(RL_w-L_{\text{nz}}+1)\times(RL_w-L_{\text{nz}}+1)}$ is defined as $\bar{\mathbf{D}}_{j,n} \triangleq \mathbf{C}_n^H\mathbf{D}_j\mathbf{C}_n$, vector $\bar{\mathbf{b}}_n \in \mathbb{C}^{(RL_w-L_{\text{nz}}+1)\times 1}$ is given by $\bar{\mathbf{b}}_n^H \triangleq \mathbf{b}_n^H\mathbf{C}_n$; and matrix $\bar{\mathbf{C}}_n \in \mathbb{C}^{(RL_w-L_{\text{nz}}+1)\times(RL_w-L_{\text{nz}}+1)}$ is expressed as $\bar{\mathbf{C}}_n \triangleq \mathbf{C}_n^H\mathbf{C}_n$. To solve (4.42) for $\bar{\mathbf{w}}$, we define a new auxiliary variable z as

$$z \triangleq \frac{(\beta_1+\beta_2)\,\bar{\delta}_{2,n}(\bar{\mathbf{w}})}{\| \bar{\mathbf{b}}_n^H\bar{\mathbf{w}} \|^2} \tag{4.43}$$

Using (4.43), the inner minimization in (4.42) can be rewritten as

$$\begin{aligned} \min_{\bar{\mathbf{w}},\, z} \quad & z + z\bar{\mathbf{w}}^H\bar{\mathbf{D}}_{1,n}\bar{\mathbf{w}} + \bar{\mathbf{w}}^H\bar{\mathbf{C}}_n\bar{\mathbf{w}} \\ \text{subject to} \quad & \frac{z(\bar{\mathbf{w}}^H\,\bar{\mathbf{b}}_n\bar{\mathbf{b}}_n^H\,\bar{\mathbf{w}})}{\bar{\mathbf{w}}^H\bar{\mathbf{D}}_{2,n}\bar{\mathbf{w}}+1} = (\beta_1+\beta_2). \end{aligned} \tag{4.44}$$

or, equivalently, as

$$\begin{aligned} \min_{z} \quad & z + \min_{\bar{\mathbf{w}}}\ \bar{\mathbf{w}}^H\mathbf{E}_n(z)\bar{\mathbf{w}} \\ \text{s.t.} \quad & \bar{\mathbf{w}}^H(z\bar{\mathbf{b}}_n\bar{\mathbf{b}}_n^H - (\beta_1+\beta_2)\bar{\mathbf{D}}_{2,n})\bar{\mathbf{w}} = (\beta_1+\beta_2) \end{aligned} \tag{4.45}$$

where we define $\mathbf{E}_n(z) \triangleq z\bar{\mathbf{D}}_{1,n} + \bar{\mathbf{C}}_n$. The optimization problem in (4.45) is infeasible for those values of z which satisfy the following condition:

$$z\bar{\mathbf{b}}_n\bar{\mathbf{b}}_n^H - (\beta_1+\beta_2)\bar{\mathbf{D}}_{2,n} \prec \mathbf{0}. \tag{4.46}$$

We observe that, for $j \in \{1,2\}$, $\mathbf{D}_j$ is full-rank, and thus, $\bar{\mathbf{D}}_j$ is positive semi-definite. Therefore, the infeasibility condition in (4.46) can be written as

$$z\bar{\mathbf{D}}_{2,n}^{-1/2}\bar{\mathbf{b}}_n\bar{\mathbf{b}}_n^H\bar{\mathbf{D}}_{2,n}^{-H/2} - (\beta_1+\beta_2)\mathbf{I}_{RL_w} \prec \mathbf{0}. \tag{4.47}$$

or, equivalently, as

$$\begin{aligned} 0 >& \lambda_{\max}\left(z\bar{\mathbf{D}}_{2,n}^{-1/2}\bar{\mathbf{b}}_n\bar{\mathbf{b}}_n^H\bar{\mathbf{D}}_{2,n}^{-H/2} - (\beta_1+\beta_2)\mathbf{I}_{RL_w}\right) \\ =& z \parallel \bar{\mathbf{D}}_{2,n}^{-1/2}\bar{\mathbf{b}}_n \parallel^2 - (\beta_1+\beta_2). \end{aligned} \tag{4.48}$$

where the equality follows from the fact that the largest eigenvalue of any matrix in the form of $u\mathbf{a}\mathbf{a}^H + z\mathbf{I}$ is equal to $u\mathbf{a}^H\mathbf{a} + z$. Using (4.48), we can find the range of z over which the inner minimization in (4.45) is feasible as

$$z \geq \frac{(\beta_1+\beta_2)}{\parallel \bar{\mathbf{D}}_{2,n}^{-1/2}\bar{\mathbf{b}}_n \parallel^2}. \tag{4.49}$$

For any z satisfying (4.49), the solution to the inner minimization in (4.45), which is a quadratic programming optimization, is given by

$$\bar{\mathbf{w}}^{\mathrm{o}} = \sqrt{\frac{\beta_1+\beta_2}{\mathbf{u}^H(z)\mathbf{P}_n(z)\mathbf{u}(z)}}\mathbf{E}_n^{-1/2}(z)\mathbf{u}(z) \tag{4.50}$$

where the matrix $\mathbf{P}_n(z)$ is defined as

$$\mathbf{P}_n(z) \triangleq \mathbf{E}_n^{-H/2}(z)(z\bar{\mathbf{b}}_n\bar{\mathbf{b}}_n^H - (\beta_1+\beta_2)\bar{\mathbf{D}}_{2,n})\mathbf{E}_n^{-1/2}(z) \tag{4.51}$$

and $\mathbf{u}_n(z) \triangleq \mathcal{P}\{\mathbf{P}_n(z)\}$ is the normalized principal eigenvector of the matrix $\mathbf{P}_n(z)$. Now, to obtain z, we substitute $\bar{\mathbf{w}}^{\mathrm{o}}$ from (4.50) back into (4.45), and rewrite the optimization problem in (4.45) as

$$\min_z \quad z + \frac{\beta_1+\beta_2}{\lambda_n(z)}, \qquad \text{s.t.} \quad z \geq \frac{(\beta_1+\beta_2)}{\parallel \bar{\mathbf{D}}_{2,n}^{-1/2}\bar{\mathbf{b}}_n \parallel^2} \tag{4.52}$$

where $\lambda_n(z)$ denotes the principal eigenvalue of the matrix $\mathbf{P}_n(z)$. For any $z \in (\frac{(\beta_1+\beta_2)}{\|\bar{\mathbf{D}}_{2,n}^{-1/2}\bar{\mathbf{b}}_n\|^2}, +\infty)$, the principal eigenvalue $\lambda_n(z)$ can be found as the provably unique positive value of υ which satisfies[11]

$$z\bar{\mathbf{b}}_n^H((\beta_1+\beta_2)\bar{\mathbf{D}}_{2,n}+\upsilon\mathbf{E}_n(z))^{-1}\bar{\mathbf{b}}_n = 1. \tag{4.53}$$

Lemma 4.2.1. *There exists a unique global minimum for the objective function of (4.52) in the interval* $\left(\frac{(\beta_1+\beta_2)}{\| \bar{\mathbf{D}}_{2,n}^{-1/2}\bar{\mathbf{b}}_n \|^2}, +\infty\right)$.

Proof. see Appendix B.5. □

In light of Lemma 4.2.1, the unique optimal value of z can be obtained when the derivative of the cost function in (4.52) with respect to (w.r.t.) z vanishes. Denoting the derivative of the cost function in (4.52) w.r.t. z as $f(z)$, we can write

$$f_n(z) = 1-(\beta_1+\beta_2)\frac{\frac{\partial}{\partial z}\lambda_n(z)}{\lambda_n^2(z)}. \tag{4.54}$$

It can be shown that $\frac{\partial}{\partial z}\lambda_n(z)$ is given by[12]

$$\frac{\partial\lambda_n(z)}{\partial z} = \frac{z^{-2}-\lambda_n(z)\bar{\mathbf{b}}_n^H\mathbf{\Lambda}_n^{-1}(z)\bar{\mathbf{D}}_{1,n}\mathbf{\Lambda}_n^{-1}(z)\bar{\mathbf{b}}_n}{\bar{\mathbf{b}}_n^H\mathbf{\Lambda}_n^{-1}(z)\mathbf{E}_n(z)\mathbf{\Lambda}_n^{-1}(z)\bar{\mathbf{b}}_n} \tag{4.55}$$

where $\mathbf{\Lambda}_n(z) \triangleq (\beta_1+\beta_2)\bar{\mathbf{D}}_{2,n}+\lambda_n(z)\mathbf{E}_n(z)$. Substituting (4.55) in (4.54), we arrive at

$$f_n(z) = 1-(\beta_1+\beta_2)\frac{z^{-2}-\lambda_n(z)\bar{\mathbf{b}}_n^H\mathbf{\Lambda}_n^{-1}(z)\bar{\mathbf{D}}_{1,n}\mathbf{\Lambda}_n^{-1}(z)\bar{\mathbf{b}}_n}{\lambda_n^2(z)\bar{\mathbf{b}}_n^H\mathbf{\Lambda}_n^{-1}(z)\mathbf{E}_n(z)\mathbf{\Lambda}_n^{-1}(z)\bar{\mathbf{b}}_n}. \tag{4.56}$$

Equating $f_n(z)$ to zero does not yield a closed-form solution for z. Therefore, to find a closed-form solution for z (which we denote as z_n), we can resort to numerical approaches such as Newton-Raphson or bisection method. To implement the Newton-Raphson or bisection method, from (4.56), it can be seen that for each intermediate value of z, $\lambda_n(z)$ must be calculated. For any $z \in (\frac{(\beta_1+\beta_2)}{\|\bar{\mathbf{D}}_{2,n}^{-1/2}\bar{\mathbf{b}}_n\|^2}, +\infty)$, the parameter $\lambda_n(z)$ can be found numerically by solving (4.53) for υ using the Newton-Raphson method[13]. Given z_n and $\lambda_n(z_n)$, we can

[11] For derivation of (4.53), see Appendix B.3 and for the proof of the existence of a unique positive solution to (4.53), see Appendix B.4.

[12] For derivations see Appendix B.3.

[13] For the use in Newton-Raphson method, the derivative of the LHS of (4.53) with respect to υ is given by $-z\bar{\mathbf{b}}_n^H((\beta_1+\beta_2)\bar{\mathbf{D}}_{2,n}+\upsilon\mathbf{E}_n(z))^{-1}\mathbf{E}_n(z)((\beta_1+\beta_2)\bar{\mathbf{D}}_{2,n}+\upsilon\mathbf{E}_n(z))^{-1}\bar{\mathbf{b}}_n$.

obtain a closed-form solution for the optimal weight vector. Let $\bar{\mathbf{w}}_n^{\mathrm{o}}$ denote the optimal weight vector solution when only the n-th tap of the end-to-end CIR is non-zero. Using (4.50), we can write

$$\bar{\mathbf{w}}_n^{\mathrm{o}} = \sqrt{\frac{z_n(\beta_1+\beta_2)}{\kappa_n \lambda_n(z_n)}}[(\beta_1+\beta_2)\bar{\mathbf{D}}_{2,n} + \lambda_n(z_n)\mathbf{E}_n(z_n)]^{-1}\bar{\mathbf{b}}_n \tag{4.57}$$

where we use the fact that $\lambda_n(z) = \mathbf{u}^H(z)\mathbf{P}_n(z)\mathbf{u}(z)$ holds true, and define

$$\kappa_n = z_n \bar{\mathbf{b}}_n^H \Big[(\beta_1+\beta_2)\mathbf{E}_n^{-1/4}(z_n)\bar{\mathbf{D}}_{2,n}\mathbf{E}_n^{-1/4}(z_n) + \lambda(z_n)\mathbf{E}_n^{1/2}(z_n)\Big]^{-2}\bar{\mathbf{b}}_n. \tag{4.58}$$

Using (4.57), we obtain the optimal value of the cost function in (4.42) for the n-th tap of end-to-end CIR, $P_T^{(n)}(\bar{\mathbf{w}}_n^{\mathrm{o}})$ as

$$P_T^{(n)}(\bar{\mathbf{w}}_n^{\mathrm{o}}) = \frac{\bar{\delta}_{1,n}(\bar{\mathbf{w}}_n^{\mathrm{o}})\bar{\delta}_{2,n}(\bar{\mathbf{w}}_n^{\mathrm{o}})}{\|\bar{\mathbf{b}}_n^H \bar{\mathbf{w}}_n^{\mathrm{o}}\|^2}(\beta_1+\beta_2) + \bar{\mathbf{w}}_n^{\mathrm{o},H}\bar{\mathbf{C}}_n\bar{\mathbf{w}}_n^{\mathrm{o}}. \tag{4.59}$$

The optimal tap of the end-to-end CIR, n_{opt}, corresponds to the tap index which yields the minimum total transmit power among all the values of $P_T^{(n)}(\bar{\mathbf{w}}_n^{\mathrm{o}})$ attained for the set of weight vectors $\{\bar{\mathbf{w}}_n^{\mathrm{o}}\}_{n\in\mathcal{N}}$. In other words, this optimal tap n_{opt} can be achieved by

$$n_{\mathrm{opt}} = \arg \min_{n\in\mathcal{N}} P_T^{(n)}(\bar{\mathbf{w}}_n^{\mathrm{o}}). \tag{4.60}$$

Let $\mathbf{w}_{\mathrm{opt}}$ signify the $RL_w \times 1$ optimal distributed equalization weight vector. For the given n_{opt}, the optimal distributed equalization weight vector can be given as

$$\mathbf{w}_{\mathrm{opt}} = \mathbf{C}_{n_{\mathrm{opt}}}\bar{\mathbf{w}}_{n_{\mathrm{opt}}}^{\mathrm{o}}. \tag{4.61}$$

Using the sub-carriers' transmit power expression in (4.35), we can derive the optimal sub-carriers' transmit power over the i-th subcarrier at TR_j as

$$P_{ij}^{\mathrm{o}} = \delta_{\bar{j}}(\mathbf{w}_{\mathrm{opt}})\left(\frac{2^{\frac{r_{\bar{j}}}{N}}-1}{\|\ \mathbf{B}^*\mathbf{w}_{\mathrm{opt}}\ \|^2}\right) = \frac{\beta_{\bar{j}}(1+\mathbf{w}_{\mathrm{opt}}^H\mathbf{D}_{\bar{j}}\mathbf{w}_{\mathrm{opt}})}{\|\ \mathbf{B}^*\mathbf{w}_{\mathrm{opt}}\ \|^2}. \tag{4.62}$$

The proposed algorithm is summarized in Algorithm 2.

Algorithm 2 Proposed frequency-flat CIR algorithm

1. Define $\mathbf{B}$ as the Toeplitz matrix with the first column and the first row given by vectors $[\tilde{h}_r[0] \;\; \tilde{h}_r[1] \;\; \cdots \tilde{h}_r[L_{\tilde{h}}-1] \;\; \mathbf{0}_{1\times(L_h-L_{\tilde{h}})}]^T$ and $[\tilde{h}_r[0] \;\; \mathbf{0}_{1\times(L_w-1)}]^T$. Define $\mathcal{N} \triangleq \{0 \leq n \leq L_h-1|$ the $(n+1)$th row of $\mathbf{B}^*$ is not zero$\}$. Stack the non-zero rows of $\mathbf{B}^*$ in a new matrix $\tilde{\mathbf{B}} \in \mathbb{C}^{L_{\rm nz}\times RL_w}$, where $L_{\rm nz}$ is the number of non-zero rows of $\mathbf{B}^*$. Form matrices $\mathbf{\Pi}$ and $\{\mathbf{D}_j\}_{j=1}^2$ as in (4.18) and (4.19), respectively.

2. Set $n=0$.

3. If $n \in \mathcal{N}$, go to the next step, otherwise go to Step 12.

4. Let $\mathbf{b}_n^H$ be the $(n+1)$-th row of matrix $\mathbf{B}^*$, while $\mathbf{B}_{-n} \in \mathbb{C}^{(L_{\rm nz}-1)\times RL_w}$ symbolizes matrix $\mathbf{B}$ after all its $L_{\rm nz}$ zero rows as well as its $(n+1)$-th row (which is nonzero) is removed.

5. Use matrix $\mathbf{B}_{-n}$ to find matrix $\mathbf{C}_n$ according to the procedure presented in Appendix B.2.

6. Obtain $\bar{\mathbf{b}}_n^H = \mathbf{b}_n^H\mathbf{C}_n$, $\bar{\mathbf{C}}_n = \mathbf{C}_n^H\mathbf{C}_n$, and $\bar{\mathbf{D}}_{j,n} = \mathbf{C}_n^H\mathbf{D}_j\mathbf{C}_n$, for $j \in \{1,2\}$. For the sum-rate threshold, r_j, at TR$_j$, set $\beta_j = (2^{\frac{r_j}{N}}-1)$, for $j \in \{1,2\}$.

7. Define function $f_n(z)$ as in (4.56). where $\mathbf{E}_n(z) \triangleq z\bar{\mathbf{D}}_{1,n} + \bar{\mathbf{C}}_n$, and $\mathbf{\Lambda}_n(z) \triangleq (\beta_1+\beta_2)\bar{\mathbf{D}}_{2,n} + \lambda(z)\mathbf{E}_n(z)$.

8. Using the following bisection algorithm, find $z_n \in \left(\frac{(\beta_1+\beta_2)}{\|\bar{\mathbf{D}}_{2,n}^{-1/2}\bar{\mathbf{b}}_n\|^2}, +\infty\right)$ such that $f_n(z_n)=0$:

   (a) Set $\tilde{z}_{\rm l} = \frac{(\beta_1+\beta_2)}{\|\bar{\mathbf{D}}_{2,n}^{-1/2}\bar{\mathbf{b}}_n\|^2}$, and let $z_{\rm u}$ be a sufficiently large number. Also, choose an arbitrary small number ϵ. Set $k=1$.

   (b) Set $z^{(k)} = (z_{\rm l}+z_{\rm u})/2$.

   (c) Using Newton-Raphson method, obtain $\lambda_n(z^{(k)})$ as the unique positive value of υ which satisfies (4.53) for $z=z^{(k)}$. Obtain $f_n(z^{(k)})$. If $f_n(z^{(k)})>0$, then set $z_{\rm u}=z^{(k)}$. If $f_n(z^{(k)})<0$, then set $z_{\rm l}=z^{(k)}$.

   (d) Set $z^{(k+1)} = (z_{\rm l}+z_{\rm u})/2$. If $|z^{(k+1)}-z^{(k)}|>\epsilon$, then $k=k+1$ and go to Step 8b. Otherwise, go to Step 8e.

   (e) Set $z_n = z^{(k+1)}$, and using Newton-Raphson method, obtain $\lambda_n(z_n)$ as the positive value of υ which satisfies (4.53)

9. Calculate κ as in (4.58).

10. Obtain the optimal weight vector $\bar{\mathbf{w}}_n^{\rm o}$ for the n-th tap of the end-to-end CIR, $h[\cdot]$, as in (4.57).

11. Calculate $P_T^{(n)}(\bar{\mathbf{w}}_n^{\rm o})$ as in (4.59).

12. Set $n=n+1$. If $n \geq L_h$, go to the next step, otherwise go to Step 3.

13. Find the optimal $n_{\rm opt}$ over $n \in \mathcal{N}$ such that $n_{\rm opt} = \arg\min_{n\in\mathcal{N}} P_T^{(n)}(\bar{\mathbf{w}}_n^{\rm o})$.

14. Obtain the $RL_w \times 1$ optimal distributed equalization weight vector $\mathbf{w}_{\rm opt}$ as $\mathbf{w}_{\rm opt} = \mathbf{C}_{n_{\rm opt}}\bar{\mathbf{w}}_{n_{\rm opt}}^{\rm o}$.

15. Calculate the i-th sub-carrier optimal transmit power at TR$_1$ and TR$_2$ as in (4.62).

4.2.3 Lower Bound

To analyze the performance of our proposed sub-optimal solutions, we here obtain a lower bound for the original optimization problem (4.27) by using two relaxations and then solve the relaxed optimization problem. As the first relaxation, considering the inner minimization in (4.27) as in (4.28), we can rewrite the rate constraint as $\left(\prod_{i=1}^{N}(1+\frac{NP_{ij}|\mathbf{q}_i^H\bar{\mathbf{h}}(\mathbf{w})|^2}{\delta_{\bar{j}}(\mathbf{w})})\right)^{1/N} = 2^{r_{\bar{j}}/N}$ and then relax this constraint as $N^{-1}\sum_{i=1}^{N}(1+\frac{NP_{ij}|\mathbf{q}_i^H\bar{\mathbf{h}}(\mathbf{w})|^2}{\delta_{\bar{j}}(\mathbf{w})}) = 2^{r_{\bar{j}}/N}$, where we use the fact that the arithmetic mean of a set of positive numbers is greater than their geometric mean. Hence, after this relaxation, we arrive at the following optimization problem:

$$\text{min.} \quad \rho\sum_{i=1}^{N}\alpha_i, \;\; \text{s.t.} \;\; \frac{1}{N}\sum_{i=1}^{N}(1+\alpha_i\zeta_i) = c, \quad \alpha_i \geq 0. \tag{4.63}$$

where we define $\alpha_i \triangleq P_{ij}$, $\zeta_i \triangleq \frac{N|\mathbf{q}_i^H\bar{\mathbf{h}}(\mathbf{w})|^2}{\delta_{\bar{j}}(\mathbf{w})}$, $\rho \triangleq \frac{\delta_j(\mathbf{w})}{N}$ and $c \triangleq 2^{\frac{r_{\bar{j}}}{N}}$. The Karush-Kuhn-Tucker (KKT) conditions to solve (4.63) can be given as

$$\gamma = \frac{N(-\rho+\nu_i)}{\zeta_i}, \;\; \nu_i \geq 0, \;\; \nu_i\alpha_i = 0 \tag{4.64}$$

where γ and ν_i are the Lagrange multipliers. It follows from $\nu_i\alpha_i = 0$ that if $\alpha_i > 0$, for some i then $\nu_i = 0$ holds for those values of i, and hence, $\gamma = \frac{-N\rho}{\zeta_i}$ must hold for those values of i. As a result, only one of the α_i's can be non-zero because ζ_i's are different. The non-zero α_i is equal to $\frac{N(c-1)}{\zeta_i}$, and thus, the index of this non-zero α_i should be chosen as $\bar{i} = \arg\ \max_i\ \zeta_i = \arg\ \max_i\ |\mathbf{q}_i^H\bar{\mathbf{h}}(\mathbf{w})|^2$ in order to minimize the cost function in (4.63). As a result, we need to choose $P_{\bar{i}j} = \frac{\beta_j\delta_{\bar{j}}(\mathbf{w})}{|\mathbf{q}_{\bar{i}}^H\bar{\mathbf{h}}(\mathbf{w})|^2}$, for $j = 1, 2$. Based on this result, the outer minimization in (4.27) can be written as

$$\min_{\mathbf{w}} \;\; \frac{(1+\mathbf{w}^H\mathbf{D}_1\mathbf{w})(1+\mathbf{w}^H\mathbf{D}_2\mathbf{w})}{|\mathbf{q}_{\bar{i}}^H\bar{\mathbf{h}}|^2}(\beta_1+\beta_2)+\mathbf{w}^H\mathbf{w}\,. \tag{4.65}$$

We now apply the second relaxation to (4.65). From the Parseval theorem, we know that the equality $\sum_{i=1}^{N}\left|\mathbf{q}_i^H\bar{\mathbf{h}}\right|^2 = \|\mathbf{B}^*\mathbf{w}\|^2$ must be satisfied. Therefore, the inequality $\left|\mathbf{q}_{\bar{i}}^H\bar{\mathbf{h}}\right|^2 \leq \|\ \mathbf{B}^*\mathbf{w}\ \|^2$ holds true for any i. Substituting the right-hand side of this inequality in (4.65) results in a lower bound optimization for (4.65) and thus, a lower bound for (4.27). Doing

so, we can rewrite (4.65) as

$$\min_{\mathbf{w}} \ \frac{(1+\mathbf{w}^H\mathbf{D}_1\mathbf{w})(1+\mathbf{w}^H\mathbf{D}_2\mathbf{w})}{\parallel \mathbf{B}^*\mathbf{w} \parallel^2}(\beta_1+\beta_2)+\mathbf{w}^H\mathbf{w}. \tag{4.66}$$

To solve (4.66), we define an auxiliary variable, v, as $v \triangleq \frac{(\beta_1+\beta_2)(1+\mathbf{w}^H\mathbf{D}_1\mathbf{w})}{(\mathbf{w}^H\mathbf{B}^T\mathbf{B}^*\mathbf{w})}$, and rewrite (4.66) as the following minimization over v and $\mathbf{w}$:

$$\begin{aligned} &\min_{v} \ (v+\min_{\mathbf{w}} \ v\mathbf{w}^H\mathbf{D}_2\mathbf{w}+\mathbf{w}^H\mathbf{w}) \\ &\text{s.t.} \ \ v(\mathbf{w}^H\mathbf{B}^T\mathbf{B}^*\mathbf{w})-(\beta_1+\beta_2)(\mathbf{w}^H\mathbf{D}_1\mathbf{w})=(\beta_1+\beta_2). \end{aligned} \tag{4.67}$$

We can rewrite (4.67) in a quadratic format as

$$\begin{aligned} \min_{v} \quad & v+\min_{\mathbf{w}} \ \mathbf{w}^H(v\mathbf{D}_2+\mathbf{I})\mathbf{w} \\ \text{s.t.} \quad & \mathbf{w}^H(v\mathbf{B}^T\mathbf{B}^*-(\beta_1+\beta_2)\mathbf{D}_1)\mathbf{w}=(\beta_1+\beta_2). \end{aligned} \tag{4.68}$$

The optimization problem in (4.68) is infeasible for those values of v which result in $v\mathbf{B}^T\mathbf{B}^*-(\beta_1+\beta_2)\mathbf{D}_1$ being non-negative definite. Hence, v should chosen such that $\lambda_{\max}\left[v\mathbf{D}_1^{-1/2}\mathbf{B}^T\mathbf{B}^*\mathbf{D}_1^{-H/2}-(\beta_1+\beta_2)\mathbf{I}\right] > 0$, or equivalently, $v > \frac{\beta_1+\beta_2}{\lambda_{\max}\left[\mathbf{D}_1^{-1/2}\mathbf{B}^T\mathbf{B}^*\mathbf{D}_1^{-H/2}\right]}$. Hence we can rewrite the optimization problem (4.68) as

$$\min_{v} \ \ v+\frac{\beta_1+\beta_2}{\lambda_{\max}(\mathbf{W}(v))}, \qquad \text{s.t. } v > \frac{\beta_1+\beta_2}{\lambda_{\max}\left[\mathbf{D}_1^{-1/2}\mathbf{B}^T\mathbf{B}^*\mathbf{D}_1^{-H/2}\right]} \tag{4.69}$$

where we define $\mathbf{W}(v) \triangleq (v\mathbf{D}_2+\mathbf{I})^{-1}(v\mathbf{B}^T\mathbf{B}^*-(\beta_1+\beta_2)\mathbf{D}_1)$ and we used the fact that the inner minimization in (4.68) is a quadratic programming optimization. The optimization problem can be solved using a numerical search in the interval $(\frac{\beta_1+\beta_2}{\lambda_{\max}\left[\mathbf{D}_1^{-1/2}\mathbf{B}^T\mathbf{B}^*\mathbf{D}_1^{-H/2}\right]}, +\infty)$. Doing so will lead us to a lower bound on the total transmit power consumption. Such a lower bound will give a measure of the maximum performance gap between the proposed schemes and the seemingly unattainable optimal solution.

4.2.4 Complexity Analysis

Defining $M \triangleq RL_w - L_{\text{nz}} + 1$, we can see that $\bar{\mathbf{b}}_n$ is $M \times 1$, and matrices $\bar{\mathbf{D}}_{1,n}$, $\mathbf{E}_n(z)$, and $\mathbf{\Lambda}_n^{-1}(z)$ are $M \times M$. The complexity of computing the numerator in (4.56) is $\mathcal{O}(M^3)$.

Similarly, the complexity of computing the denominator in (4.56) is $\mathcal{O}(M^3)$. Therefore, the complexity of evaluating (4.56) is $\mathcal{O}(M^3)$. On the other hand, the complexity of evaluating (4.53) is $\mathcal{O}(M^3)$. Bisection and Newton-Raphson algorithms converge fast within a few iterations regardless of the problem size. As such, their computational complexities are mostly independent of the problem size i.e., they are constant, see [102], and hence, do not contribute to the *order* of computational complexity. The above computations are repeated for each tap of the end-to-end CIR, for $L_{\text{nz}} = |\mathcal{N}|$ taps, the overall complexity of the proposed algorithm is $\mathcal{O}(L_{\text{nz}}M^3)$. Note that the maximum number of end-to-end CIR taps is $L_{\text{nz}} = L_h = 2L + L_w - 2$, thus, the complexity is $\mathcal{O}(L_h(RL_w - L_h + 1)^3)$.

4.3 Remarks

Remark 1: It is worth mentioning that to tackle the frequency-selectivity of the links, one could use a multi-carrier relaying protocol, where each relay uses DFT followed by sub-carrier-dependent weights and IDFT, thereby implementing a frequency-domain filtering. Such a multi-carrier relaying scheme was studied in [43]. The proposed schemes, which rely on time-domain filtering at the relays, have several important advantages compared to the solution of [43]. The first advantage is that implementation of filtering in time-domain requires the optimization of only a few filter taps at each relay, while the multi-carrier scheme of [43] asks for optimizing as many weights as the number of sub-carriers at each relay. Hence, obtaining the solutions to the proposed schemes requires less computational complexity, as compared to the multi-carrier scheme of [43]. Moreover, OFDM-based relays require more complexity as compared to FIR-based relays with only a few taps. Last but not least, the performance of the multi-carrier relaying scheme of [43] is significantly inferior to the proposed schemes, as shown in the next section on simulation results. Indeed, we show through numerical examples that the proposed schemes significantly outperform the multi-carrier scheme of [43]. This could be attributed to the fact that the multi-carrier scheme of [43] amounts to circular convolution at the relays while the proposed schemes rely on linear convolution, which is known to be an efficient method for equalization.

Remark 2: It is a common approach to assume prefect CSI at the algorithm design stage as it allows us to gain insights with perfect CSI. Also, algorithms which rely on perfect CSI provide ultimate performance bounds. Such bounds in turn will be quite useful once one aims to design schemes that are robust in the presence of imperfect CSI. Indeed, designing robust schemes for the considered system will be the next natural direction in this line of work. Such robust schemes can rely on worst-case performance optimization based schemes [107] or on chance constrained approaches [108].

Remark 3: Assuming that the transceivers have the knowledge of all the channels between all the relays and both transceivers is realistic in cloud radio access network (C-RAN) architectures, where the global CSI is collected at a central unit, thereby allowing centralized processing.

Remark 4: We herein assumed perfect self-interference cancellation. In case perfect self-interference cancelation cannot be achieved (for example, due to imperfect CSI), one can always model the residual self-interference as noise and still use the proposed schemes to obtain an upper-bound performance for more practical scenarios.

Remark 5: Note that the diagonalization of the end-to-end channel, as implied in (4.13) and (4.14), requires that the CP is longer than the delay spread of the end-to-end channel. Large end-to-end delay spreads will result in rate loss in any OFDM-based system and the proposed scheme with the gradient-based solution is no exception. However, our proposed frequency-flat CIR solution does not suffer from large delay spreads as this solution forces the end-to-end channel to be frequency-flat, allowing a CP with length zero (no CP). This is yet another reason why one may prefer our proposed frequency-flat CIR solution over the gradient-based solution. Even the gradient based solution is expected to require shorter CP as the task of end-to-end channel equalization is distributed in the network and at the relays and is not carried out at the two end-nodes.

4.4 Numerical Results

In this section, we study the performance of the two proposed algorithms which are referred to as gradient steepest descent solution and frequency-flat CIR solution. We consider two

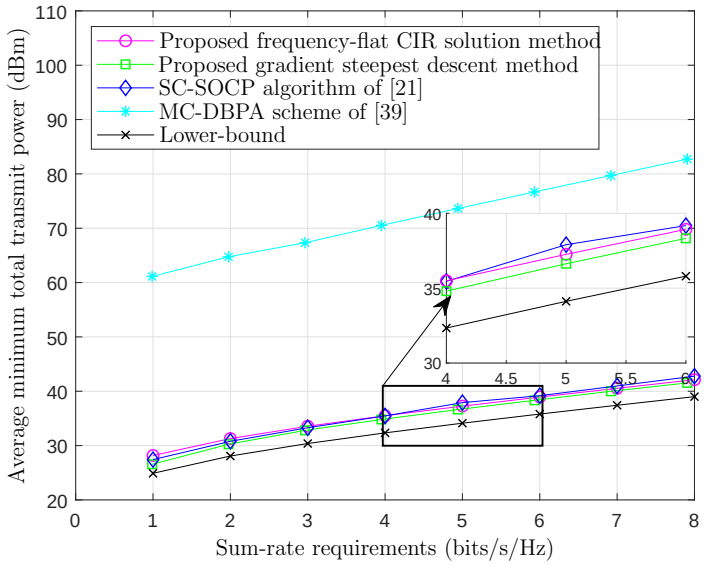

Figure 4.2: Power consumption performance versus the required sum-rates with $R = 10$, $L_{\rm ds} = 3$, $L = 46$, $L_w = 5$, $N = 1024$, and $L_{\rm cp} = 12$.

OFDM-based transceivers in a 10 MHz bandwidth with $N = 1024$ sub-carriers communicating at carrier frequency 2.3 GHz through R relay nodes which employ FIR filters of order of L_w. The carrier frequency is 2.3 GHz. Transceivers are stationary and are located at the Cartesian coordinates of $(-1, 0)$ km and $(1, 0)$ km. The R relay nodes are randomly located over an area of 500 meters by 500 meters centered at $(0, 0)$ km. Each relay-transceiver channel is considered quasi-static frequency-selective with a delay spread of $L_{\rm ds}$, i.e., only $L_{\rm ds}$ consecutive taps of $\{f_r[\cdot]\}_{r=1}^R$ and $\{g_r[\cdot]\}_{r=1}^R$ are non-zero. With this geometry and assuming a sampling rate of 10 M samples/sec, we can obtain $L_0 = 25$ and $L = L_{\rm ds} + 43$. The Okumura-Hata model for urban environment is used to model the path loss as $137.03 + 35 \log_{10}(d)$, with the path loss exponent being 3.5. We assume shadowing standard deviation to be 8 dB. The small scale fading coefficients are modeled as independent and identically distributed complex Gaussian random variables with zero mean and unit variance. The noise at the transceivers and the relays are also modeled as zero-mean white Gaussian random variables with variance $\sigma^2 = -104$ dBm, which is equivalent to the noise level in a 10 MHz transmission bandwidth. Throughout our simulations, we compare different techniques in terms of the minimum total transmit power in (4.20) achieved by them under the sum-rate constraints. We plot the average minimum total transmit power, which is the minimum total transmit power averaged over all channel realizations.

In our first numerical experiment, we set $R = 10$ and $L_w = 5$, and assume each relay-transceiver channel to have $L_{\rm ds} = 3$ non-zero taps, leading to $L = 46$. Fig. 4.2 compares the performance of our proposed schemes with the lower bound that we obtained in Subsection 4.2.3 as well as with the performance of the single-carrier SOCP-based (SC-SOCP) algorithm of [21], and the multi-carrier scheme of [43]. Assuming FF relay nodes, the SC-SOCP algorithm minimizes the total transmit power subject to SINR constraints at the two transceivers. For comparison, we use β_1 and β_2 as the transceivers' SINR requirements for the SC-SOCP algorithm[14].

We need to stress that as the SC-SOCP method is not always feasible for arbitrary channel realizations, the performance of this method is averaged only over the feasible cases, see [21]. The multi-carrier scheme of [43] is a suboptimal iterative algorithm which aims to minimize the total transmit power subject to sum-rate constraints for a TWR network where all the nodes employ OFDM transmission and reception schemes. We herein refer to this algorithm as the multi-carrier distributed beamforming and power allocation (MC-DBPA) method. We point out that for the SC-SOCP algorithm, no CP insertion is needed. Also, for the frequency-flat CIR solution, the CP insertion is not required either as the end-to-end channel will result in a zero delay spread by the design. However, for the proposed gradient steepest descent solution and for the MC-DBPA method of [39], we need to insert a CP of length of $L_{\rm cp} = 12$. This value of $L_{\rm cp}$ is obtained based on the geometry of the scenario detailed earlier and is equal to the difference between the time of arrival of the first sample of the signal with the shortest travel time possible and the time of arrival of the last sample of the signal with the longest travel time possible. Note that to compare the gradient steepest descent method with the frequency-flat CIR method at the same effective data rates per subcarrier r_1/N and r_2/N, we need to take into account the CP overhead for the loss of data rate in the gradient steepest descent method. Thus, the corresponding data rate requirement in problem (4.26) for the gradient steepest descent method (including the initialization using the frequency-flat CIR method) should be scaled as $r_j(N + L_{\rm cp})/N$,

[14]In terms of computational complexity, the SC-SOCP method involves a two dimensional search over a grid, which covers all possible values of transmit powers of the two transceivers, followed by solving an SOCP over each vertex of this grid. However, the computational complexity of the grid search method is too high for practical implementation. As such, this method is used in our simulation results only to benchmark the performance of the proposed solutions.

$j = 1, 2$, that is we initiate the gradient steepest descent solution with the solution of the frequency-flat CIR method with r_1 and r_2 scaled by $(N + L_{\rm cp})/N$.

We observe from Fig. 4.2 that our proposed algorithms substantially outperforms the MC-DBPA algorithm. The reason is that the MC-DBPA scheme is an iterative coordinate-descent method whose performance largely depends on the initial values of the weight vectors, thereby leaving the solution readily susceptible to trapping in a local minimum. In particular, our proposed frequency-flat CIR solution with $L_w = 5$ can approximately achieve an improvement in the range of $35 - 47$ dB compared to the MC-DBPA method. Our proposed gradient steepest descent based algorithm is also sensitive to the initial values of the weight vector and can also trap in a poor local minimum. However, initiated by the solution obtained from our frequency-flat CIR solution, the gradient steepest descent based algorithm can marginally perform better than the frequency-flat CIR solution for the parameters chosen in this example[15]. Note that as shown in Fig. 4.2, although both proposed algorithms perform close to the SC-SOCP method, our algorithms are always feasible and the SC-SOCP technique may not always be feasible, see [21]. Moreover, the SC-SOCP technique requires a much higher computational complexity, compared to the proposed scheme. As can be seen in this figure, the proposed methods are within less than 3 dB from the (unknown) optimal solution as the performance gap between our proposed methods and that lower-bound is less than 3 dB.

Fig. 4.3 displays the average minimum total transmit power of the proposed algorithms versus the order of the FIR filters, L_w, at the relays, for two different effective data rates of 1 and 4 bits/s/Hz. In this example, we have to choose $L_{\rm cp} = 2L_{\rm ds} + L_w + 1 = L_w + 7$ for the gradient steepest descent solution. According to Fig. 4.3, for a TWR network with $R = 10$ relay nodes, increasing the order of the relays' FIR filter L_w reduces the total transmit power consumed in the network, at the expense of increased end-to-end delay. As can be seen from this figure, the gradient steepest descent based algorithm outperforms the frequency-flat CIR solution when the order of the relays' FIR filters are low. In particular, when we choose $L_w = 1$ (i.e., AF relaying), the gradient descent steepest method outperforms the frequency-

[15]In our next examples, we soon show that our gradient steepest descent based algorithm can outperform our frequency-flat CIR solution. Indeed, a good initialization for the MC-DBPA scheme is not known, and thus, this scheme is very susceptible to the choice of initial point.

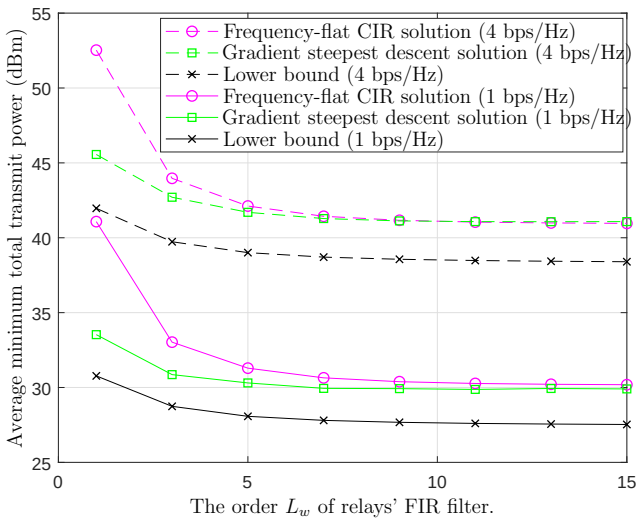

Figure 4.3: The effects of the relays' FIR filter order, L_w, on power consumption performance for $L_{\rm ds} = 3, R = 10$, $N = 1024$, and $\frac{r_1}{N} = \frac{r_2}{N} = 1$ or 4 (bits/s/Hz) for the frequency-flat CIR solution and $\frac{r_1}{N+L_{\rm cp}} = \frac{r_2}{N+L_{\rm cp}} = 1$ or 4 (bits/s/Hz) for the gradient steepest descent solution.

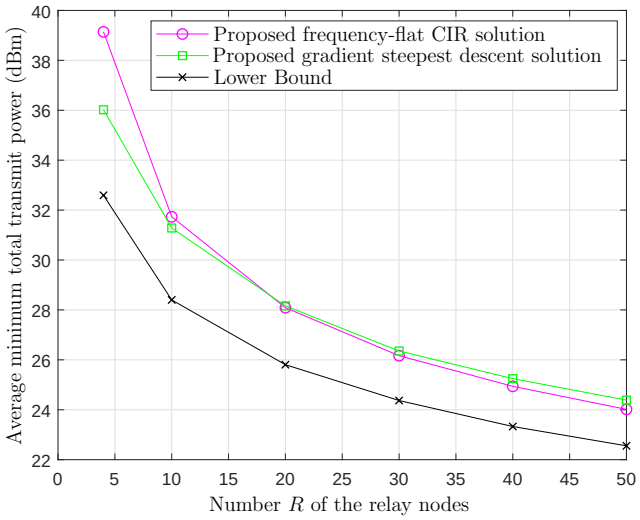

Figure 4.4: The effects of the number of the relays, R, on power consumption performance with $L_{\rm ds} = 3$, $L = 46$, $L_w = 5$, $N = 1024$, and $\frac{r_1}{N} = \frac{r_2}{N} = 1$ (bits/s/Hz) for the frequency-flat CIR solution and $\frac{r_1}{N+L_{\rm cp}} = \frac{r_2}{N+L_{\rm cp}} = 1$ (bits/s/Hz) for the gradient steepest descent solution.

flat CIR solution by about 7 dB. Hence, the gradient descent steepest method can lead to a lower power consumption with lower end-to-end lower delay at the price of increased computational complexity. It can also be seen from Fig. 4.3 that the performances of the two proposed techniques do not improve much beyond $L_w \geq 7$. This figure also shows that as the required effective rates are increased from 1 bit/s/Hz to 4 bits/s/Hz, the performance gap between the two proposed methods diminishes for $L_w \geq 7$, indicating that we can rely on the frequency-flat CIR solution and avoid the additional iterations involved in the gradient steepest descent solution. Nevertheless, for lower values of L_w, the gradient steepest descent solution remains the winner method.

The effect of increasing the number of relay nodes, R, is studied in Fig. 4.4. In this figure, we assume frequency-selective relay-transceivers channels with $L_{\rm ds} = 3$ taps and choose $L_w = 5$, with sum-rate requirements of $r_1/N = r_2/N = 1$ (bit/s/Hz) for the frequency-flat CIR solution and sum-rate requirements of $r_1/(N + L_{\rm cp}) = r_2/(N + L_{\rm cp}) = 1$ (bit/s/Hz) for the gradient steepest descent solution. We also have to choose $L_{\rm cp} = 2L_{\rm ds} + L_w + 1 = 12$ for the gradient steepest descent solution. Fig. 4.4 demonstrates that as the number of relay nodes is increased, the average minimum total transmit power is reduced. From this figure, we observe that increasing the number of relay nodes in the network can consistently reduce the average minimum total transmit power. One reason for this behaviour is the enhanced channel diversity when more relay-transceiver paths exist in the network. Another reason is that as the number of relay nodes increases in the network, gain of the distributed relay beamforming becomes higher as the degrees of freedom in the relay channel are increased. It is worth mentioning that in Fig. 4.4, the frequency-flat CIR solution outperforms the gradient steepest descent method for $R > 30$. This seems to counter the fact that the latter method is designed to improve the performance of the former technique. To explain this, we stress that in order to fairly compare the sum-rates achieved by the gradient steepest descent method and the frequency-flat CIR method, one has to take into account the overhead of the CP length for the data rate loss in the former method. Hence, for the gradient steepest descent method using the CP, a higher sum-rate requirement must be enforced in (4.26) with $r_1 = r_2 = N + L_{\rm cp}$, to achieve the same data rate of that uses the frequency-float CIR solution. These higher sum-rate requirements

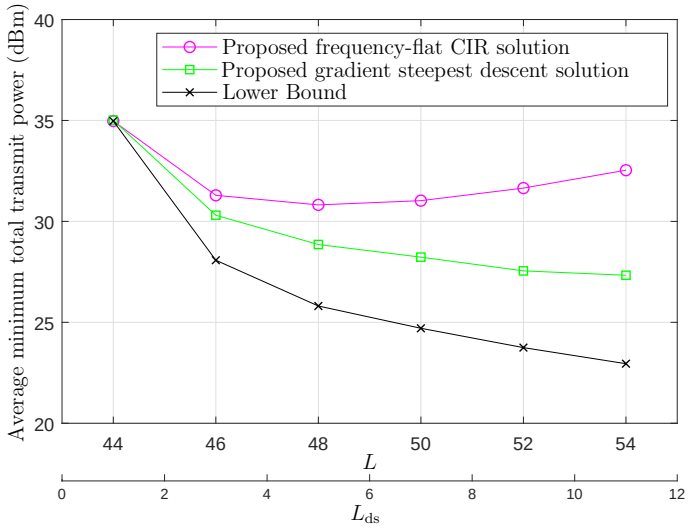

Figure 4.5: The average minimum total transmit power versus the number of taps in the frequency-selective channels, when $R = 10$, $L_w = 5$, $N = 1024$, and $\frac{r_1}{N} = \frac{r_2}{N} = 1$ (bits/s/Hz), for the frequency-flat CIR solution and $\frac{r_1}{N+L_{\text{cp}}} = \frac{r_2}{N+L_{\text{cp}}} = 1$ (bits/s/Hz) for the gradient steepest descent solution.

appear not to be compensable by the performance improvement offered by the gradient steepest descent method over the frequency-flat CIR method, for $R > 30$..

Fig. 4.5 studies the performance of the proposed algorithms in TWR networks, where the frequency-selective channels have a different number of taps. In this experiment, we choose $L_{\text{cp}} = 2L_{\text{ds}} + L_w + 1 = 2L_{\text{ds}} + 6$ for the gradient steepest descent solution. As can be seen from this figure, the performance of the frequency-flat CIR solution is first improved when $1 \leq L_{\text{ds}} \leq 5$ and then is worsened when $L_{\text{ds}} > 5$. This behavior can be associated with the trade-off between channel diversity and available degrees of freedom. When L_{ds} is increased, the diversity in the end-to-end channel is increased, and at the same time, it becomes increasingly more difficult to force the end-to-end channel to be frequency-flat with a given number of relays and a given order for the relays' FIR filters. Fig. 4.5 shows that for $L_{\text{ds}} < 5$, the advantages of channel diversity prevails while for $L_{\text{ds}} > 5$, the limited degree of freedom is the dominant factor in deteriorating the performance of the frequency-flat CIR solution. Such a trade-off does not exist in the gradient steepest descent method as this method does not aim to force the end-to-end channel to be frequency-flat. As such, the performance of the latter method monotonically improves as L_{ds} is increased.

Chapter 5

Unsupervised User clustering and Power Allocation Design

In this chapter, we consider the problem of joint user clustering and power allocation in downlink transmission of NOMA-aided massive MIMO networks, where both co-located and distributed structures are considered for the massive MIMO system. We formulate a total transmit power minimization problem subject to SINR constraints at the users to jointly design the user clustering and power allocation coefficients. This study is the first attempt which considers a joint problem of power allocation and user clustering design for minimizing the total transmit power in both co-located and distributed massive MIMO-NOMA networks. We present a three-step solution for the formulated minimization, where we first employ a machine-learning-based method to perform the NOMA user clustering task, then we design the beamforming weights, and lastly, we solve a linear programming optimization solely for obtaining the power allocation coefficients.

The rest of this chapter is organized as follows: System description is presented in Section 5.1. In Section 5.2, the minimization problem is formulated and a solution for user clustering and power allocation is developed. Case study and Simulation results are discussed in Section 5.3.

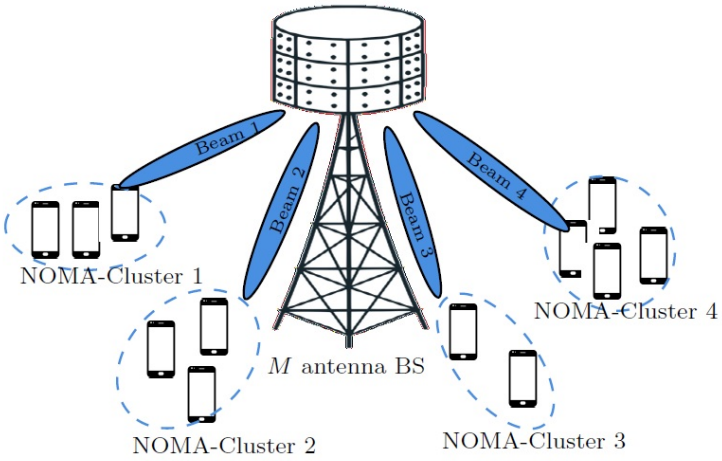

Figure 5.1: A co-located massive MIMO-NOMA setup where K_{t} single-antenna UEs are grouped into $R = 4$ clusters and M transmitting antennas are located at one BS.

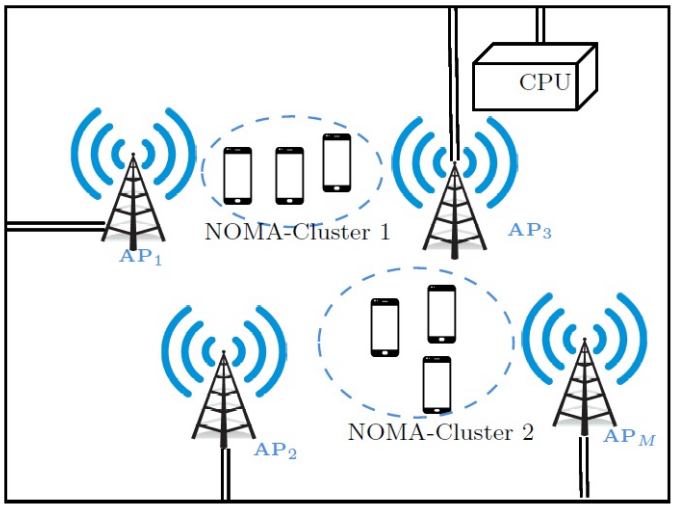

Figure 5.2: A distributed massive MIMO-NOMA setup where M single-antenna APs are serving K_{t} single-antennas UEs which are grouped into $R = 2$ clusters.

5.1 System Description

We consider downlink transmission in a NOMA-aided massive MIMO system with M transmit antennas at base station(s), BS(s), and a total of K_{t} single-antenna users, with $K_{\mathrm{t}} \ll M$. The M transmit antennas can be either co-located at one BS as the conventional multi-antenna BS, as shown in Fig. 5.1, or be distributed in a serving area, as depicted in Fig. 5.2. We refer to the former scenario with co-located antennas as a C-MIMO system and the latter with distributed antennas as a D-MIMO system. The cell-free massive MIMO system recently proposed is an example of such D-MIMO system, where the distributed M single-antenna access points are connected together via a CPU [8, 9, 24–26]. All APs simultaneously serve the K_t users. To simplify the notations, we hereafter use AP_m to refer to either the m-th antenna in the C-MIMO system, or the m-th AP in the D-MIMO system, for $m \in \mathcal{M} \triangleq \{1, \ldots, M\}$.

5.1.1 Clustering Model

For a NOMA-aided MIMO system, we assume the UEs are grouped into R clusters, where $R \leq K_{\mathrm{t}}$. Let $\mathcal{R} \triangleq \{1, 2, \ldots, R\}$. Data transmission to the UEs in each cluster are using the same MISO beam formed by the M antennas, but with different power allocations via the power-domain NOMA technique. Different clusters are served on separate beams. Let $\mathcal{K} = \{1, 2, ..., K_{\mathrm{t}}\}$. Let $\mathcal{K}_r$ denote the index set of UEs that belong to cluster r, with the size of the cluster being $K_r = |\mathcal{K}_r| \geq 1$, for $r \in \mathcal{R}$. We assume each UE only belongs to one cluster. Thus, we have $\mathcal{K}_r \cap \mathcal{K}_i = \emptyset$, $r \neq i$, $\forall i, r \in \mathcal{R}$, $\cup_{r=1}^{R} \mathcal{K}_r = \mathcal{K}$, and

$$\sum_{r=1}^{R} K_r = K_{\mathrm{t}}. \tag{5.1}$$

5.1.2 Channel Model

To simplify the analysis, the independent and identically distributed (i.i.d.) Rayleigh fading channel model is widely used in massive MIMO literature. However, in practical scenarios, the Rayleigh fading model cannot account for the effects of the LoS path between each

AP and each UE, as well as the correlation among non-LoS pathes which is caused by scattering clusters [100, 109]. LoS transmissions are commonly expected in ultra-dense applications of 5G networks where propagation distance is short. Therefore, we consider spatially correlated Rician fading channels in this work, where physically close UEs can experience highly correlated channels. It is known that spatial correlation can undermine the performance of MIMO systems. Hence, we later design a clustering algorithm which is able to deploy the correlation between channels as a feature to decide whether to integrate NOMA into the MIMO system and ameliorate an otherwise weak performance, or to keep using the existing spatial degrees of freedom without adopting NOMA clustering.

We assume the channels are frequency-flat and constant in each coherence time block. Let h_{mk} denote the complex channel coefficient at AP_m to UE_k, and $\mathbf{h}_k \triangleq [h_{1k}, \ldots, h_{Mk}]^T$ denote the channel vector from all APs to UE_k, $k \in \mathcal{K}$. In many 5G network deployment scenarios, such as densely deployed systems, the transmission propagation distance is short, and the channels commonly contain an LoS path. In this work, we consider the spatially correlated Rician channel model, consisting of both an LoS path and non-LoS components caused by multipath propagation. For UEs that are physically close by, their channels from the APs may be highly correlated to each other. In our case studies in Section 5.3, we consider two different Rician fading models for the C-MIMO system and the D-MIMO system, respectively [100, 109]. We assume APs have a perfect knowledge of CSI.

5.1.3 Signal Model

We assume downlink transmissions for the aforementioned NOMA-aided massive MIMO network where perfect CSI is available at AP node(s). In practice, such systems can operate in time division duplex (TDD) mode by transmitting uplink pilot sequences to estimate the CSI. However, it is a common practice to assume perfect knowledge of CSI at the system design stages, in virtue of garnering insights about the ultimate performance bounds of the designed algorithm [90, 91, 101]. In this section, we aim to develop a generalized signal model for NOMA-aided massive MIMO downlink transmissions which can be used for both D-MIMO and C-MIMO systems. Note that in our unified system model, only the employed channel model is slightly different as it was defined in (5.27) and (5.21) for the D-MIMO

systems and the C-MIMO systems, respectively.

Recall that UEs in the same cluster are served on the same downlink beam. The data of these UEs in the cluster are superimposed for transmission. Let w_{rm} denote the complex beamforming weight coefficient at AP_m for cluster r, and $\mathbf{w}_r \triangleq [w_{r1},\ w_{r2},\ \ldots,\ w_{rM}]^T$ denote the $M \times 1$ beamforming vector from all APs to cluster r. We assume $\mathbf{w}_r$ is normalized as $\|\mathbf{w}_r\| = 1$. The received signal at UE_k in cluster r from all M APs is given by

$$y_k = \underbrace{\sqrt{p_k}\mathbf{w}_r^H \mathbf{h}_k s_k}_{\text{desired signal}} + \underbrace{\mathbf{w}_r^H \mathbf{h}_k \sum_{j \neq k, j \in \mathcal{K}_r} \sqrt{p_j} s_j}_{\text{intra-cluster interference}} + \underbrace{\sum_{r'=1, r' \neq r}^{R} \mathbf{w}_{r'}^H \mathbf{h}_k \sum_{j \in \mathcal{K}_{r'}} \sqrt{p_j} s_j}_{\text{inter-cluster interference}} + n_k, \quad k \in \mathcal{K}_r, r \in \mathcal{R} \tag{5.2}$$

where s_k is the symbol intended for UE_k with $E\{s_k\} = 0$ and $E\{|s_k|^2\} = 1$, p_k denotes the total power from all APs allocated to UE_k, and $n_{rk} \sim \mathcal{CN}(0,\ 1)$ is the receiver additive Gaussian noise at UE_k in cluster r. We assume that all the users have the same noise power. The second term in (5.2) is the intra-cluster interference from signals intended for other UEs in the cluster who share the same beam, and the third term is the inter-cluster interference from other clusters who use different transmission beam.

By the power-domain NOMA technique, a user with a stronger channel is assigned a lower power, while a user with a weaker channel is assigned a higher power. Within each cluster, each user applies the SIC operation to successively decode and remove the interfering signals for those users whose channels are weaker than this user's channel. The remaining intra-cluster interference at the user consists of the signals of those users whose channels are stronger than this user. Without loss of generality, the users within each cluster r are indexed according to the decreasing order of their instantaneous beamed channel gains:[1]

$$\left|\mathbf{w}_r^H \mathbf{h}_k\right|^2 \geq \left|\mathbf{w}_r^H \mathbf{h}_j\right|^2 \quad \forall k, j \in \mathcal{K}_r \text{ and } k < j. \tag{5.3}$$

Given the ordering in (5.3), UE_k in cluster r can decode and remove interference from any UE_j, where $j > k$, $j, k \in \mathcal{K}_r$, by the SIC processing. As a result, after SIC, the

[1]User ordering problem is not trivial, and analyzing such methods is beyond the scope of this work.

post-processed signal at UE_k is given by

$$\tilde{y}_k = \underbrace{\sqrt{p_k}\mathbf{w}_r^H \mathbf{h}_k s_k}_{\text{desired signal}} + \underbrace{\mathbf{w}_r^H \mathbf{h}_k \sum_{j<k, j\in\mathcal{K}_r} \sqrt{p_j} s_j}_{\text{intra-cluster interference}} + \underbrace{\sum_{r'=1, r'\neq r}^{R} \mathbf{w}_{r'}^H \mathbf{h}_k \sum_{j\in\mathcal{K}_{r'}} \sqrt{p_j} s_j}_{\text{inter-cluster interference}} + n_k, \quad k \in \mathcal{K}_r, r \in \mathcal{R} \tag{5.4}$$

where the second term shows the residual interference from those users which have stronger channel than UE_k.

5.1.4 Expressions for SINR and Total Transmit Power

Let Γ_k^k denote the instantaneous SINR after the SIC operation at UE_k to detect symbol s_k. From (5.4), Γ_k^k is given by

$$\Gamma_k^k = \frac{p_k |\mathbf{w}_r^H \mathbf{h}_k|^2}{1 + |\mathbf{w}_r^H \mathbf{h}_k|^2 \sum_{j\in\mathcal{K}_r, j<k} p_j + \sum_{r'\neq r} |\mathbf{w}_{r'}^H \mathbf{h}_k|^2 \sum_{j\in\mathcal{K}_{r'}} p_j}, \qquad k \in \mathcal{K}_r, r \in \mathcal{R}. \tag{5.5}$$

The details of the derivation of (5.5) are given in Appendix C.2.

The total transmit power from all APs is given by

$$P_{\text{total}} = \sum_{k=1}^{K_{\text{t}}} p_k = \mathbf{1}^T \mathbf{p} \tag{5.6}$$

where $\mathbf{p} \triangleq [p_1, \ldots, p_{K_{\text{t}}}]^T$ is the power allocation vector.

5.1.5 Condition for Successful SIC Operation

Let $\bar{\Gamma}_k^j$ denote the instantaneous SINR at UE_k to decode s_j intended for UE_j, and let $\bar{\Gamma}_j^j$ denote the instantaneous SINR at UE_j to decode its own symbol s_j, $k, j \in \mathcal{K}_r$. We use subscript to indicate which user the signal is received at, and the superscript to indicate which user's symbol to be detected. Note that, different from Γ_k^k, both $\bar{\Gamma}_k^j$ and $\bar{\Gamma}_j^j$ are SINRs without SIC processing. From information theoretic perspective, the necessary condition for the SIC at UE_k to successfully decode s_j intended for UE_j in the same cluster is given

$$\bar{\Gamma}_k^j = \frac{p_j \, |\mathbf{w}_r^H \mathbf{h}_k|^2}{1 + |\mathbf{w}_r^H \mathbf{h}_k|^2 \sum_{k' \neq k, k' \in \mathcal{K}_r} p_{k'} + \sum_{r' \neq r} |\mathbf{w}_{r'}^H \mathbf{h}_k|^2 \sum_{k' \in \mathcal{K}_{r'}} p_{k'}}, \qquad \forall k, j \in \mathcal{K}_r. \quad (5.8)$$

$$\bar{\Gamma}_j^j = \frac{p_j \, |\mathbf{w}_r^H \mathbf{h}_j|^2}{1 + |\mathbf{w}_r^H \mathbf{h}_j|^2 \sum_{k' \neq k, k' \in \mathcal{K}_r} p_{k'} + \sum_{r' \neq r} |\mathbf{w}_{r'}^H \mathbf{h}_j|^2 \sum_{k' \in \mathcal{K}_{r'}} p_{k'}}, \qquad \forall j \in \mathcal{K}_r. \quad (5.9)$$

by [86]

$$\bar{\Gamma}_k^j \geq \bar{\Gamma}_j^j, \quad k < j, \; k, j \in \mathcal{K}_r, \; r \in \mathcal{R}. \quad (5.7)$$

It should be noted that the aforementioned SIC condition in (5.7) must be holds true at each UE_k for conducting the SIC operation. The instantaneous SINRs, $\bar{\Gamma}_k^j$ and $\bar{\Gamma}_j^j$, can be obtained using (5.2). Similar to (5.5), the instantaneous SINR of receiving data symbol s_j at UE_k in cluster r, $\bar{\Gamma}_k^j$, can be obtained by (5.8). Similarly, the instantaneous SINR of receiving data symbol s_j at UE_j in cluster r, $\bar{\Gamma}_j^j$, is given by (5.9). To further simplify the SIC condition in (5.7), using (5.8) and (5.9), we can write[2]

$$|\mathbf{w}_r^H \mathbf{h}_k|^2 a(\mathbf{p}_{-r}, \mathbf{h}_j) \geq |\mathbf{w}_r^H \mathbf{h}_j|^2 a(\mathbf{p}_{-r}, \mathbf{h}_k) \quad (5.10)$$

where for any given vector $\mathbf{h}$, we define $a(\mathbf{p}_{-r}, \mathbf{h}) \triangleq 1 + \sum_{r' \neq r} |\mathbf{w}_{r'}^H \mathbf{h}|^2 \sum_{k \in \mathcal{K}_{r'}} p_k$. The vector $\mathbf{p}_{-r}$ is defined as a subset of power allocation vector, $\mathbf{p}$, including those power coefficients which do not belong to cluster r, i.e., p_k for $k \in \{\mathcal{K}_{r'}\}_{r' \neq r}$. It is evident from (5.10) that successful SIC decoding depends on the values of the channel gains as well as the power allocation coefficients. An important point to highlight here is that the performance of the SIC process also depends on the accuracy of CSI estimations. That is, in practice, there exists some residual interference after performing SIC, which is known as the imperfections in SIC operation. However, as it is especially emphasized before, in this work we assume a perfect knowledge of CSI in order to focus on the ultimate performance bounds of our proposed solution. The effects of such imperfections can be considered in future work.

[2] See Appendix C.3 for derivation details.

5.2 Joint Design Optimization

We consider the joint design of beamforming, user clustering, and power allocation for NOMA-aided massive MIMO systems. Our goal is to minimize the total transmit power subject to the SINR requirement at each user. The user clusters can be specified by the number of clusters R, and the user association to each of R clusters $\{\mathcal{K}_r\}_{r=1}^{R}$. Thus, the joint optimization problem is formulated as follows

$$\min_{R,\{\mathcal{K}_r\},\{\mathbf{w}_r\},\mathbf{p}} \quad \sum_{k=1}^{K_\mathrm{t}} p_k \tag{5.11a}$$

$$\text{s.t.} \quad \Gamma_k^k \geq \gamma_k, \quad k \in \mathcal{K} \tag{5.11b}$$

$$\bar{\Gamma}_k^j \geq \bar{\Gamma}_j^j, \quad j > k,\ j,k \in \mathcal{K}_r, r \in \mathcal{R} \tag{5.11c}$$

$$p_k \geq 0, \quad k \in \mathcal{K} \tag{5.11d}$$

$$|\mathcal{K}_r| \geq 1, \quad r \in \mathcal{R} \tag{5.11e}$$

$$\mathcal{K}_r \cap \mathcal{K}_j = \emptyset, \quad r \neq j,\ r,j \in \mathcal{R} \tag{5.11f}$$

$$\sum_{r=1}^{R} |\mathcal{K}_r| = K_\mathrm{t} \tag{5.11g}$$

where γ_k denotes the SINR requirement at UE_k. The constraint in (5.11b) sets the SINR requirement for each UE. The constraint in (5.11c) ensures successful SIC operation in each cluster, and the clustering constraints are specified in (5.11e)–(5.11g).

The optimization problem in (5.11) is a mixed-integer program. The SINR expression is non-convex with respect to $\{\mathbf{w}_r\}$ and $\mathbf{p}$. This joint optimization problem is very challenging to solve. To make the problem more tractable, we consider a specific type of beamforming method and decompose the joint optimization problem in (5.11) into two subproblems: the clustering subproblem and the power allocation subproblem. We propose a three-step procedure to solve them:

1. We develop a novel fast user clustering algorithm based on an unsupervised learning technique, utilizing the correlation characteristics of the user channels.

2. We consider a zero-forcing (ZF) beamformer scheme and design the beamforming coefficients for a given clustering set.

3. Lastly, for the given clustering solution and the beamforming method, we reformulate the minimization problem in (5.11) into a linear programming problem for power allocation optimization.

5.2.1 Learning-Based User Clustering Approach

We propose a novel learning-based clustering algorithm. It utilizes the correlation among users' channel vectors, $\{\mathbf{h}_k\}_{k=1}^{K_\mathrm{t}}$ to form a metric to make the user clustering decision. It is known that with multi-antenna transmitters, the spatial domain can be explored to separate users' data. However, in a correlated propagation environment, users' channels may be highly correlated. This limits the degrees of freedom that can be explored at the transmitters to eliminate interference among users. As a result, only relying on transmit beamforming may result in poor performance. To address this, for the correlated users, we leverage NOMA techniques to group them in the same cluster and use the power domain to separation their data. The virtue of our proposed method is the ability to automatically switch between using the spatial domain MIMO (SD-MIMO) and power domain NOMA-MIMO for multi-user transmission, depending on the availability of degrees of freedom presented in the system. That is, upon lack of enough spatial dimension, our proposed clustering algorithm assembles more correlated users into the same cluster to operate on the so-called NOMA-aided mode. In contrast, when enough degrees of freedom are available on spatial dimension through the usage of a massive number of APs, our proposed algorithm tends to stay in the conventional SD-MIMO mode and deploy the spatial dimension to serve fewer users on each separate beam. In other words, our proposed clustering algorithm is able to automatically decide on the number clusters, R, and on the size of each cluster, K_r.

We develop a clustering algorithm based on a modified version of the unsupervised mean-shift clustering to form NOMA clusters. The mean-shift clustering [110–113] is a mode-seeking iterative procedure, in which the local maxima (modes) in data distribution are found by using a window kernel density estimation technique. As a result, the mean-shift algorithm is able to determine the cluster members as well as the number of clusters for a given set of data points.

Selection of a suitable feature space makes a significant contribution toward the reduction of dimensionality in the mean-shift clustering. Motivated by the fact that the correlation among channels can undermine the transmit beamforming performance of MIMO systems, we span a feature space based on the normalized complex-valued channel vectors, i.e., $\mathbf{x}_k = \frac{\mathbf{h}_k}{\|\mathbf{h}_k\|}$ for $k \in \mathcal{K}$. In other words, we aim to group users into the same clusters based on how correlated their channels are. With such clustering, we can employ the NOMA technique within each cluster to separate users using the power domain and to overcome the limitation of spatial dimension for user separation due to channel correlation in the conventional SD-MIMO systems. Specifically, correlated users inside each cluster perform the SIC operation to remove an otherwise irremovable intra-cluster interference from other users with weaker channels.

Let $\mathcal{X} = \{\mathbf{x}_k : \ \mathbf{x}_k = \frac{\mathbf{h}_k}{\|\mathbf{h}_k\|} e^{-j\angle h_{1k}}, \ \ \forall k \in \mathcal{K}\}$ denote a M-dimensional phased aligned data set[3]. In the context of kernel density estimation for the mean-shift algorithm, the notion of kernel *profile* is often used for symmetric kernels. For given kernel $F(\cdot)$ and variable vector $\mathbf{x}$, the kernel profile $f(\cdot)$ satisfies $F(\mathbf{x}) = \beta \ k(\|\mathbf{x}\|^2)$ for the non-negative entries of the vector, $x \geq 0$ [113], where the constant β serves as the normalization factor such that $F(\mathbf{x})$ integrates to one. Using the kernel profile concept, we can define a kernel density estimator (KDE) as

$$\psi(\mathbf{x}) = \frac{\beta}{K_t \lambda^M} \sum_{k=1}^{K_t} \ f\left(\| \frac{\mathbf{x} - \mathbf{x}_k}{\lambda} \|^2 \right) \tag{5.12}$$

where $\lambda > 0$ denotes the kernel estimator bandwidth which affects the shape of the final KDE function. The underlying principle of the mean-shift algorithm is to find the modes[4] of the KDE function in (5.12). For a large kernel bandwidth, the KDE surface tends to have less peaks, i.e, a fewer number of clusters, whereas with a smaller kernel bandwidth, the KDE results in more clusters. In its original format, the mean-shift clustering chooses a centroid point from the set of data points, $\mathbf{t} \in \mathcal{X}$, and computes a new centroid, $\mathbf{t}^{\text{new}}$, as

[3]We later propose the usage of the inner product operation as a criterion for our proposed clustering task. Therefore, we must precede by a caveat on redefining the co-phased data points. To do so, one can use a simple phase-alignment operation on data points such that the first entry of each data point vector has zero phase.

[4]The modes are the points that make the gradient of the density function equals to zero.

follows

$$\mathbf{t}^{\text{new}} = \frac{\sum\limits_{\mathbf{x}_i \in \mathcal{X}_r} \mathbf{x}_i \; f\left(\| \frac{\mathbf{x}_i - \mathbf{t}}{\lambda} \|^2 \right)}{\sum\limits_{\mathbf{x}_i \in \mathcal{X}_r} f\left(\| \frac{\mathbf{x}_i - \mathbf{t}}{\lambda} \|^2 \right)}. \tag{5.13}$$

Here, *mean-shift* refers to the shifts of the current centroid toward the new centroid, $\mathbf{t}^{\text{new}}$.

In the original mean-shift clustering, the clustering criterion is defined based on the Euclidean distance between data point vectors using the norm operation. This metric is not applicable to our problem to indicate the correlation level of two channels [5]. To tackle this problem, we propose a modified version of the mean-shift clustering method which resorts to the inner product operation to measure the correlation among data points instead of using the Euclidean distance measurements[6].

For a correlation threshold of τ, $(0 < \tau \leq 1)$, let $\mathcal{X}_r$ signify the set of those data points associated with the cluster r which satisfy the condition $|\mathbf{t}_r^H \mathbf{x}_k| > \tau$ i.e., $\mathcal{X}_r = \{\mathbf{x}_k : |\mathbf{t}_r^H \mathbf{x}_k| > \tau, \; \forall \mathbf{x}_k \in \mathcal{X}\}$, where $\mathbf{t}_r$ is a measure of normalized centroid of current points owned by cluster r. As such, we measure the inner product between any data point and the normalized cluster center of each cluster r to determine whether or not that data point can be associated to the cluster r. Consequently, with this modification, the conventional kernel estimation expression in (5.13) is given by

$$\bar{\mathbf{t}}_r = \frac{\sum\limits_{\mathbf{x}_k \in \mathcal{X}_r} \mathbf{x}_k \, f\left(\frac{1 - |\mathbf{t}_r^H \, \mathbf{x}_k|}{1 - \tau} \right)}{\sum\limits_{\mathbf{x}_k \in \mathcal{X}_r} f\left(\frac{1 - |\mathbf{t}_r^H \, \mathbf{x}_k|}{1 - \tau} \right)}, \tag{5.14}$$

$$\mathbf{t}_r^{\text{new}} \triangleq \frac{\bar{\mathbf{t}}_r}{\|\bar{\mathbf{t}}_r\|} \tag{5.15}$$

where $\mathbf{t}_r^{\text{new}}$ is the new normalized centroid, and the Gaussian kernel profile $f(\cdot)$ is used.

[5] The metric is sensitive to phase shift perturbations when complex-valued data points are being used.

[6] The aforementioned drawback of the original mean-shift clustering can be easily seen by considering two highly correlated vectors, $\mathbf{t}$ and $\mathbf{x}$, which only differ on some phase shift of θ, as $\mathbf{t} = \mathbf{h}$ and $\mathbf{x} = \mathbf{h}e^{j\theta}$. The conventional mean-shift method fails to correctly capture the correlation between these two vectors as the Euclidean distance $\|\mathbf{t} - \mathbf{x}\|$ is a function of θ, i.e., $|1 - e^{j\theta}|$. However, in our proposed method, the dot product operation, $\frac{|\mathbf{t}^H \mathbf{x}|}{\|\mathbf{t}\| \|\mathbf{x}\|}$, can accurately capture the correlation between any two vectors.

Note that in (5.14), the "*distance* " between data points is measured by the correlation threshold level τ, while in (5.13) this distance is determined by the Euclidean scale of the kernel bandwidth λ.

The main steps of the proposed mean-shift clustering algorithm are summarized in Algorithm 3. Note that as the number of APs (M) increases, the dimension of data point vectors increases and the correlation of two different channel vectors (data points) decreases. As a result, as the degrees of freedom increases with M, the proposed algorithm can automatically form more clusters with fewer users per cluster to use the spatial domain, instead of power domain, to separate the users.

Algorithm 3 The correlation-based mean-shift clustering

1. Define each data point as $\mathbf{x}_k = \frac{\mathbf{h}_k}{\|\mathbf{h}_k\|} e^{-j\angle h_{1k}}$ for $k \in \mathcal{K}$; let $\mathcal{X} = \{\mathbf{x}_k, k \in \mathcal{K}\}$; Set the correlation threshold $\tau \in (0, 1]$; Set the iteration threshold ϵ.
2. Let $\mathcal{T} \subseteq \mathcal{X}$ denote the cluster center. Initialize $\mathcal{T} = \mathcal{X}$, and set $r = 1$.
3. Set $l = 0$, and randomly select a centroid point $\mathbf{t}_r^{(l)} \in \mathcal{T}$.
4. Obtain the set of data points associated to cluster r, such that $\mathcal{X}_r = \{\mathbf{x}_k : \ |\mathbf{t}_r^H \mathbf{x}_k| > \tau, \ \forall \mathbf{x}_k \in \mathcal{X}\}$.
5. Update centroid: For $\mathcal{X}_r$, compute

$$\mathbf{t}_r^{(l+1)} = \frac{\sum_{\mathbf{x}_k \in \mathcal{X}_r} \mathbf{x}_k \, f(\frac{1-|\mathbf{t}_r^{(l)H} \mathbf{x}_k|}{1-\tau})}{\sum_{\mathbf{x}_k \in \mathcal{X}_r} f(\frac{1-|\mathbf{t}_r^{(l)H} \mathbf{x}_k|}{1-\tau})},$$

   and $\mathbf{t}_r^{(l+1)} \leftarrow \frac{\mathbf{t}_r^{(l+1)}}{\|\mathbf{t}_r^{(l+1)}\|}$.
6. If $|\mathbf{t}_r^{(l)} - \mathbf{t}_r^{(l+1)}| > \epsilon$, set $l \leftarrow l + 1$, and go to Steps 4; Otherwise, go to Step 7.
7. Update $\mathcal{T} \leftarrow \mathcal{T} \backslash \mathcal{X}_r$. If $\mathcal{T} \neq \emptyset$, then set $r \leftarrow r + 1$ and go to Step 3. Otherwise, clustering is complete.

5.2.2 Complexity Analysis of Proposed Clustering Algorithm

In this section, the complexity of the proposed modified mean-shift clustering algorithm is analyzed. The computation of the inner product between $\mathbf{t}_r$ and $\mathbf{x}_k$ in (5.14) is M flops with a total of $K_t M$ flops for all data points. The complexity of computing all centroids is cK_tM

where $c > 0$ is a constant. If I_a denotes the average number of iterations required to obtain the data points associated with cluster r, i.e., $\mathcal{X}_r$, then the complexity of the proposed mean-shift clustering algorithm amounts to $\mathcal{O}(I_a M K_{\mathrm{t}})$. We will show through numerical simulations that the average number of required iterations, I_a, is a approximately constant value which is independent from the problem dimension M. In summary, the complexity of the proposed algorithm is $\mathcal{O}(K_t M)$ which is linear with respect to the problem dimension.

5.2.3 Beamforming Design

To determine beamforming weights $\{\mathbf{w}_r\}$, we use the ZF beamforming approach to suppress the inter-cluster interferences. The ZF beamformer can nullify the interference among clusters by projecting the received signal onto the interference null space. Since the same beam is used for each cluster, to effectively design the ZF beamformer, we propose to use form the desired beam using the centroid $\mathbf{t}_r$ in each cluster r, and project it into the interference null space.

Let us first define the channel matrix $\mathbf{H}_r \in \mathbb{C}^{M \times K_r}$, whose columns are the collection of user channels in the cluster r, $\{\mathbf{h}_k\}$ for $k \in \mathcal{K}_r$. Now, for the cluster r, we define its inter cluster interference matrix, $\mathbf{H}_{-r}$, as

$$\mathbf{H}_{-r} \triangleq [\mathbf{H}_1,\ \ldots,\ \mathbf{H}_{r-1},\ \mathbf{H}_{r+1},\ \ldots,\ \mathbf{H}_R] \in \mathbb{C}^{M \times (K_{\mathrm{t}} - K_r)}. \tag{5.16}$$

The basis for the null space of $\mathbf{H}_{-r}$ can be found through the QR-decomposition of $\mathbf{H}_{-r}$ [114]. Specifically, the QR-decomposition of $\mathbf{H}_{-r}$ is given by

$$\mathbf{H}_{-r} = \mathbf{Q}_r\, \mathbf{R}_r = \left[\mathbf{Q}_r^{'},\ \mathbf{Q}_r^{''}\right] \begin{bmatrix} \mathbf{R}_r^{'} \\ \mathbf{0} \end{bmatrix} = \mathbf{Q}_r^{'}\, \mathbf{R}_r^{'}, \tag{5.17}$$

where $\mathbf{Q}_r^{''}$ aaawis the basis matrix of the null space of $\mathbf{H}_{-r}$, i.e., $\mathbf{H}_{-r}^H\, \mathbf{Q}_r^{''} = \mathbf{0}$. If the basis matrix of the null space, $\mathbf{Q}_r^{''}$ is not empty, the ZF beamforming vector is given by

$$\mathbf{w}_r^{\mathrm{ZF}} = \frac{\bar{\mathbf{P}}_r\, \mathbf{t}_r}{\|\bar{\mathbf{P}}_r\, \mathbf{t}_r\|}, \qquad \text{for} \quad r \in \mathcal{R}, \tag{5.18}$$

where $\bar{\mathbf{P}}_r \triangleq \mathbf{Q}_r^{''}(\mathbf{Q}_r^{''H}\mathbf{Q}_r^{''})^{-1}\mathbf{Q}_r^{''H}$. If $\mathbf{Q}_r^{''}$, is empty, e.g. there is no inter-cluster interference, and there is only one cluster in the system, we resort to a simple maximum ratio transmission

(MRT) beamforming design as

$$\mathbf{w}_r^{\mathrm{MRT}} = \frac{\mathbf{t}_r}{\|\mathbf{t}_r\|}, \quad \forall r \in \mathcal{R}. \tag{5.19}$$

5.2.4 Power Allocation Problem

Given the clustering solution $\{\mathcal{K}_r\}_{r=1}^{R}$ and beamforming weights $\{\mathbf{w}_r\}_{r=1}^{R}$ obtained in Sections 5.2.1 and 5.2.3, respectively, we can rewrite the power allocation optimization problem in (5.11) as the following power minimization problem

$$\begin{aligned} \min_{\{p_k\}} \quad & \sum_{k=1}^{K_{\mathrm{t}}} p_k \\ \text{s.t.} \quad & \Gamma_k^k \geq \gamma_k, \qquad \forall k \in \mathcal{K}_r, r \in \mathcal{R} \\ & \frac{|\mathbf{w}_r^H \mathbf{h}_k|^2}{|\mathbf{w}_r^H \mathbf{h}_j|^2} a(\mathbf{p}_{-r}, \mathbf{h}_j) \geq \ a(\mathbf{p}_{-r}, \mathbf{h}_k), \ \ \forall j > k, \ j,k \in \mathcal{K}_r, \\ & p_k \geq 0, \qquad \forall k \in \mathcal{K} \end{aligned} \tag{5.20}$$

Note that both the objective and constraint functions in the minimization problem in (5.20) are linear with respect to power variables $\{\mathbf{p}_k\}$, therefore, the problem is a linear program (LP). To solve (5.20), LP solvers such as CVX [115], or linprog function in MATLAB Optimization Toolbox can be employed to obtain the set of power allocation coefficients for each user, $\{p_k\}_{k=1}^{K_{\mathrm{t}}}$.

5.3 Case Studies

In this section, we provide two case studies for C-MIMO and D-MIMO, respectively, to evaluate the performance of the proposed NOMA-aided systems for downlink transmission. We focus on spatially correlated Rician channel model among UEs, which presents limited degrees of freedom in the system. The corresponding channel models are different in the two cases, due to the different scenarios considered.

In both case studies, we set the carrier frequency of $f_c = 2.3$ GHz. For the channel path loss model, we assume the path loss exponent of 3.5, and the shadowing standard deviation of 8 dB. For the noise figure of NF = 6 dB, and the transmission bandwidth of $B = 20$

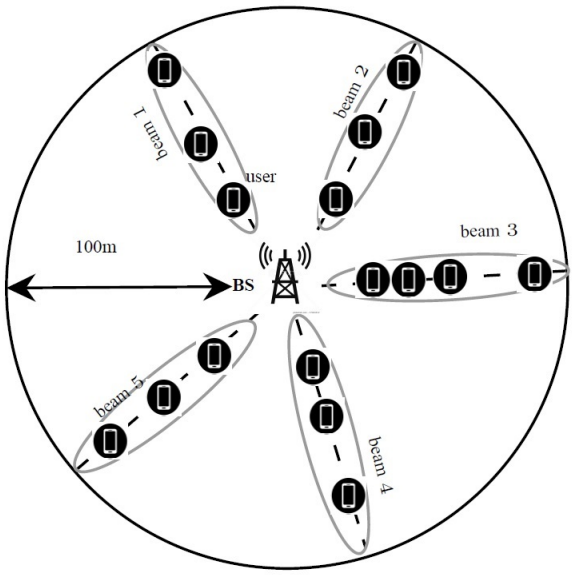

Figure 5.3: Illustration of C-MIMO Scenario.

MHz, the receiver noise power is $\sigma^2 = -174 + 10\log(B) + \text{NF} = -94\text{dBm}$. In practical situations, when the nodes are in close vicinity of each other, they experience correlated shadow fading [8]. Therefore, we also consider the correlated shadow fading model proposed in [8, 116].

5.3.1 Case 1: Co-located MIMO Scenario

We consider a propagation environment in which a central BS with a linear array of M antennas, positioned at the origin, serves $K_{\text{t}} = 16$ UEs positioned within a circle of radius 100 m, centered at the BS, as shown in Fig. 5.3. The UEs are randomly located at five fixed angles from the BS with random distance to the BS. Note that this scenario can be seen as an extremely correlated environment where the BS cannot rely on spatial domain to separate those UEs positioned at the same direction from the BS.

5.3.2 Correlated Rician Channel Model for C-MIMO:

Let $\mathbf{\Delta}_k$ denote an $M \times M$ correlation matrix due to the BS's M antennas seen at UE_k. The (m_i, m_j)-th element is defined as $[\mathbf{\Delta}_k]_{m_i,m_j} = r_k^{|m_i - m_j|}$, for a given correlation coefficient r_k at UE_k, for $0 < r_k \leq 1$. Also, let d_k denote the distance (in meter) between the BS

and the UE$_k$. Assuming the LoS path between the BS and UE$_k$, we consider the Rician model for the channel vector $\mathbf{h}_k$, with the Rician K-factor $K(d_k)$. The Rician K-factor $K(d_k)$ describes the energy ratio between the LoS and non-LoS components and defined as $K(d_k) = 10^{1.3-0.003d_k}$. Therefore, the Rician channel model is given by [117]

$$\mathbf{h}_k = \bar{h}_k \, \boldsymbol{\alpha}_k(\phi_k, \theta_k) + \boldsymbol{\Delta}_k^{\frac{1}{2}} \, \mathbf{g}_k, \qquad \forall m, \;\; \forall k \tag{5.21}$$

where $\bar{h}_k \, \boldsymbol{\alpha}_k(\phi_k, \theta_k)$ is the LoS component with $\boldsymbol{\alpha}_k(\phi_k, \theta_k)$ being the $M \times 1$ array steering vector, and $\boldsymbol{\Delta}_k^{\frac{1}{2}} \, \mathbf{g}_k$ term represents the non-Los component with $\mathbf{g}_k \sim \mathcal{CN}(\mathbf{0}, \, \beta_k \mathbf{I}_M)$ capturing scattered components from the BS to UE$_k$ in which the variance β_k is defined as

$$\beta_k = \frac{1}{1 + K(d_k)} \mathrm{PL}_k, \tag{5.22}$$

where PL$_k$ denotes the path loss (PL) between the BS and UE$_k$ and it can be modeled (in dB) based on COST 231 Walfish-Ikegami model as [109]

$$\mathrm{PL}_k = -35.4 - 26 \log_{10}(\frac{d_k}{1 \text{ m}}) + 20 \log_{10}(f_c) + F_k. \tag{5.23}$$

In (5.23), f_c is the carrier frequency in MHz, and F_k represents the shadow fading coefficient. The LoS component in (5.21) comprises of a large scale fading component $\bar{h}_k$

$$\bar{h}_k = \sqrt{\frac{K(d_k)}{1 + K(d_k)}} \sqrt{\mathrm{PL}_k}, \tag{5.24}$$

and the array steering vector defined as follow for an array with an arbitrary geometry [118]

$$\boldsymbol{\alpha}_k(\phi_k, \theta_k) = [e^{j\mathbf{k}(\phi_k, \theta_k)^T \mathbf{u}_1}, \ldots, e^{j\mathbf{k}(\phi_k, \theta_k)^T \mathbf{u}_M}]^T \tag{5.25}$$

where the angles ϕ_k and θ_k denote the azimuth and the elevation angles from the BS to UE$_k$, respectively, the vector $\mathbf{u}_m = [x, y, z]^T$ is the 3D Cartesian coordinate of the m-th antenna, and $\mathbf{k}(\phi_k, \theta_k)$ denotes the phase shift vector experienced at the location $\mathbf{u}_m$ and it is given by

$$\mathbf{k}(\phi_k, \theta_k) = \frac{2\pi}{\lambda_c} \begin{bmatrix} \cos(\theta_k) \cos(\phi_k) \\ \cos(\theta_k) \sin(\phi_k) \\ \sin(\theta_k) \end{bmatrix} \tag{5.26}$$

where λ_c is the corresponding wavelength of f_c.

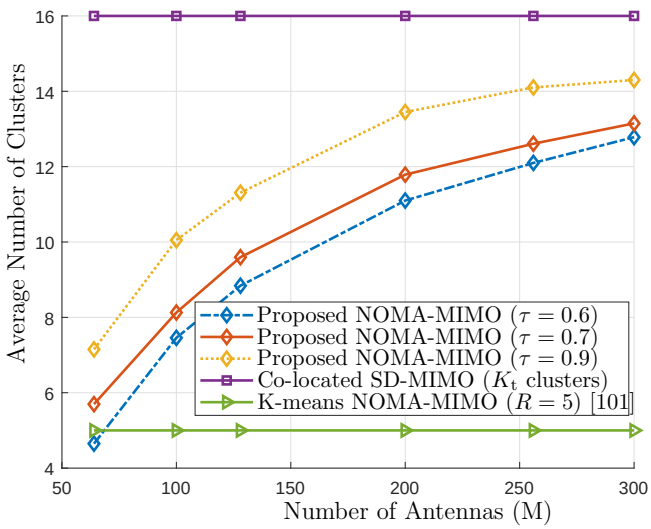

Figure 5.4: Average number of clusters versus number of antennas for $K_t = 16$, runs= 100, and 20 user drops.

5.3.3 Simulation Results for C-MIMO Case

For the purpose of comparison, we have considered two other methods:1) a no-clustering approach that only relies on spatial domain (SD) to separate all users via conventional transmit beamforming, we name it as SD-MIMO; 2) the clustering method proposed in [101]. The authors in [101] proposed a machine-learning-based approach, i.e., K-means clustering algorithm, for user clustering and power allocation problem for a NOMA-aided MIMO system. However, their approach is not applicable to our problem because of two reasons: First, as opposed to our proposed mean-shift clustering, the K-means clustering in [101] cannot separate the users based on their channel correlation because it uses Euclidean distance measures as criteria to group the users. Moreover, K-means clustering requires the pre-knowledge of number of clusters, R, whereas the mean-shift clustering does not; Second, the power allocation design proposed in [101] is based on a sum-rate maximization problem subject to power constraints while in our design a total power minimization subject to SINR constraints is considered. As a result, we consider the K-means-based clustering method proposed in [101] in conjunction with our proposed power allocation solution, where this scheme hereafter is referred to as K-means NOMA-MIMO scheme. In the following simulations, UEs' locations are generated for 20 drops and 100 independent Monte Carlo channel realizations for each user drop.

Fig. 5.4 shows the average number clusters versus the number of antennas (M) under different clustering methods. For the proposed NOMA-MIMO different values of the correlation threshold τ is considered. Note that our proposed clustering method in NOMA-MIMO is able to estimate the number of clusters R, while the K-means NOMA-MIMO requires to know the number of clusters R. We consider the K-means NOMA-MIMO scheme with $R = 5$ clusters. In practice, the K-means NOMA-MIMO scheme requires an extra step to estimate R. As it can be seen from Fig. 5.4, the average number of clusters in our proposed NOMA-MIMO, gradually increases as the number of antennas grows. The reason is that by increasing the number of antennas there are more degrees of freedom to separate users' channels. In this case, users' channels are less correlated and they no longer need to be clustered together. Instead, they can rely on beamforming to separate each other. Note that a higher number of clusters amounts to having fewer UEs at each cluster. In fact, such behavior potentially gives our proposed clustering algorithm the ability to automatically decide on the best mode of transmissions, namely NOMA-aided mode, or the conventional SD-MIMO mode. In other words, our proposed NOMA-MIMO scheme groups automatically trade off between the available degrees of freedom in the spatial domain and the power domain for multi-user transmission. In contrast, the K-means NOMA-MIMO scheme resorts to a fixed number of clusters and cannot adapt to the available degrees of freedom which is provided by a massive number of antennas at BS.

In Fig. 5.5, we evaluate the probability of having feasible solutions for power allocation problem (5.20) versus M for an SINR threshold of $\gamma_k = 5$ dB, $k \in \mathcal{K}$. As it was expected, with the considered highly correlated channel scenario, the SD-MIMO method demonstrates a very poor feasibility performance due to its inability to distinguish between users which are seen on the same beam direction. It can also be seen from Fig. 5.5 that the K-means NOMA-MIMO approach achieves an even worse feasibility performance than the SD-MIMO method at higher values of M. Such poor performance can be explained by the fact that K-means NOMA-MIMO clustering method resorts to the Euclidean distance to group the users which does not reflect the existing correlations among the users. As a result, the feasibility performance of the K-means NOMA-MIMO method suffers from both miss-clustering of the users, and utilizing a fixed number of clusters throughout all values of

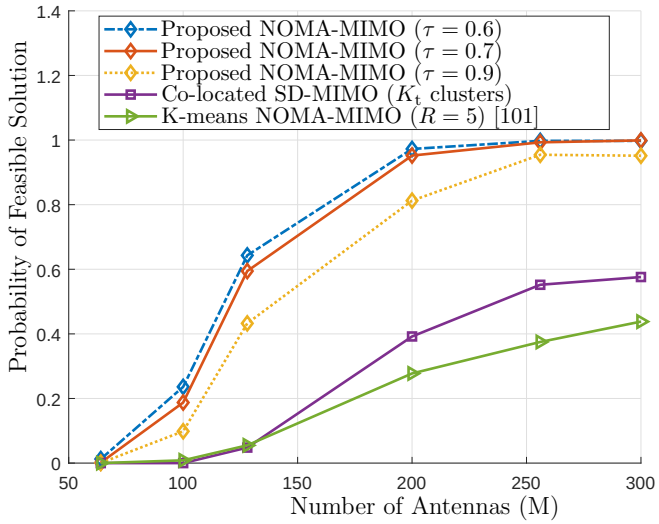

Figure 5.5: Comparison of probability of having feasible solution versus number of antennas for $\gamma_k = 5$ dB, $K_t = 16$, runs= 100, and 20 user drops are used.

M. Fig. 5.5 shows that our proposed NOMA-aided solution can significantly improve the feasibility performance for the highly correlated channel scenario in the C-MIMO systems. This is because our method effectively utilizes the power domain to separate users, leading to higher percentage of feasible solutions for the original problem (5.11). Moreover, as it is compared in Fig. 5.5, higher values of correlation thresholds, e.g. $\tau = 0.9$ can slightly undermine the viability of the proposed NOMA-MIMO in terms of feasibility performance. The reason for that is when higher values of correlation thresholds are used, less UEs are grouped into clusters, which means the performance of the proposed method moves closer to that of the SD-MIMO system in which each user is assigned to a separate cluster/beam.

The total transmit power consumption of the C-MIMO systems versus the number of antennas at BS for the proposed NOMA-MIMO scheme is shown in Fig. 5.6, where our proposed method with $\tau = 0.6, 0.7, 0.9$ is compared with the SD-MIMO scheme and K-means NOMA-MIMO method with $R = 5$ clusters. As we expect, increasing the number of antennas at BS yields more array gain, therefore, it diminishes the overall total transmit power in all methods. We observe from Fig. 5.6 that, in the correlated setups, the proposed NOMA-MIMO scheme can significantly outperform the conventional SD-MIMO and the K-means NOMA-MIMO systems. For instance, our proposed NOMA-MIMO method with $\tau = 0.7$ can approximately improve the performance of the conventional SD-MIMO systems by

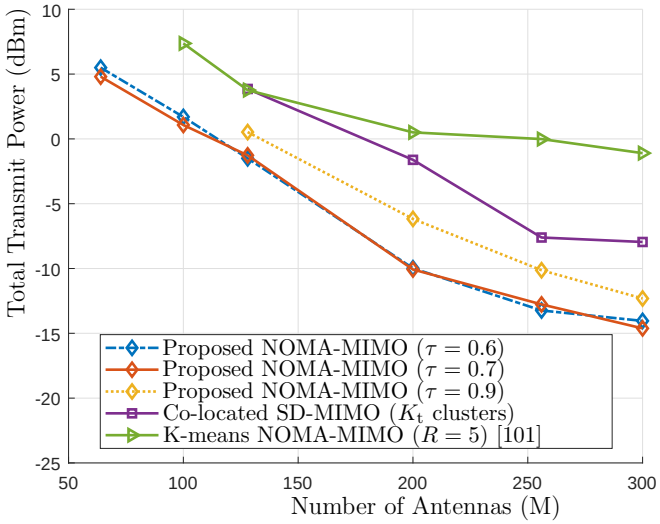

Figure 5.6: Total transmit power versus number of antennas in C-MIMO systems for $\gamma_k = 5$ dB, $K_t = 16$, runs= 100, and 20 user drops.

5 dB. The reason for such superior performance is the ability of the proposed NOMA-aided method to efficiently group the most correlated UEs into clusters and to remove the intra-cluster interference of those UEs which have weaker channel conditions from those which have stronger channel conditions. It is also evident from Fig. 5.6 that when the number of antennas increases the K-means NOMA-MIMO scheme has the worse performance among all compared methods, simply because of its inability to adaptively take advantage of the existing degrees of freedom.

Fig. 5.7 demonstrates the average number of iterations required for the convergence of our proposed mean-shift clustering algorithm with respect to the number of antennas. It is revealed that our proposed NOMA-MIMO algorithm requires only $2-3$ iterations for convergence. Moreover, the number of iterations does not grow with M.

5.3.4 Case 2: Distributed MIMO Scenario

In this case study, we consider a cell-free massive MIMO scenario where M distributed AP nodes are simultaneously serving $K_t = 10$ UEs. It is well-known that the distributed antenna architectures can outperform the co-located ones due to the diversity gains. As a result, an otherwise correlated scenario for C-MIMO systems is typically appeared as uncorrelated for the D-MIMO systems. However, there are still practical scenarios in which

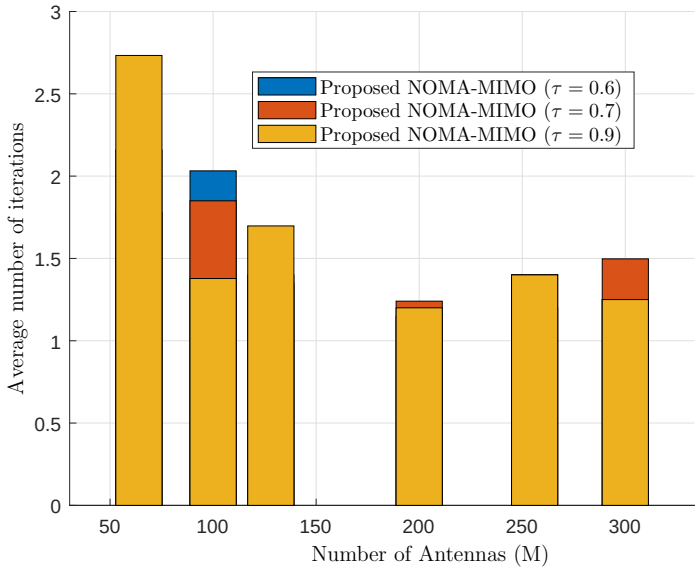

Figure 5.7: Average number of iterations versus number of antennas in C-MIMO systems.

the topology leads to correlated user channels. One example is multiple APs are distributed over a one-dimensional space (e.g. in a train, or on a corridor). We consider a range of length 200 meter, with M APs and $K_{\mathrm{t}} = 10$ UEs. The APs are equally spaced over the range and UEs are randomly dropped. To avoid near-field, there is a minimum distance from UEs to each AP.

5.3.5 Correlated Rician Channel Model for D-MIMO:

The Rician fading channel coefficients between AP_m and UE_k, for $m = 1, 2, \ldots, M$ and $k = 1, 2, \ldots, K_{\mathrm{t}}$, can be modeled as [109]

$$h_{mk} = \bar{h}_{mk}\, e^{j\phi_{mk}} + g_{mk}, \qquad \forall m, \;\; \forall k \tag{5.27}$$

where the first term represents LoS component, with $\bar{h}_{mk} \geq 0$ and ϕ_{mk} being the channel gain and the LoS angle between AP_m and UE_k, respectively. In (5.27), $g_{mk} \sim \mathcal{CN}(0, \beta_{mk})$ is the non-LoS component. Note that $|h_{mk}|$ in (5.27) is Rician distributed with the K-factor K_{mk} between AP_m and UE_k. The Rician K-factor is defined as $K(d_{mk}) = 10^{1.3-0.003 d_{mk}}$, with d_{mk} denoting the distance (in meter) between AP_m and UE_k. Given K-factor $K(d_{mk})$,

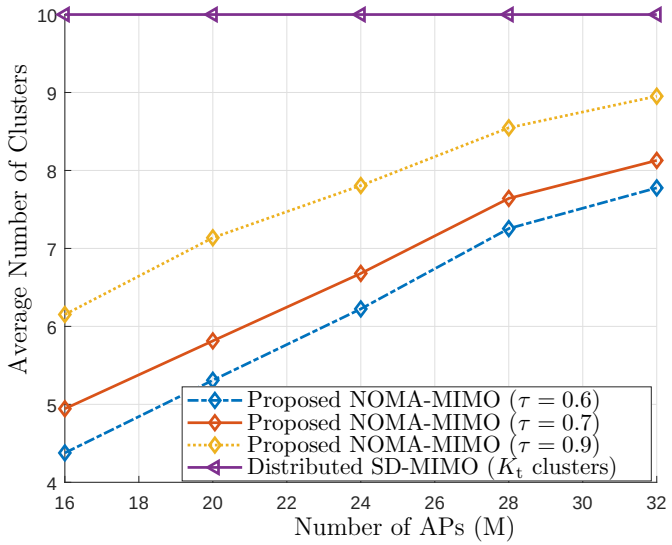

Figure 5.8: Average number of clusters versus number of APs for D-MIMO scenarios with $\gamma_k = 5$ dB, and $K_t = 10$.

we have

$$\bar{h}_{mk} = \sqrt{\frac{K(d_{mk})}{1 + K(d_{mk})}} \sqrt{\text{PL}_{mk}} \tag{5.28}$$

$$\beta_{mk} = \frac{1}{1 + K(d_{mk})} \text{PL}_{mk}, \tag{5.29}$$

where PL_{mk} denotes the PL between AP_m and UE_k. In our simulation, it is modeled based on COST 231 Walfish-Ikegami model as follows [109]

$$\text{PL}_{mk} = -35.4 - 26 \log_{10}(\frac{d_{mk}}{1 \text{ m}}) + 20 \log_{10}(f_c) + F_{mk}, \tag{5.30}$$

where F_{mk} represents the shadow fading between AP_m and UE_k.

For the following simulations, 20 random drops of UEs' locations with 100 independent Monte Carlo channel realizations for each drop are used.

5.3.6 Simulation Results for D-MIMO Case

Fig. 5.8 plots the average number of clusters formed by our proposed in our propose NOMA-MIMO algorithm versus the number of APs. A similar trend as in Fig. 5.4 for the C-MIMO

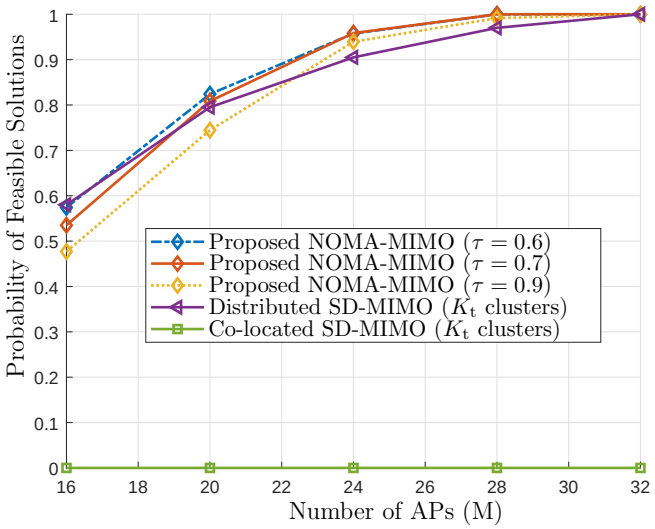

Figure 5.9: Probability of feasible solution versus the number of APs in D-MIMO systems for $\gamma_k = 5$ dB, and $K_t = 10$.

scenario can be seen here in Fig. 5.8. That is, as the number of APs increases, more clusters are formed by the proposed clustering method. Our proposed solution is able to take advantage of the increased degrees of freedom to use spatial dimension to serve users. This behavior indicates an automatic trade-off between two modes, the NOMA-aided mode and the SD-MIMO mode.

In Fig. 5.9, we show the percentage of having feasible solutions to problem (5.20) versus the number of APs for SINR requirement of $\gamma_k = 5$ dB. It is clear that for this 1D scenario, while the co-located SD-MIMO method fails to separate users via spatial domain. The proposed NOMA-MIMO and the distributed SD-MIMO achieve a satisfactory feasibility performance when M is large enough. For example, the feasible solutions can be obtained at 90 percent of time when $M > 24$. Also, the performance difference in the proposed algorithm appears to be insensitive to different threshold value τ.

Fig. 5.10 shows the average transmit power versus the number of APs under the NOMA MIMO method and the SD-MIMO method for SINR requirement $\gamma_k = 5$ dB. The proposed NOMA-based method has noticeable performance improvement over the SD-MIMO approach. It can be seen that as M is increased from 16 to 32, the proposed NOMA-MIMO can outperform the SD-MIMO by 1.6 dB to 5.9 dB. The reason for the superior performance of our proposed method is the ability of NOMA to suppress the intra-cluster interferences

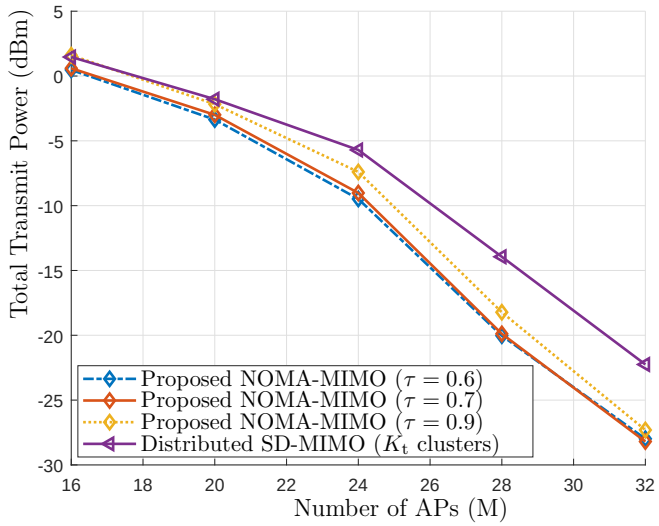

Figure 5.10: Total transmit power versus number of APs in D-MIMO systems for $\gamma_k = 5$ dB, and $K_t = 10$.

among clusters by performing SIC operations at the receiving terminals. Therefore, it is evident that the combination of the two techniques, NOMA and transmit beamforming, is highly beneficial for the correlated channel scenario.

Chapter 6

Conclusions and Future Work

6.1 Conclusions

In Chapter 3 of this dissertation, we studied the joint problem of power allocation and distributed beamforming for a multi-carrier asynchronous two-way multi-relay network. We considered two OFDM-based transceivers communicating with the aid of multiple amplify-and-forward relay nodes. Since each relaying path has its own propagation delay, the end-to-end channel manifests multipath propagation phenomenon, and is thus prone to ISI at high data rates. To tackle this ISI, the transceivers are equipped with OFDM to equalize the end-to-end channel. We formulated the total transmit power minimization problem s subject to the rate constraints at the transceivers. We proposed an optimal solution which enjoys a simple semi-closed form for the distributed beamforming weight vector and sub-carrier powers at the transceivers. We showed that at the optimum, the end-to-end CIR has only one non-zero tap, which means our solution leads to a relay selection scheme in which only those relays contributing to this optimal tap can stay active. We provided a complexity analysis for our proposed method and demonstrated that the worst-case complexity of our algorithm is linear with respect to the number of relays. Our numerical results revealed that the proposed algorithm dramatically outperforms the best-relay selection scheme when the number of relay nodes is grown large. In particular, the proposed scheme consumes 1 dB less power, as compared with the best-relay selection technique, when the number of relays is 10, while for 100 relays, the power saving offered by our solution is more than 2.5 dB.

In Chapter 4, we considered a multi-carrier two-way relaying network consisting of two

OFDM-based transceivers and multiple filter-and-forward relays. We studied the design of joint subcarrier power allocation and relaying distributed beamforming coefficients to minimize the total transmit power minimization subject to data rate constraints. We proposed two algorithms to solve this minimization: The first solution was obtained by employing a gradient steepest descent technique, whose performance is sensitive to the choice of the initial points. Thus, we proposed a second solution in which we imposed an additional constraint on the original minimization problem such that at the optimum, an otherwise frequency-selective end-to-end channel is forced to become a flat-frequency channel. As a result of adding such constraint, a fast and simple semi-closed-form solution was rigorously derived for the total power minimization problem. By relaxing the original optimization, we further derived a lower bound for the optimization cost function that served as a benchmark to evaluate the performances of the proposed algorithms. We also conducted a complexity analysis for our second solution. Finally, by comparison with the lower bound, our simulation results showed that both algorithms are within 3 dB from the optimal (unknown) performance. Moreover, the superiority of the proposed algorithm was demonstrated against two existing methods for similar networks.

In Chapter 5, we investigated the joint problem of user clustering and power allocation design for the downlink transmissions of NOMA-aided massive MIMO networks. We considered networks which consist of multiple single-antenna users and multiple access points where the access points can be arranged either in a distributed manner or a co-located fashion. We formulated a total transmit power minimization subject to the SINR constraints at the users. We proposed a three-step solution to this problem. In the first step, we proposed an unsupervised novel clustering algorithm which deploys the correlation among users' channels to group the *correlated users* into the same cluster. Our proposed clustering method benefits from the ability to automatically switch between using the spatial dimension, in conventional MIMO systems, and the power dimension, in NOMA-aided MIMO systems. In the second step, we designed a ZF beamforming based on our clustering results to effectively suppress the inter-cluster interference. In the final step, for given clustering and beamforming designs, we rewrote the original minimization as a linear programming optimization and solved this problem to obtain power allocation coefficients. We further

performed the complexity analysis of our proposed clustering algorithm and showed that the worst-complexity is linear with respect to the number of access points. We evaluated and compared the performance of our proposed solution with that of the existing work through numerical simulations for two specials cases, namely the co-located scenario and the distributed scenario. We showed that our proposed method, compared to the existing methods, can greatly improve the feasibility probability and substantially decrease the total transmit power in highly-correlated environments.

6.2 Future work

In the following, we present some possible extensions of the research work studied in this dissertation:

- In this dissertation, we assumed that the perfect knowledge of CSI is known in the problems studied in Chapters 3, 4, and 5. However, in practical scenarios, this assumption is often unrealistic. Therefore, studying the aforementioned problems under unknown/uncertain CSI can be an interesting practical extension for future work.

- In Chapters 3 and 4, we considered multi-carrier two-way relay networks with two transceivers, under the assumption that no direct link exists between the transceivers. Therefore, as future work, one can consider a more challenging problem assuming the existence of a direct link between transceivers, which in turn, leads to a more complicated system model and optimization problem.

- In this dissertation, we aimed to minimize the total transmit power in order to design the power allocation and beamforming coefficients in two-way relay networks (Chapters 3 and 4), and to find a solution for user clustering and power allocation problem in NOMA-aided massive MIMO networks (Chapter 5). However, a similar design can be studied under different optimization problems. For example, minimizing the mean square error, minimizing the average transmit power at certain nodes, maximizing the energy efficiency, or maximizing the sum-rates can be considered as the objective functions.

- In this dissertation, we focused on wireless networks with single-antenna user nodes. An interesting extension to our study can be taking into account multi-antenna user nodes and study the detrimental effects of the antenna correlations on the overall performance in more practical scenarios.

- In Chapter 5, we studied the problem of user clustering and power allocation design to minimize the total transmit power in NOMA-aided massive MIMO systems. We proposed an unsupervised clustering algorithm which leads to a suboptimal clustering solution. Another possible interesting problem to consider can be using analytical methods to approach the joint optimization problem of Chapter 5, as an attempt to find an optimal solution for the clustering problem.

Bibliography

[1] S. Kiani, S. Shahbazpanahi, M. Dong, and G. Boudreau, "Power-optimal distributed beamforming for multi-carrier asynchronous bidirectional relay networks," *IEEE Transactions on Signal and Information Processing over Networks*, pp. 1–1, 2020.

[2] S. KianiHarchegani, S. ShahbazPanahi, M. Dong, and G. Boudreau, "Distributed equalization and power allocation for multi-carrier bidirectional filter-and-forward relay networks," in *ICASSP 2020 - 2020 IEEE International Conference on Acoustics, Speech and Signal Processing (ICASSP)*, 2020, pp. 4752–4756.

[3] S. KianiHarchehgani, S. ShahbazPanahi, M. Dong, and G. Boudreau, "Joint power allocation and distributed beamforming design for multi-carrier asynchronous two-way relay networks," in *2019 IEEE 20th International Workshop on Signal Processing Advances in Wireless Communications (SPAWC)*, 2019, pp. 1–5.

[4] J. G. Andrews, S. Buzzi, W. Choi, S. V. Hanly, A. Lozano, A. C. Soong, and J. C. Zhang, "What will 5G be?" *IEEE Journal on selected areas in communications*, vol. 32, no. 6, pp. 1065–1082, 2014.

[5] T. L. Marzetta, "Noncooperative cellular wireless with unlimited numbers of base station antennas," *IEEE Trans. Wireless Commun.*, vol. 9, pp. 3590–3600, Nov. 2010.

[6] L. Lu, G. Y. Li, A. L. Swindlehurst, A. Ashikhmin, and R. Zhang, "An overview of massive MIMO: Benefits and challenges," *IEEE Journal of Selected Topics in Signal Processing*, vol. 8, no. 5, pp. 742–758, 2014.

[7] Shidong Zhou, Ming Zhao, Xibin Xu, Jing Wang, and Yan Yao, "Distributed wireless communication system: a new architecture for future public wireless access," *IEEE Communications Magazine*, vol. 41, no. 3, pp. 108–113, 2003.

[8] H. Q. Ngo, A. Ashikhmin, H. Yang, E. G. Larsson, and T. L. Marzetta, "Cell-free massive MIMO versus small cells," *IEEE Transactions on Wireless Communications*, vol. 16, pp. 1834–1850, March 2017.

[9] Z. Chen and E. Bjornson, "Channel hardening and favorable propagation in cell-free massive MIMO with stochastic geometry," *IEEE Transactions on Communications*, pp. 1–1, 2018.

[10] L. Dai, B. Wang, Y. Yuan, S. Han, C. I, and Z. Wang, "Non-orthogonal multiple access for 5G: solutions, challenges, opportunities, and future research trends," *IEEE Communications Magazine*, vol. 53, no. 9, pp. 74–81, 2015.

[11] X. Chen, Z. Zhang, C. Zhong, R. Jia, and D. W. K. Ng, "Fully non-orthogonal communication for massive access," *IEEE Transactions on Communications*, vol. 66, no. 4, pp. 1717–1731, 2018.

[12] S. M. R. Islam, N. Avazov, O. A. Dobre, and K. Kwak, "Power-domain non-orthogonal multiple access (NOMA) 5G systems: Potentials and challenges," *IEEE Communications Surveys Tutorials*, vol. 19, no. 2, pp. 721–742, 2017.

[13] R. Vahidnia and S. ShahbazPanahi, "Single-carrier equalization for asynchronous two-way relay networks," *IEEE Trans. Signal Process.*, vol. 62, pp. 5793– 5808, Nov. 2014.

[14] C. K. Ho, R. Zhang, and Y. . Liang, "Two-way relaying over OFDM: Optimized tone permutation and power allocation," in *2008 IEEE International Conference on Communications*, May 2008, pp. 3908–3912.

[15] Y. Jang, E. Jeong, and Y. H. Lee, "A two-step approach to power allocation for OFDM signals over two-way amplify-and-forward relay," *IEEE Transactions on Signal Processing*, vol. 58, no. 4, pp. 2426–2430, April 2010.

[16] R. Vahidnia and S. Shahbazpanahi, "Multi-carrier asynchronous bi-directional relay networks: Joint subcarrier power allocation and network beamforming," *IEEE Trans. Wireless Commun.*, vol. 12, pp. 3796–3812, Aug. 2013.

[17] S. Shahbazpanahi and M. Dong, "A semi-closed-form solution to optimal distributed beamforming for two-way relay networks," *IEEE Trans. Signal Process.*, vol. 60, no. 3, pp. 1511–1516, Mar. 2012.

[18] Y.-W. Liang, A. Ikhlef, W. Gerstacker, and R. Schober, "Cooperative filter-and-forward beamforming for frequency-selective channels with equalization," *IEEE Trans. Wireless Commun.*, vol. 10, pp. 228 –239, Jan. 2011.

[19] Y. Liang, A. Ikhlef, W. Gerstacker, and R. Schober, "Filter-and-forward beamforming for multiple multi-antenna relays," in *Communications and Networking in China (CHINACOM), 2010 5th International ICST Conference on*, aug. 2010, pp. 1 –8.

[20] H. Chen, A. Gershman, and S. Shahbazpanahi, "Filter-and-forward distributed beamforming in relay networks with frequency selective fading," *IEEE Trans. Signal Process.*, vol. 58, no. 3, pp. 1251–1262, Mar. 2010.

[21] H. Chen, S. ShahbazPanahi, and A. B. Gershman, "Filter-and-forward distributed beamforming for two-way relay networks in frequency selective channels," *IEEE Trans. Signal Process.*, vol. 60, pp. 1927–1941, Mar. 2012.

[22] A. Goldsmith, *Wireless Communications*. Cambridge University Press, 2005.

[23] E. G. Larsson, O. Edfors, F. Tufvesson, and T. L. Marzetta, "Massive mimo for next generation wireless systems," *IEEE Communications Magazine*, vol. 52, no. 2, pp. 186–195, 2014.

[24] E. Nayebi, A. Ashikhmin, T. L. Marzetta, H. Yang, and B. D. Rao, "Precoding and power optimization in cell-free massive MIMO systems," *IEEE Transactions on Wireless Communications*, vol. 16, pp. 4445–4459, July 2017.

[25] H. Q. Ngo, L. Tran, T. Q. Duong, M. Matthaiou, and E. G. Larsson, "On the total energy efficiency of cell-free massive MIMO," *IEEE Transactions on Green Communications and Networking*, vol. 2, pp. 25–39, March 2018.

[26] T. M. Hoang, H. Q. Ngo, T. Q. Duong, H. D. Tuan, and A. Marshall, "Cell-free massive mimo networks: Optimal power control against active eavesdropping," *IEEE Transactions on Communications*, pp. 1–1, 2018.

[27] M. S. Ali, H. Tabassum, and E. Hossain, "Dynamic user clustering and power allocation for uplink and downlink non-orthogonal multiple access (NOMA) systems," *IEEE Access*, vol. 4, pp. 6325–6343, 2016.

[28] Y. Liu, M. Elkashlan, Z. Ding, and G. K. Karagiannidis, "Fairness of user clustering in MIMO non-orthogonal multiple access systems," *IEEE Communications Letters*, vol. 20, no. 7, pp. 1465–1468, 2016.

[29] M. Zeng, A. Yadav, O. A. Dobre, G. I. Tsiropoulos, and H. V. Poor, "Capacity comparison between MIMO-NOMA and MIMO-OMA with multiple users in a cluster," *IEEE Journal on Selected Areas in Communications*, vol. 35, no. 10, pp. 2413–2424, 2017.

[30] C. I, C. Rowell, S. Han, Z. Xu, G. Li, and Z. Pan, "Toward green and soft: a 5G perspective," *IEEE Communications Magazine*, vol. 52, no. 2, pp. 66–73, 2014.

[31] Z. Hasan, H. Boostanimehr, and V. K. Bhargava, "Green cellular networks: A survey, some research issues and challenges," *IEEE Communications Surveys Tutorials*, vol. 13, no. 4, pp. 524–540, 2011.

[32] J. Hoydis, M. Kobayashi, and M. Debbah, "Green small-cell networks," *IEEE Vehicular Technology Magazine*, vol. 6, no. 1, pp. 37–43, 2011.

[33] G. Zheng, K.-K. Wong, A. Paulraj, and B. Ottersten, "Collaborative-relay beamforming with perfect CSI: Optimum and distributed implementation," *IEEE Signal Processing Letters*, vol. 16, pp. 257 –260, Apr. 2009.

[34] V. Havary-Nassab, S. Shahbazpanahi, and A. Grami, "Optimal distributed beamforming for two-way relay networks," *IEEE Trans. Signal Process.*, vol. 58, no. 3, pp. 1238–1250, Mar. 2010.

[35] H. Wang, Q. Yin, and X. Xia, "Distributed beamforming for physical-layer security of two-way relay networks," *IEEE Transactions on Signal Processing*, vol. 60, no. 7, pp. 3532–3545, July 2012.

[36] T. Koike-Akino, P. Popovski, and V. Tarokh, "Optimized constellations for two-way wireless relaying with physical network coding," *IEEE J. Sel. Areas Commun.*, vol. 27, pp. 773–787, june 2009.

[37] R. Vahidnia, S. Shahbazpanahi, and A. Minasian, "Pre-channel equalization and distributed beamforming in asynchronous single-carrier bi-directional relay networks," *IEEE Trans. Signal Process.*, vol. 64, pp. 3968–3983, Aug 2016.

[38] F. Eshaghian-Dorcheh and S. Shahbazpanahi, "Jointly optimal pre- and post-channel equalization and distributed beamforming in asynchronous bidirectional relay networks," *IEEE Transactions on Signal Processing*, vol. 65, pp. 4593–4608, Sept 2017.

[39] R. AliHemmati and S. Shahbazpanahi, "Sum-rate optimal network beamforming and subcarrier power allocation for multi-carrier asynchronous two-way relay networks," *IEEE Trans. Signal Process.*, vol. 63, pp. 4129–4143, Aug 2015.

[40] J. Mirzaei and S. ShahbazPanahi, "On achievable SNR region for multi-user multi-carrier asynchronous bidirectional relay networks," *IEEE Trans. Wireless Commun.*, vol. 14, pp. 3219–3230, Jun. 2015.

[41] Y.-U. Jang, E.-R. Jeong, and Y. Lee, "A two-step approach to power allocation for OFDM signals over two-way amplify-and-forward relay," *IEEE Trans. Signal Process.*, vol. 58, pp. 2426–2430, Apr. 2010.

[42] Y.-W. Liang, A. Ikhlef, W. Gerstacker, and R. Schober, "Two-way filter-and-forward beamforming for frequency-selective channels," *IEEE Trans. Wireless Commun.*, vol. 10, pp. 4172–4183, Dec. 2011.

[43] R. AliHemmati, S. ShahbazPanahi, and M. Dong, "Joint spectrum sharing and power allocation for OFDM-based two-way relaying," *IEEE Trans. Wireless Commun.*, vol. 14, no. 6, pp. 3294–3308, Jun. 2015.

[44] S. Bastanirad, S. Shahbazpanahi, and A. Grami, "Jointly optimal distributed beamforming and power control in asynchronous two-way relay networks," in *2015 49th Asilomar Conference on Signals, Systems and Computers*, Nov 2015, pp. 963–967.

[45] D. Kim, J. Seo, and Y. Sung, "Filter-and-forward transparent relay design for OFDM systems," *IEEE Transactions on Vehicular Technology*, vol. 62, no. 9, pp. 4392–4407, Nov 2013.

[46] D. Kim, Y. Sung, and J. Chung, "Filter-and-forward relay design for MIMO-OFDM systems," *IEEE Transactions on Communications*, vol. 62, no. 7, pp. 2329–2339, July 2014.

[47] L. Lu, G. Y. Li, A. L. Swindlehurst, A. Ashikhmin, and R. Zhang, "An overview of massive MIMO: Benefits and challenges," *IEEE Journal of Selected Topics in Signal Processing*, vol. 8, no. 5, pp. 742–758, 2014.

[48] H. V. Cheng, E. Bjornson, and E. G. Larsson, "Performance analysis of NOMA in training-based multiuser MIMO systems," *IEEE Transactions on Wireless Communications*, vol. 17, no. 1, pp. 372–385, 2018.

[49] Z. Ding, F. Adachi, and H. V. Poor, "The application of MIMO to non-orthogonal multiple access," *IEEE Transactions on Wireless Communications*, vol. 15, no. 1, pp. 537–552, 2016.

[50] Z. Ding and H. V. Poor, "Design of massive-MIMO-NOMA with limited feedback," *IEEE Signal Processing Letters*, vol. 23, no. 5, pp. 629–633, 2016.

[51] M. F. Hanif, Z. Ding, T. Ratnarajah, and G. K. Karagiannidis, "A minorization-maximization method for optimizing sum rate in the downlink of non-orthogonal multiple access systems," *IEEE Transactions on Signal Processing*, vol. 64, no. 1, pp. 76–88, 2016.

[52] J. Choi, "Minimum power multicast beamforming with superposition coding for multiresolution broadcast and application to NOMA systems," *IEEE Transactions on Communications*, vol. 63, no. 3, pp. 791–800, 2015.

[53] W. A. Al-Hussaibi and F. H. Ali, "Efficient user clustering, receive antenna selection, and power allocation algorithms for massive MIMO-NOMA systems," *IEEE Access*, vol. 7, pp. 31 865–31 882, 2019.

[54] M. Iwamura, H. Takahashi, and S. Nagata, "Relay technology in LTE-advanced," *NTT Docomo Technical Journal*, vol. 12, no. 2, pp. 29–36, 2010.

[55] S. W. Peters, A. Y. Panah, K. T. Truong, and R. W. Heath, "Relay architectures for 3GPP LTE-advanced," *EURASIP Journal on Wireless Communications and Networking*, vol. 2009, no. 1, pp. 618–787, 2009.

[56] Z. Yang and M. Dong, "Low-complexity coordinated relay beamforming design for multi-cluster relay interference networks," *IEEE Transactions on Wireless Communications*, vol. 18, no. 4, pp. 2215–2228, 2019.

[57] J. Chen and M. Dong, "Multi-antenna relay network beamforming design for multiuser peer-to-peer communications," in *2014 IEEE International Conference on Acoustics, Speech and Signal Processing (ICASSP)*, 2014, pp. 7594–7598.

[58] W. Li and M. Dong, "Distributed alamouti relay beamforming scheme in multiuser relay networks," *IEEE Signal Processing Letters*, vol. 24, no. 10, pp. 1527–1531, 2017.

[59] B. Rankov and A. Wittneben, "Spectral efficient protocols for half-duplex fading relay channels," *IEEE J. Sel. Areas Commun.*, vol. 25, no. 2, pp. 379–389, Feb. 2007.

[60] S. Atapattu, Y. Jing, H. Jiang, and C. Tellambura, "Relay selection schemes and performance analysis approximations for two-way networks," *IEEE Trans. Commun.*, vol. 61, no. 3, pp. 987–998, Mar. 2013.

[61] B. Rankov and A. Wittneben, "Achievable rate regions for the two-way relay channel," in *2006 IEEE International Symposium on Information Theory*, July 2006, pp. 1668–1672.

[62] W. Li and M. Dong, "Joint relay beamforming and receiver processing for multi-way multi-antenna relay networks," *IEEE Transactions on Communications*, vol. 66, no. 2, pp. 576–588, 2018.

[63] M. Chang, M. Dong, F. Zuo, and S. ShahbazPanahi, "Joint subchannel pairing and power allocation in multichannel MABC-based two-way relaying," *IEEE Trans. Wireless Commun.*, vol. 15, pp. 620–632, Jan. 2016.

[64] M. Dong and S. Shahbazpanahi, "Optimal spectrum sharing and power allocation for OFDM-based two-way relaying," in *Proc. ICASSP'10*, Mar. 2010, pp. 3310–3313.

[65] C. Yuen, W. H. Chin, Y. L. Guan, W. Chen, and T. Tee, "Bi-directional multi-antenna relay communications with wireless network coding," in *Proc. IEEE Vehicular Technology Conference, (VTC-Spring 2008)*, Singapore, May 2008, pp. 1385–1388.

[66] T. Cui and J. Kliewer, "Memoryless relay strategies for two-way relay channels: Performance analysis and optimization," in *Proc. IEEE International Conference on Communications*, Beijing, May 2008, pp. 1139–1143.

[67] S. Shahbazpanahi, "A semi-closed-form solution to optimal decentralized beamforming for two-way relay networks," in *Proc. IEEE CAMSAP'09*, Aruba, Dec. 13-16 2009, pp. 101–104.

[68] R. Vaze and R. W. Heath, "Optimal amplify and forward strategy for two-way relay channel with multiple relays," in *Proc. IEEE ITW 2009*, Volos, Greece, Jun. 12–10, 2009, pp. 181–185.

[69] T. P. Do, J. S. Wang, I. Song, and Y. H. Kim, "Joint relay selection and power allocation for two-way relaying with physical layer network coding," *IEEE Communications Letters*, vol. 17, no. 2, pp. 301–304, 2013.

[70] S. Talwar and S. Shahbazpanahi, "A total power minimization approach to relay selection for two-way relay networks," in *Conference Record of the Forty Sixth Asilomar Conference on Signals, Systems and Computers (ASILOMAR), 2012*, 2012, pp. 2001–2005.

[71] S. Bastanirad, S. Shahbazpanahi, R. Rahimi, and A. Grami, "On total transmission power minimization approach to decentralized beamforming in single-carrier asynchronous bidirectional relay-assisted communication networks," *IEEE Access*, vol. 7, pp. 30 966–30 979, 2019.

[72] R. Rahimi and S. ShahbazPanahi, "Asynchronous two-way MIMO relaying: A multi-relay scenario," *IEEE Transactions on Wireless Communications*, vol. 17, no. 7, pp. 4270–4287, 2018.

[73] R. Rahimi and S. ShahbazPanahi, "Multiple peer-to-peer bidirectional cooperative communications using massive mimo relays," in *2018 IEEE International Conference on Acoustics, Speech and Signal Processing (ICASSP)*, 2018, pp. 3784–3788.

[74] T. C. Ng and W. Yu, "Joint optimization of relay strategies and resource allocations in cooperative cellular networks," *IEEE Journal on Selected Areas in Communications*, vol. 25, no. 2, pp. 328–339, February 2007.

[75] W. Dang, M. Tao, H. Mu, and J. Huang, "Subcarrier-pair based resource allocation for cooperative multi-relay OFDM systems," *IEEE Transactions on Wireless Communications*, vol. 9, no. 5, pp. 1640–1649, May 2010.

[76] T. Miyajima, H. Teshiromori, and Y. Sugitani, "Adaptive self-interference suppression for full duplex filter-and-forward relaying," *IEEE Wireless Communications Letters*, vol. 9, no. 10, pp. 1701–1704, 2020.

[77] Z. Chen, Z. Ding, X. Dai, and G. K. Karagiannidis, "On the application of quasi-degradation to MISO-NOMA downlink," *IEEE Transactions on Signal Processing*, vol. 64, no. 23, pp. 6174–6189, 2016.

[78] W. Shin, M. Vaezi, B. Lee, D. J. Love, J. Lee, and H. V. Poor, "Coordinated beamforming for multi-cell MIMO-NOMA," *IEEE Communications Letters*, vol. 21, no. 1, pp. 84–87, 2017.

[79] Z. Ding, R. Schober, and H. V. Poor, "A general MIMO framework for NOMA downlink and uplink transmission based on signal alignment," *IEEE Transactions on Wireless Communications*, vol. 15, no. 6, pp. 4438–4454, 2016.

[80] D. Zhang, Z. Zhou, C. Xu, Y. Zhang, J. Rodriguez, and T. Sato, "Capacity analysis of NOMA with mmwave massive MIMO systems," *IEEE Journal on Selected Areas in Communications*, vol. 35, no. 7, pp. 1606–1618, 2017.

[81] S. Kusaladharma, W. P. Zhu, W. Ajib, and G. Amarasuriya, "Achievable rate analysis of NOMA in cell-free massive MIMO: A stochastic geometry approach," in *ICC 2019 - 2019 IEEE International Conference on Communications (ICC)*, 2019, pp. 1–6.

[82] Y. Li and G. A. Aruma Baduge, "NOMA-aided cell-free massive MIMO systems," *IEEE Wireless Communications Letters*, vol. 7, no. 6, pp. 950–953, 2018.

[83] D. L. Galappaththige and G. Amarasuriya, "NOMA-aided cell-free massive MIMO with underlay spectrum-sharing," in *ICC 2020 - 2020 IEEE International Conference on Communications (ICC)*, 2020, pp. 1–6.

[84] F. Rezaei, C. Tellambura, A. A. Tadaion, and A. R. Heidarpour, "Rate analysis of cell-free massive MIMO-NOMA with three linear precoders," *IEEE Transactions on Communications*, vol. 68, no. 6, pp. 3480–3494, 2020.

[85] M. Bashar, K. Cumanan, A. G. Burr, H. Q. Ngo, L. Hanzo, and P. Xiao, "NOMA-OMA mode selection-based cell-free massive MIMO," in *ICC 2019 - 2019 IEEE International Conference on Communications (ICC)*, 2019, pp. 1–6.

[86] H. V. Cheng, E. Bjornson, and E. G. Larsson, "Performance analysis of NOMA in training-based multiuser MIMO systems," *IEEE Transactions on Wireless Communications*, vol. 17, no. 1, pp. 372–385, 2018.

[87] K. Senel, H. V. Cheng, E. Bjornson, and E. G. Larsson, "NOMA versus massive MIMO in rayleigh fading," in *2019 IEEE 20th International Workshop on Signal Processing Advances in Wireless Communications (SPAWC)*, 2019, pp. 1–5.

[88] K. Senel, H. V. Cheng, E. Björnson, and E. G. Larsson, "What role can NOMA play in massive MIMO?" *IEEE Journal of Selected Topics in Signal Processing*, vol. 13, no. 3, pp. 597–611, 2019.

[89] J. Cui, Y. Liu, Z. Ding, P. Fan, and A. Nallanathan, "Optimal user scheduling and power allocation for millimeter wave NOMA systems," *IEEE Transactions on Wireless Communications*, vol. 17, no. 3, pp. 1502–1517, 2018.

[90] L. Zhu, J. Zhang, Z. Xiao, X. Cao, D. O. Wu, and X. Xia, "Joint power control and beamforming for uplink non-orthogonal multiple access in 5G millimeter-wave communications," *IEEE Transactions on Wireless Communications*, vol. 17, no. 9, pp. 6177–6189, 2018.

[91] B. Wang, L. Dai, Z. Wang, N. Ge, and S. Zhou, "Spectrum and energy-efficient beamspace MIMO-NOMA for millimeter-wave communications using lens antenna array," *IEEE Journal on Selected Areas in Communications*, vol. 35, no. 10, pp. 2370–2382, 2017.

[92] O. Elijah, C. Y. Leow, T. A. Rahman, S. Nunoo, and S. Z. Iliya, "A comprehensive survey of pilot contamination in massive MIMO-5G system," *IEEE Communications Surveys Tutorials*, vol. 18, no. 2, pp. 905–923, 2016.

[93] E. G. Larsson and H. V. Poor, "Joint beamforming and broadcasting in massive MIMO," *IEEE Transactions on Wireless Communications*, vol. 15, no. 4, pp. 3058–3070, 2016.

[94] J. Jose, A. Ashikhmin, T. L. Marzetta, and S. Vishwanath, "Pilot contamination and precoding in multi-cell tdd systems," *IEEE Transactions on Wireless Communications*, vol. 10, no. 8, pp. 2640–2651, 2011.

[95] K. Selvam and K. Kumar, "A novel energy-efficient resource allocation algorithm for non-orthogonal multiple access (NOMA) based M2M communication," in *2020 7th International Conference on Signal Processing and Integrated Networks (SPIN)*, 2020, pp. 776–780.

[96] F. Fang, H. Zhang, J. Cheng, and V. C. M. Leung, "Energy-efficient resource allocation for downlink non-orthogonal multiple access network," *IEEE Transactions on Communications*, vol. 64, no. 9, pp. 3722–3732, 2016.

[97] S. Lee and J. H. Lee, "Joint user scheduling and power allocation for energy efficient millimeter wave NOMA systems with random beamforming," in *2018 IEEE 88th Vehicular Technology Conference (VTC-Fall)*, 2018, pp. 1–5.

[98] D. Zhai, R. Zhang, L. Cai, B. Li, and Y. Jiang, "Energy-efficient user scheduling and power allocation for NOMA-based wireless networks with massive IoT devices," *IEEE Internet of Things Journal*, vol. 5, no. 3, pp. 1857–1868, 2018.

[99] X. Zhang, X. Zhu, and H. Zhu, "Joint user clustering and multi-dimensional resource allocation in downlink MIMO–NOMA networks," *IEEE Access*, vol. 7, pp. 81 783–81 793, 2019.

[100] X. Hu, C. Zhong, X. Chen, W. Xu, and Z. Zhang, "Cluster grouping and power control for angle-domain mmwave MIMO NOMA systems," *IEEE Journal of Selected Topics in Signal Processing*, vol. 13, no. 5, pp. 1167–1180, 2019.

[101] J. Cui, Z. Ding, P. Fan, and N. Al-Dhahir, "Unsupervised machine learning-based user clustering in millimeter-wave-NOMA systems," *IEEE Transactions on Wireless Communications*, vol. 17, no. 11, pp. 7425–7440, 2018.

[102] S. Boyd and L. Vandenberghe, *Convex Optimization*. New York, NY: Cambridge University Press, 2004.

[103] A. V. Oppenheim and R. W. Schafer, *Discrete-Time Signal Processing*. Pearson Education, 2014.

[104] J. Mirzaee, S. ShahbazPanahi, and R. Vahidnia, "Sum-rate maximization for active channels," *IEEE Signal Processing Letters*, vol. 20, pp. 771–774, Aug 2013.

[105] J. Mirzaei and S. ShahbazPanahi, "Sum-rate maximization for active channels with unequal subchannel noise powers," *IEEE Trans. Signal Processing*, vol. 62, pp. 4187–4198, Aug 2014.

[106] P. Abbasi-Saei and S. Shahbazpanahi, "Sum-rate maximization for two-way active channels," *IEEE Trans. Signal Process.*, vol. 64, pp. 1369–1382, 2016.

[107] S. Shahbazpanahi, A. B. Gershman, Z.-Q. Luo, and K. M. Wong, "Robust adaptive beamforming for general-rank signal models," *IEEE Trans. Signal Process.*, vol. 51, no. 9, pp. 2257–2269, Sep. 2003.

[108] B. K. Chalise, S. Shahbazpanahi, A. Czylwik, and A. B. Gershman, "Robust downlink beamforming based on outage probability specifications," *IEEE Trans. Wireless Commun.*, vol. 6, no. 10, pp. 3498–3503, Oct. 2007.

[109] O. Ozdogan, E. Bjornson, and J. Zhang, "Performance of cell-free massive MIMO with rician fading and phase shifts," *IEEE Transactions on Wireless Communications*, vol. 18, no. 11, pp. 5299–5315, 2019.

[110] Yizong Cheng, "Mean shift, mode seeking, and clustering," *IEEE Transactions on Pattern Analysis and Machine Intelligence*, vol. 17, no. 8, pp. 790–799, Aug 1995.

[111] K. Fukunaga and L. Hostetler, "The estimation of the gradient of a density function, with applications in pattern recognition," *IEEE Transactions on Information Theory*, vol. 21, no. 1, pp. 32–40, 1975.

[112] Y. Cheng and K. Fu, "Conceptual clustering in knowledge organization," *IEEE Transactions on Pattern Analysis and Machine Intelligence*, vol. PAMI-7, no. 5, pp. 592–598, 1985.

[113] D. Comaniciu and P. Meer, "Mean shift: a robust approach toward feature space analysis," *IEEE Transactions on Pattern Analysis and Machine Intelligence*, vol. 24, no. 5, pp. 603–619, 2002.

[114] R. Chen, R. W. Heath, and J. G. Andrews, "Transmit selection diversity for unitary precoded multiuser spatial multiplexing systems with linear receivers," *IEEE Transactions on Signal Processing*, vol. 55, no. 3, pp. 1159–1171, 2007.

[115] M. Grant and S. Boyd, "CVX: Matlab software for disciplined convex programming, version 2.1," http://cvxr.com/cvx, Mar. 2014.

[116] H. Q. Ngo, A. Ashikhmin, H. Yang, E. G. Larsson, and T. L. Marzetta, "Cell-free massive MIMO versus small cells," *IEEE Transactions on Wireless Communications*, vol. 16, no. 3, pp. 1834–1850, March 2017.

[117] S. Jin, D. Yue, and H. H. Nguyen, "Spectral and energy efficiency in cell-free massive MIMO systems over correlated rician fading," *IEEE Systems Journal*, pp. 1–12, 2020.

[118] A. Manikas, A. Sleiman, and I. Dacos, "Manifold studies of nonlinear antenna array geometries," *IEEE Transactions on Signal Processing*, vol. 49, no. 3, pp. 497–506, 2001.

[119] Z. Zhao, M. Schellmann, X. Gong, Q. Wang, R. Böhnke, and Y. Guo, "Pulse shaping design for OFDM systems," *EURASIP Journal on Wireless Communications and Networking*, vol. 2017, no. 1, p. 74, 2017.

[120] G. Matz, H. Bolcskei, and F. Hlawatsch, "Time-frequency foundations of communications: Concepts and tools," *IEEE Signal Processing Magazine*, vol. 30, no. 6, pp. 87–96, 2013.

[121] G. Matz, D. Schafhuber, K. Grochenig, M. Hartmann, and F. Hlawatsch, "Analysis, optimization, and implementation of low-interference wireless multicarrier systems," *IEEE Transactions on Wireless Communications*, vol. 6, no. 5, pp. 1921–1931, 2007.

[122] B. Le Floch, M. Alard, and C. Berrou, "Coded orthogonal frequency division multiplex," *Proceedings of the IEEE*, vol. 83, no. 6, pp. 982–996, 1995.

[123] Z. Zhao, M. Schellmann, Q. Wang, X. Gong, R. Boehnke, and W. Xu, "Pulse shaped ofdm for asynchronous uplink access," in *2015 49th Asilomar Conference on Signals, Systems and Computers*, 2015, pp. 3–7.

Appendix A

Appendices in Chapter 3

A.1 Derivation of the discrete-time channel model

Assuming that the channel between each transceiver and each relay is frequency flat and reciprocal, the effective continuous-time linear time-invariant channels between the two transceivers can be represented by the channel impulse response. Based on these assumptions, the relay channel from Transceiver 1 to Transceiver 2, (or vice vera) can be viewed as a *multipath end-to-end channel* whose impulse response is given by

$$h(t) \triangleq h_{21}(t) = h_{12}(t) = \sum_{l=1}^{L} \alpha_l \delta(t - \tau_l),$$

where $\alpha_l \triangleq w_l g_{l1} g_{l2}$ is the total attenuation/amplification factor applied to the signal going through the l-th relay, w_l is the complex beamforming weight of the l-th relay, and g_{lq} is the frequency flat channel coefficient between Transceiver q and the l-th relay. For the sake of simplicity let us focus on one direction of the communication, namely from Transceiver 1 to Transceiver 2. The signal $\check{s}_1(t)$ transmitted by Transceiver 1 to the relays is given by

$$\check{s}_1(t) = \sum_{k=-\infty}^{\infty} \check{s}_1[k] \varphi(t - kT_{\mathrm{s}}), \tag{A.1}$$

where $\varphi(t)$ is the response of the pulse shaping filter, $\check{s}_1[k]$ is the k-th data sample[1] transmitted by Transceiver 1, and T_s is the sampling period. The signal $\check{s}_1(t)$ produces, at Transceiver 2, the following signal:

$$\begin{aligned} r_2(t) &= \check{s}_1(t) \star_\mathrm{c} h(t) \\ &= \sum_{k=-\infty}^{\infty} \check{s}_1[k] \sum_{l=1}^{L} \alpha_l \varphi(t - kT_\mathrm{s} - \tau_l) \end{aligned} \tag{A.2}$$

where $\star_\mathrm{c}$ denotes the continuous-time convolution operation. Sampling $r_1(t)$ at the sampling rate $1/T_\mathrm{s}$, we express the discrete-time received sequence $r_1[nT_\mathrm{s}]$ as

$$\begin{aligned} r_2[nT_\mathrm{s}] &= r_2(t)\Big|_{t=nT_\mathrm{s}} \\ &= \sum_{k=-\infty}^{\infty} \check{s}_1[k] \sum_{l=1}^{L} \alpha_l \varphi((n-k)T_\mathrm{s} - \tau_l) \\ &= \check{s}_1[n] \star_\mathrm{d} h[n] \end{aligned} \tag{A.3}$$

where $\star_\mathrm{d}$ represents the discrete-time convolution and

$$h[n] \triangleq \sum_{l=1}^{L} \alpha_l \varphi(nT_\mathrm{s} - \tau_l) \tag{A.4}$$

is the equivalent discrete-time impulse response corresponding to the end-to-end channel between Transceivers 1 and 2. Assuming a rectangular pulse[2] shape

$$\varphi(t) = \begin{cases} 1 & 0 \le t < T_s \\ 0 & \text{otherwise} \end{cases} \tag{A.5}$$

[1] In this dissertation, $\check{s}_1[k]$ is the kth sample of the serial signal obtained by serializing the vector $\mathbf{T}_\mathrm{cp}\mathbf{F}^H\mathbf{A}_m\mathbf{s}_m$, which is the output of CP insertion operation that follows the IFFT operation at Transceiver m.

[2] Note that rectangular pulse shape is indeed quite popular and has already been used in the 4G networks [119–123] for the co-called CP-OFDM schemes which is exactly the same scheme we are considering in this dissertation. Indeed, conventional OFDM which relies on rectangular transmit and receive pulses and a cyclic prefix, often referred to as CP-OFDM, is part of several wireless standards such as digital audio and video broadcasting (DRM, DAB, DVB), wireless personal area networks (IEEE 802.15), fixed broadband wireless access (IEEE 802.16), and WLANs (IEEE 802.11a,g,n, Hiperlan/2) [121].

we can write

$$\varphi(nT_s - \tau_l) = \begin{cases} 1, & \text{for } 0 \leq nT_s - \tau_l < T_s \\ 0, & \text{otherwise} \end{cases} \tag{A.6}$$

or equivalently,

$$\varphi(nT_s - \tau_l) = \begin{cases} 1, & (n-1)T_s < \tau_l \leq nT_s \\ 0, & \text{otherwise.} \end{cases} \tag{A.7}$$

It follows from (A.7) that

$$\varphi(nT_s - \tau_l) = I_n(\tau_l) \tag{A.8}$$

where $I_n(\tau_l)$ is an indicator function whose value is equal to 1, when $\tau_l \in ((n-1)T_s, nT_s]$, and zero otherwise. Using (A.8) in (A.4) and dropping the subscripts 12, will lead us to (3.1).

A.2 Derivation of (3.20)

Inserting (3.19) back into the constraint in (3.17), we can write

$$\begin{aligned} 2r_2 = \sum_{i=1}^{N} \log_2(1 + \beta_i(\mathbf{w})P_{i1}) = \\ \sum_{i=1}^{N} \log_2 \left(\frac{N|\mathbf{f}_i^H \mathbf{B}\mathbf{w}|^2}{\sigma^2(1 + \mathbf{w}^H \mathbf{D}_2 \mathbf{w})} \times \frac{\gamma N}{2\ln 2(1 + \mathbf{w}^H \mathbf{D}_1 \mathbf{w})} \right). \end{aligned} \tag{A.9}$$

We can rewrite (A.9) as

$$2^{2r_2} = \left[\frac{\gamma N^2}{2\ln 2(1 + \mathbf{w}^H \mathbf{D}_1 \mathbf{w})\sigma^2(\mathbf{w}^H \mathbf{D}_2 \mathbf{w} + 1)} \right] \prod_{i=1}^{NN} |\mathbf{f}_i^H \mathbf{B}\mathbf{w}|^2 \tag{A.10}$$

Using (A.10), we obtain γ as

$$\gamma = \Gamma(\mathbf{w}) \left(\frac{2^{2r_2}}{\prod_{i=1}^{N} |\mathbf{f}_i^H \mathbf{B}\mathbf{w}|^2} \right)^{\frac{1}{N}} \tag{A.11}$$

where we define $\Gamma(\mathbf{w}) \triangleq \frac{2\ln 2(1+\mathbf{w}^H\mathbf{D}_1\mathbf{w})(1+\mathbf{w}^H\mathbf{D}_2\mathbf{w})\sigma^2}{N^2}$.

A.3 Derivation of (3.21)

To derive (3.21), we substitute (3.20) in (3.19), and simplify the result as shown in the sequel:

$$\begin{aligned}
P_{i1} &= \frac{\Gamma(\mathbf{w}) \left(\frac{2^{2r_2}}{\prod_{i=1}^{N} |\mathbf{f}_i^H \mathbf{B}\mathbf{w}|^2} \right)^{\frac{1}{N}} N}{2\ln 2(1+\mathbf{w}^H\mathbf{D}_1\mathbf{w})} - \frac{\sigma^2(1+\mathbf{w}^H\mathbf{D}_2\mathbf{w})}{N|\mathbf{f}_i^H\mathbf{B}\mathbf{w}|^2} \\
&= \frac{2\ln 2(1+\mathbf{w}^H\mathbf{D}_1\mathbf{w})(1+\mathbf{w}^H\mathbf{D}_2\mathbf{w})\sigma^2}{N^2} \times \\
&\left[\frac{2^{2r_2}}{\prod_{i=1}^{N} |\mathbf{f}_i^H \mathbf{B}\mathbf{w}|^2} \right]^{\frac{1}{N}} \frac{N}{2\ln 2(1+\mathbf{w}^H\mathbf{D}_1\mathbf{w})} \\
&- \frac{\sigma^2(1+\mathbf{w}^H\mathbf{D}_2\mathbf{w})}{N|\mathbf{f}_i^H\mathbf{B}\mathbf{w}|^2} = \\
&\frac{\sigma^2(1+\mathbf{w}^H\mathbf{D}_2\mathbf{w})}{N} \left(\frac{2^{\frac{2r_2}{N}}}{\left[\prod_{i=1}^{N} |\mathbf{f}_i^H \mathbf{B}\mathbf{w}|^2 \right]^{\frac{1}{N}}} - \frac{1}{|\mathbf{f}_i^H\mathbf{B}\mathbf{w}|^2} \right).
\end{aligned}$$

A.4 Proof of Lemma 3.2.1

Let P_T^{min} denote the minimum total power achieved by solving the OP in (3.14). Consider the following OP:

$$\max_{\mathbf{p}_1,\mathbf{p}_2,\mathbf{w}} R_1(\mathbf{p}_2,\mathbf{w}) \text{ s.t.} R_2(\mathbf{p}_1,\mathbf{w}) = r_2, P_T(\mathbf{p}_1,\mathbf{p}_2,\mathbf{w}) \leq P_T^{min} \tag{A.12}$$

The optimization problem (A.12) was solved in [39]. We now show that for any feasible value of r_1 in the first constraint of (3.14), the optimal rate of TR_1 obtained by solving the

optimization problem (A.12), denoted by R_1^{max}, cannot be less than or greater than r_1, i.e., $R_1^{max} = r_1$ must hold at the optimum of (A.12). Let $(\mathbf{w}^{o}, \mathbf{p}_1^{o}, \mathbf{p}_2^{o})$ be the optimum solution to the optimization problem (3.14), while $(\hat{\mathbf{w}}, \hat{\mathbf{p}}_1, \hat{\mathbf{p}}_2)$ stands for the optimal solution to the optimization problem (A.12). Note that $P_T(\mathbf{w}^{o}, \mathbf{p}_1^{o}, \mathbf{p}_2^{o}) = P_T^{min}$ holds true in (A.12). First, consider a case where at the optimum of (A.12), $R_1(\hat{\mathbf{p}}_2, \hat{\mathbf{w}}) = R_1^{max}$ is less than r_1. This implies that the optimum solution to (3.14), which leads to $R_1(\mathbf{p}_2^{o}, \mathbf{w}^{o}) = r_1$, provides a higher achievable rate at TR_1 than the optimum solution to (A.12) does, since $R_1(\hat{\mathbf{p}}_2, \hat{\mathbf{w}}) = R_1^{max} < r_1$. This result contradicts the assumption that the $(\hat{\mathbf{w}}, \hat{\mathbf{p}}_1, \hat{\mathbf{p}}_2)$ is optimal, for the optimization problem (A.12). As a result, R_1^{max} cannot be less than r_1.

We now show that $R_1(\hat{\mathbf{p}}_2, \hat{\mathbf{w}}) = R_1^{max}$ cannot be greater than r_1. Because, otherwise one of the entries of the transmission power vector of $\hat{\mathbf{p}}_2$ at TR_2 can be decreased such that the new transmission power vector, say $\tilde{\mathbf{p}}_2$, yields a new achievable rate at TR_1, $R_1(\tilde{\mathbf{p}}_2, \mathbf{w})$ which is equal to r_1. Now, this new solution for the optimization problem (A.12), i.e., $(\hat{\mathbf{w}}, \hat{\mathbf{p}}_1, \tilde{\mathbf{p}}_2)$, yields a value for the total network power which is smaller than $P_T^{min} = P_T(\mathbf{p}_1^{o}, \mathbf{p}_2^{o}, \mathbf{w}^{o})$ obtained by solving the optimization problem (3.14). This, in turn, contradicts the assumption that $(\mathbf{w}^{o}, \mathbf{p}_1^{o}, \mathbf{p}_2^{o})$ is optimal for the optimization problem (3.14). As a result, R_1^{max} cannot be greater than r_1. Hence, the equality, $R_1^{max} = r_1$, must hold at the optimum of (A.12).The fact that $R_1^{max} = r_1$ holds true at the optimum of (A.12) implies that any solution to the optimization problem (A.12) is also a solution to the optimization problem (3.14). It is shown in [39] that at the optimum of (A.12), $|\mathbf{f}_i^H \mathbf{B}\mathbf{w}| = |\mathbf{f}_j^H \mathbf{B}\mathbf{w}|$ holds true for any i and j. Accordingly, at the optimum, the optimization problem (3.14) enjoys the same attributes of the optimization problem (A.12), i.e., at the optimum of (3.14), $|\mathbf{f}_i^H \mathbf{B}\mathbf{w}| = |\mathbf{f}_j^H \mathbf{B}\mathbf{w}|$ holds for any i and j, and the proof is now complete.

Appendix B

Appendices in Chapter 4

B.1 Derivation of (4.29)

Consider the following minimization problem:

$$\min_{\alpha_i \geq 0} \ \rho \sum_{i=1}^{N} \alpha_i, \text{ subject to } \quad \sum_{i=1}^{N} \log_2(1+\alpha_i \zeta_i) = c.$$

The Lagrangian function of (B.1), $L(\boldsymbol{\alpha}, \gamma, \boldsymbol{\nu})$, can be given by

$$L(\boldsymbol{\alpha}, \gamma_1, \boldsymbol{\nu}) = \rho \sum_{i=1}^{N} \alpha_i + \gamma_1 \left[c - \sum_{i=1}^{N} \log_2(1+\alpha_i \zeta_i) \right] - \boldsymbol{\nu}^T \boldsymbol{\alpha} \tag{B.1}$$

where γ_1 as well as ν_i are the Lagrange multipliers, $\boldsymbol{\alpha} \triangleq [\alpha_1, \ldots, \alpha_N]^T$, and $\boldsymbol{\nu} \triangleq [\nu_1, \ldots, \nu_N]^T$.

From KKT conditions, we can write

$$0 = \frac{\partial}{\partial \alpha_i} L(\boldsymbol{\alpha}, \gamma_1, \boldsymbol{\nu}) = \rho - \gamma_1 \frac{\zeta_i}{\ln 2(1+\alpha_i \zeta_i)} - \nu_i \tag{B.2}$$

and hence

$$\frac{(\rho - \nu_i)(1+\alpha_i \zeta_i) \ln 2}{\zeta_i} = \gamma_1. \tag{B.3}$$

Since from KKT conditions, $\nu_i \geq 0$ and $\nu_i \alpha_i = 0$, therefore, for $\nu_i = 0$, α_i is positive and for $\nu_i > 0$, $\alpha_i = 0$. As a result, (B.2) can be expressed as

$$\alpha_i = \left[\frac{\gamma}{\rho \ln 2} - \frac{1}{\zeta_i} \right]^+ \tag{B.4}$$

For $j = 1, 2$, let us define $\alpha_i \triangleq P_{ij}^{\mathrm{o}}(\mathbf{w})$, $\rho \triangleq \frac{1+\mathbf{w}^H \mathbf{D}_j \mathbf{w}}{N}$, $\gamma = \gamma_j(\mathbf{w})$, and $\zeta_i \triangleq \frac{N}{1+\mathbf{w}^H \mathbf{D}_{\bar{j}} \mathbf{w}} |\mathbf{q}_i^H \bar{\mathbf{h}}|^2$. Given these definitions, it can easily be observed that (B.4) becomes (4.29).

B.2 Finding matrix $\mathbf{C}_n$

To obtain $\mathbf{C}_n$, for any $n \in \mathcal{N}$, we rewrite (4.38) as

$$\mathbf{0} = \mathbf{B}_{-n}\mathbf{w} = \mathbf{B}_{-n}\tilde{\mathbf{\Pi}}_n \tilde{\mathbf{\Pi}}_n^T \mathbf{w} = \mathbf{0} \tag{B.5}$$

where $\tilde{\mathbf{\Pi}}_n$ can be any $RL_w \times RL_w$ permutation matrix which permutes the columns of $\mathbf{B}_{-n}$, and hence, $\tilde{\mathbf{\Pi}}_n^T$ permutes the entries of $\mathbf{w}$. As $\mathbf{B}_{-n}$ is of rank $L_{\mathrm{nz}} - 1$, we can write

$$\mathbf{B}_{-n}\tilde{\mathbf{\Pi}}_n = [\mathbf{C}_{1,n} \;\; \mathbf{C}_{2,n}] \tag{B.6}$$

where $\mathbf{C}_{1,n} \in \mathbb{C}^{(L_{\mathrm{nz}}-1)\times(L_{\mathrm{nz}}-1)}$ is a full rank (thus invertible) matrix ($\mathrm{rank}(\mathbf{C}_{1,n}) = L_{\mathrm{nz}} - 1$) which captures the first $L_{\mathrm{nz}}-1$ columns of the matrix $\mathbf{B}_{-n}\tilde{\mathbf{\Pi}}_n$, while $\mathbf{C}_{2,n} \in \mathbb{C}^{(L_{\mathrm{nz}}-1)\times(RL_w - L_{\mathrm{nz}}+1)}$ contains the remaining columns of $\mathbf{B}_{-n}\tilde{\mathbf{\Pi}}_n$. If $\tilde{\mathbf{w}}$ and $\bar{\mathbf{w}}$ capture the first $L_{\mathrm{nz}} - 1$ and the last $RL_w - (L_{\mathrm{nz}} - 1)$ entries of $\tilde{\mathbf{\Pi}}_n^T \mathbf{w}$, i.e., $\tilde{\mathbf{\Pi}}_n^T \mathbf{w} = [\tilde{\mathbf{w}}^T \;\; \bar{\mathbf{w}}^T]^T$, then we can use (B.6) in (B.5) to write

$$[\mathbf{C}_{1,n} \;\; \mathbf{C}_{2,n}][\tilde{\mathbf{w}}^T \;\; \bar{\mathbf{w}}^T]^T = \mathbf{0} \Rightarrow \tilde{\mathbf{w}} = -\mathbf{C}_{1,n}^{-1}\mathbf{C}_{2,n}\bar{\mathbf{w}} \tag{B.7}$$

Using (B.7), we can write

$$\mathbf{w} = \tilde{\mathbf{\Pi}}_n \tilde{\mathbf{\Pi}}_n^T \mathbf{w} = \tilde{\mathbf{\Pi}}_n \begin{bmatrix} \tilde{\mathbf{w}} \\ \bar{\mathbf{w}} \end{bmatrix} = \tilde{\mathbf{\Pi}}_n \begin{bmatrix} -\mathbf{C}_{1,n}^{-1} \mathbf{C}_{2,n} \bar{\mathbf{w}} \\ \bar{\mathbf{w}} \end{bmatrix} = \mathbf{C}_n \bar{\mathbf{w}} \tag{B.8}$$

where $\mathbf{C}_n$ is defined as

$$\mathbf{C}_n \triangleq \tilde{\mathbf{\Pi}}_n \begin{bmatrix} -\mathbf{C}_{1,n}^{-1} \mathbf{C}_{2,n} \\ \mathbf{I}_{RL_w - L_{\text{nz}}+1} \end{bmatrix}. \tag{B.9}$$

In light of (B.9), finding $\mathbf{C}_n$ hinges upon finding a full rank matrix $\mathbf{C}_{1n}$ such that (B.6) holds true. To obtain a full rank matrix $\mathbf{C}_{1,n}$ from $\mathbf{B}_{-n}$ with an acceptable condition number, the following algorithm can be used to obtain $L_{\text{nz}} - 1$ linearly independent columns of the matrix $\mathbf{B}_{-n}$.

Algorithm 4 : Finding the matrix $\mathbf{C}_{1,n}$

1. Let $\mathbf{c}_i$ be the i-th column of $\mathbf{B}_{-n}$, for $i = 1, 2 \ldots, L_{\text{nz}} - 1$. Set $\mathbf{a}_1 = \mathbf{c}_1$, and $k = 1$.
2. Set $k = k + 1$. If $k \geq L_{\text{nz}}$, go Step 4.
3. Find $\mathbf{c}_i$ which maximizes $\frac{\|(\mathbf{I} - \mathbf{A}_k (\mathbf{A}_k^H \mathbf{A}_k)^{-1} \mathbf{A}_k^H) \mathbf{c}_i\|^2}{\|\mathbf{c}_i\|^2}$, where $\mathbf{A}_k = [\mathbf{a}_1,\ \mathbf{a}_2,\ \ldots,\ \mathbf{a}_{k-1}]$, and then set $\mathbf{a}_k = \mathbf{c}_i$. Go to Step 2
4. $\mathbf{C}_{1,n} = \mathbf{A}_{L_{\text{nz}}}$.

Note that the permutation matrix $\tilde{\mathbf{\Pi}}_n$ corresponds to a matrix which re-arranges the columns of $\mathbf{B}_{-n}$ such that the columns of $\mathbf{C}_{1,n}$ becomes the first $L_{\text{nz}} - 1$ columns in $\mathbf{B}_{-n}$ (see (B.6)).

where equality (a) holds true by substituting the value of z with $\frac{(\beta_1 + \beta_2)}{\|\bar{\mathbf{D}}_{2,n}^{-1/2} \bar{\mathbf{b}}_n\|^2}$. The largest

$$\lim_{z\to\frac{(\beta_1+\beta_2)}{\|\bar{\mathbf{D}}_{2,n}^{-1/2}\bar{\mathbf{b}}_n\|^2}} \mathbf{P}_n(z) \stackrel{a}{=}$$

$$\left(\frac{(\beta_1+\beta_2)}{\| \bar{\mathbf{D}}_{2,n}^{-1/2}\bar{\mathbf{b}}_n \|^2}\bar{\mathbf{D}}_{1,n}+\bar{\mathbf{C}}_n\right)^{-1/2}\left(\frac{(\beta_1+\beta_2)}{\| \bar{\mathbf{D}}_{2,n}^{-1/2}\bar{\mathbf{b}}_n \|^2}\bar{\mathbf{b}}_n\bar{\mathbf{b}}_n^H-(\beta_1+\beta_2)\bar{\mathbf{D}}_{2,n}\right)$$

$$\left(\frac{(\beta_1+\beta_2)}{\| \bar{\mathbf{D}}_{2,n}^{-1/2}\bar{\mathbf{b}}_n \|^2}\bar{\mathbf{D}}_{1,n}+\bar{\mathbf{C}}_n\right)^{-1/2}$$

$$\stackrel{b}{=} (\frac{(\beta_1+\beta_2)}{\| \bar{\mathbf{D}}_{2,n}^{-1/2}\bar{\mathbf{b}}_n \|^2}\bar{\mathbf{D}}_{1,n}+\bar{\mathbf{C}}_n)^{-1/2}\left[(\beta_1+\beta_2)\bar{\mathbf{D}}_{2,n}^{1/2}\left(\frac{\bar{\mathbf{D}}_{2,n}^{-1/2}\bar{\mathbf{b}}_n\bar{\mathbf{b}}_n^H\bar{\mathbf{D}}_{2,n}^{-1/2}}{\| \bar{\mathbf{D}}_{2,n}^{-1/2}\bar{\mathbf{b}}_n \|^2}-\mathbf{I}\right)\bar{\mathbf{D}}_{2,n}^{1/2}\right]$$

$$\left(\frac{(\beta_1+\beta_2)}{\| \bar{\mathbf{D}}_{2,n}^{-1/2}\bar{\mathbf{b}}_n \|^2}\bar{\mathbf{D}}_{1,n}+\bar{\mathbf{C}}_n\right)^{-1/2} \tag{B.10}$$

$$\frac{\partial\lambda_n(z)}{\partial z}=\frac{z^{-2}-\lambda_n(z)\bar{\mathbf{b}}_n^H\mathbf{\Lambda}_n^{-1}(z)\bar{\mathbf{D}}_{1,n}\mathbf{\Lambda}_n^{-1}(z)\bar{\mathbf{b}}_n}{\bar{\mathbf{b}}_n^H\mathbf{\Lambda}_n^{-1}(z)\mathbf{E}_n(z)\mathbf{\Lambda}_n^{-1}(z)\bar{\mathbf{b}}_n}\stackrel{(a)}{>}\frac{z^{-2}-\lambda_n(z)\bar{\mathbf{b}}_n^H\mathbf{\Lambda}_n^{-1}(z)(\bar{\mathbf{D}}_{1,n}+z^{-1}\bar{\mathbf{C}}_n)\mathbf{\Lambda}_n^{-1}(z)\bar{\mathbf{b}}_n}{\bar{\mathbf{b}}_n^H\mathbf{\Lambda}_n^{-1}(z)\mathbf{E}_n(z)\mathbf{\Lambda}_n^{-1}(z)\bar{\mathbf{b}}_n}$$

$$=\frac{z^{-2}}{\bar{\mathbf{b}}_n^H\mathbf{\Lambda}_n^{-1}(z)\mathbf{E}_n(z)\mathbf{\Lambda}_n^{-1}(z)\bar{\mathbf{b}}_n}-\frac{\lambda_n(z)}{z}=\frac{\lambda_n(z)}{z}\left(\frac{z^{-1}}{\bar{\mathbf{b}}_n^H\mathbf{\Lambda}_n^{-1}(z)\lambda_n(z)\mathbf{E}_n(z)\mathbf{\Lambda}_n^{-1}(z)\bar{\mathbf{b}}_n}-1\right)$$

$$\stackrel{(b)}{\geq}\frac{\lambda_n(z)}{z}\left(\frac{z^{-1}}{\bar{\mathbf{b}}_n^H\mathbf{\Lambda}_n^{-1}(z)\left[(\beta_1+\beta_2)\bar{\mathbf{D}}_{2,n}+\lambda_n(z)\mathbf{E}_n(z)\right]\mathbf{\Lambda}_n^{-1}(z)\bar{\mathbf{b}}_n}-1\right)$$

$$\stackrel{(c)}{=}\frac{\lambda_n(z)}{z}\left(\frac{z^{-1}}{\bar{\mathbf{b}}_n^H\mathbf{\Lambda}_n^{-1}(z)\mathbf{\Lambda}_n(z)\mathbf{\Lambda}_n^{-1}(z)\bar{\mathbf{b}}_n}-1\right)=\frac{\lambda_n(z)}{z}\left(\frac{z^{-1}}{\bar{\mathbf{b}}_n^H\mathbf{\Lambda}_n^{-1}(z)\bar{\mathbf{b}}_n}-1\right)\stackrel{(d)}{=}\frac{\lambda_n(z)}{z}\left(\frac{z^{-1}}{z^{-1}}-1\right)=0 \tag{B.12}$$

eigenvalue of matrix $\left(\frac{\bar{\mathbf{D}}_{2,n}^{-1/2}\bar{\mathbf{b}}_n\bar{\mathbf{b}}_n^H\bar{\mathbf{D}}_{2,n}^{-1/2}}{\|\bar{\mathbf{D}}_{2,n}^{-1/2}\bar{\mathbf{b}}_n\|^2}-\mathbf{I}\right)$ can be found as

$$\lambda_{\max}\left(\frac{\bar{\mathbf{D}}_{2,n}^{-1/2}\bar{\mathbf{b}}_n\bar{\mathbf{b}}_n^H\bar{\mathbf{D}}_{2,n}^{-1/2}}{\| \bar{\mathbf{D}}_{2,n}^{-1/2}\bar{\mathbf{b}}_n \|^2}-\mathbf{I}\right)=\frac{\bar{\mathbf{b}}_n^H\bar{\mathbf{D}}_{2,n}^{-H/2}\bar{\mathbf{D}}_{2,n}^{-1/2}\bar{\mathbf{b}}_n}{\| \bar{\mathbf{D}}_{2,n}^{-1/2}\bar{\mathbf{b}}_n \|^2}-1 \tag{B.11}$$

B.3 Derivations of (4.53) and (4.55)

To find an expression for $\frac{\partial}{\partial z}\lambda_n(z)$, we start with the fact that $\lambda_n(z)$ is the largest eigenvalue of $\mathbf{P}_n(z)$. As a result, we can write

$$(\mathbf{P}_n(z) - \lambda_n(z)\mathbf{I})\mathbf{u}(z) = \mathbf{0}. \tag{B.13}$$

Substituting matrix $\mathbf{P}_n(z)$ from (4.51) into (B.13), we obtain

$$\mathbf{E}_n^{-1/2}(z)\left((z\bar{\mathbf{b}}_n\bar{\mathbf{b}}_n^H - (\beta_1+\beta_2)\bar{\mathbf{D}}_{2,n}) - \lambda_n(z)\mathbf{E}_n(z)\right)\times$$
$$\mathbf{E}_n^{-1/2}(z)\mathbf{u}(z) = \mathbf{0}. \tag{B.14}$$

Since $\mathbf{E}_n(z) = (z\bar{\mathbf{D}}_{1,n} + \bar{\mathbf{C}}_n) = \mathbf{C}_n^H(z\mathbf{D}_1 + \mathbf{I})\mathbf{C}_n$ is a full rank and Hermitian matrix, finding $\lambda_n(z)$ in (B.14) is equivalent to finding $\lambda_n(z)$ such that matrix

$$z\bar{\mathbf{b}}_n\bar{\mathbf{b}}_n^H - (\beta_1+\beta_2)\bar{\mathbf{D}}_{2,n} - \lambda_n(z)\mathbf{E}_n(z) \tag{B.15}$$

drops rank. For $z \in \left(\frac{(\beta_1+\beta_2)}{\|\bar{\mathbf{D}}_{2,n}^{-1/2}\bar{\mathbf{b}}_n\|^2}, +\infty\right)$, matrix $\left((\beta_1+\beta_2)\bar{\mathbf{D}}_{2,n} + \lambda_n(z)\mathbf{E}_n(z)\right)$ is a positive definite and full- rank matrix, and thus invertible[1]. Therefore, $\lambda_n(z)$ is such that

$$z\left((\beta_1+\beta_2)\bar{\mathbf{D}}_{2,n} + \lambda_n(z)\mathbf{E}_n(z)\right)^{-1}\bar{\mathbf{b}}_n\bar{\mathbf{b}}_n^H - \mathbf{I} \tag{B.16}$$

drops rank. Using the fact that the largest eigenvalue of any matrix in the form of $u\mathbf{b}\mathbf{a}^H - \mathbf{I}$ is equal to $u\mathbf{a}^H\mathbf{b} - 1$, while all other eigenvalues are zero, we can find $\lambda_n(z)$ by equating the largest eigenvalue of (B.16) to 0, that is, $\lambda_n(z)$ must satisfy

$$\bar{\mathbf{b}}_n^H\left(\underbrace{(\beta_1+\beta_2)\bar{\mathbf{D}}_{2,n} + \lambda_n(z)\mathbf{E}_n(z)}_{\triangleq\mathbf{\Lambda}_n(z)}\right)^{-1}\bar{\mathbf{b}}_n = \frac{1}{z}. \tag{B.17}$$

[1]This matrix is positive semi-definite and Hermitian because we can write it as $\mathbf{C}_n^H\left((\beta_1+\beta_2)\mathbf{D}_2 + \lambda(z)(z\mathbf{D}_1+\mathbf{I})\right)\mathbf{C}_n$, which is clearly positive semi-definite and Hermitian.

The derivation of (4.53) is now complete. Now, to derive $\frac{\partial}{\partial z}\lambda_n(z)$ as in (4.55), we differentiate (B.17) with respect to z, and equate it to zero. Doing so, we arrive at

$$\bar{\mathbf{b}}_n^H \mathbf{\Lambda}_n^{-1}(z) \frac{\partial \mathbf{\Lambda}_n(z)}{\partial z} \mathbf{\Lambda}_n^{-1}(z) \bar{\mathbf{b}}_n = \frac{1}{z^2} \tag{B.18}$$

where

$$\frac{\partial \mathbf{\Lambda}_n(z)}{\partial z} = \frac{\partial \lambda_n(z)}{\partial z} \mathbf{E}_n(z) + \lambda(z) \bar{\mathbf{D}}_{1,n}. \tag{B.19}$$

Substituting (B.19) in (B.18), we obtain $\frac{\partial}{\partial z}\lambda_n(z)$ as

$$\frac{\partial \lambda_n(z)}{\partial z} = \frac{z^{-2} - \lambda_n(z) \bar{\mathbf{b}}_n^H \mathbf{\Lambda}_n^{-1}(z) \bar{\mathbf{D}}_{1,n} \mathbf{\Lambda}_n^{-1}(z) \bar{\mathbf{b}}_n}{\bar{\mathbf{b}}_n^H \mathbf{\Lambda}_n^{-1}(z) \mathbf{E}_n(z) \mathbf{\Lambda}_n^{-1}(z) \bar{\mathbf{b}}_n}.$$

The derivation of (4.55) is complete.

B.4 Proof of the Existence of Unique Positive solution to (4.53)

To prove that for any $z \in (\frac{(\beta_1+\beta_2)}{\|\bar{\mathbf{D}}_{2,n}^{-1/2}\bar{\mathbf{b}}_n\|^2}, +\infty)$, (4.53) has only one unique positive solution for υ, we first define

$$g(z, \upsilon) \triangleq z \bar{\mathbf{b}}_n^H \left[(\beta_1 + \beta_2) \bar{\mathbf{D}}_{2,n} + \upsilon \ \mathbf{E}_n(z) \right]^{-1} \bar{\mathbf{b}}_n. \tag{B.20}$$

We observe that for any $z \in (\frac{(\beta_1+\beta_2)}{\|\bar{\mathbf{D}}_{2,n}^{-1/2}\bar{\mathbf{b}}_n\|^2}, +\infty)$, function $g(z, \upsilon)$ is monotonically decreasing in υ, and $\lim_{\upsilon \to +\infty} \ g(z, \upsilon) = 0$. Therefore, if we show that $g(z, \upsilon) - 1 > 0$ holds true as $\upsilon \to 0$, then we can conclude that for any $z \in (\frac{(\beta_1+\beta_2)}{\|\bar{\mathbf{D}}_{2,n}^{-1/2}\bar{\mathbf{b}}_n\|^2}, +\infty)$, there exists a unique solution for $g(z, \upsilon) = 1$, so does for (4.53). To show this, for $\upsilon = 0$, we can write

$$\lim_{\upsilon \ \to 0} \ g(z, \upsilon) = z \bar{\mathbf{b}}_n^H \left[(\beta_1 + \beta_2) \bar{\mathbf{D}}_{2,n} \right]^{-1} \bar{\mathbf{b}}_n \geq 1 \tag{B.21}$$

where the inequality holds true for $z \in \left(\frac{(\beta_1+\beta_2)}{\|\bar{\mathbf{D}}_{2,n}^{-1/2}\bar{\mathbf{b}}_n\|^2}, +\infty\right)$. As a result, $g(z,\upsilon) - 1 > 0$ holds true when υ approaches zero. The proof is now complete.

B.5 Proof of Lemma 4.2.1

Let us denote the objective function of (4.52) as $\psi(z) \triangleq z + \dfrac{\beta_1+\beta_2}{\lambda_n(z)}$. To show that $\psi(z)$ has a unique minimum, we first prove that $\psi(z) \to +\infty$ as $z \to +\infty$ or as $z \to \dfrac{(\beta_1+\beta_2)}{\| \bar{\mathbf{D}}_{2,n}^{-1/2}\bar{\mathbf{b}}_n \|^2}$. This result confirms that there exists at least one minimum for $\psi(z)$. Then, we will show that this minimum is indeed unique. First, consider the case that $z \to +\infty$. Using (4.51), we can write

$$\lim_{z\to+\infty} \quad \mathbf{P}_n(z) = \bar{\mathbf{D}}_{1,n}^{-H/2}\bar{\mathbf{b}}_n\bar{\mathbf{b}}_n^H\bar{\mathbf{D}}_{1,n}^{-1/2}. \tag{B.22}$$

It is clear from (B.22) that the maximum eigenvalue of $\mathbf{P}_n(z)$ is equal to $\mathbf{b}_n^H\bar{\mathbf{D}}_{1,n}^{-1}\mathbf{b}_n$ and thus is non-zero. As a result, $\lim_{z\to+\infty} \quad \psi(z) = +\infty$. Now, we consider the case that $z \to \dfrac{(\beta_1+\beta_2)}{\| \bar{\mathbf{D}}_{2,n}^{-1/2}\bar{\mathbf{b}}_n \|^2}$, and write as in (B.10) which is equal to zero, and hence, this matrix is negative semi-definite. As a result, when $z \to \frac{(\beta_1+\beta_2)}{\|\bar{\mathbf{D}}_{2,n}^{-1/2}\bar{\mathbf{b}}_n\|^2}$, the principal eigenvalue of $\mathbf{P}_n(z)$, $\lambda_n(z)$, also approaches zero. Therefore, with $\lambda_n(z)|_{z\to+\infty} = 0$, the objective function approaches infinity, i.e., $\psi(z) \to +\infty$. As such, there exists at least one minimum for $\psi(z)$ in the interval of $\left(\frac{(\beta_1+\beta_2)}{\|\bar{\mathbf{D}}_{2,n}^{-1/2}\bar{\mathbf{b}}_n\|^2}, +\infty\right)$. Now, in order to prove that this minimum is unique, we show that $\psi(z)$ is the summation of a monotonically increasing function, i.e. z, and one monotonically decreasing the function $\frac{\beta_1+\beta_2}{\lambda_n(z)}$, and thus, $\psi(z)$ has a unique minimum. Equivalently, we only need to prove that $\lambda_n(z)$ is a monotonically increasing function when $z \in (\frac{(\beta_1+\beta_2)}{\|\bar{\mathbf{D}}_{2,n}^{-1/2}\bar{\mathbf{b}}_n\|^2}, +\infty)$, that is the derivative of $\lambda_n(z)$ with respect to z is positive. Using (4.55), we can rewrite the derivative of $\lambda_n(z)$ as in (B.12), where inequality (a) holds true

due to the fact that $\lambda_n(z)\bar{\mathbf{b}}_n^H\mathbf{\Lambda}_n^{-1}(z)(z^{-1}\bar{\mathbf{C}}_n)\mathbf{\Lambda}_n^{-1}(z)\bar{\mathbf{b}}_n > 0$, inequality (b) is valid because $\bar{\mathbf{b}}_n^H\mathbf{\Lambda}_n^{-1}(z)\left[(\beta_1+\beta_2)\bar{\mathbf{D}}_{2,n}\right]\mathbf{\Lambda}_n^{-1}(z)\bar{\mathbf{b}}_n > 0$, in equality (c), the definition of $\mathbf{\Lambda}_n(z)$ is used, and equality (d) is obtained based on the fact (4.53) is satisfied for $\upsilon = \lambda_n(z)$. It follows from (B.12) that the derivative of $\lambda_n(z)$ with respect to z is positive, we conclude that $\lambda_n(z)$ is a monotonically increasing function of z. The proof is now complete.

Appendix C

Appendices in Chapter 5

C.1 Derivation of (5.2)

We can write the received signal as

$$y_k = \sum_{r'=1}^{R} \mathbf{w}_{r'}^H \mathbf{h}_k \sum_{k'=1}^{K_r} \sqrt{p_{k'}} s_{k'} + n_k \quad \forall k \in \mathcal{K}_r \tag{C.1}$$

We factor out the desired signal for the k-th user in (C.1), and split the remaining interference into the interference inside each clusters (intra-cluster interference) and the interference between clusters (inter-cluster interference). Adopting the user indexing $k \in \mathcal{K}_r$ for each cluster r, where $k \in \{1, 2, \ldots, K_r\}$, we can write

$$y_k = \underbrace{\sqrt{p_k}\mathbf{w}_r^H \mathbf{h}_k s_k}_{\text{Desired Signal}} + \underbrace{\mathbf{w}_r^H \mathbf{h}_k \sum_{k' \neq k, k' \in \mathcal{K}_r} \sqrt{p_{k'}} s_{k'}}_{\text{Intra Cluster Interference}}$$
$$+ \underbrace{\sum_{r' \neq r}^{R} \mathbf{w}_{r'}^H \mathbf{h}_k \sum_{k' \in \mathcal{K}_{r'}} \sqrt{p_{k'}} s_{k'}}_{\text{Inter Cluster Interference}} + \underbrace{n_k}_{\text{Received Noise}}, \forall k \in \mathcal{K}_r.$$

C.2 Derivation of SINR Expression in (5.5)

To derive the SINR in (5.5), the expressions for the power of desired signal at the numerator, the power of interference and noise at the denominator are needed. Using (5.4), for $k \in \mathcal{K}_r$, we can obtain the desired signal power as follows

$$\begin{aligned} E\left\{|\sqrt{p_k}\mathbf{w}_r^H\,\mathbf{h}_k s_k|^2\right\} &= p_k\,|\mathbf{w}_r^H\,\mathbf{h}_k|^2\;E\left\{|\;s_k|^2\right\} \\ &= p_k\,|\mathbf{w}_r^H\,\mathbf{h}_k|^2. \end{aligned} \tag{C.2}$$

Similarly, for $k \in \mathcal{K}_r$, the intra-cluster interference power can be obtained as

$$\begin{aligned} & E\left\{|\mathbf{w}_r^H\mathbf{h}_k \sum_{k'\neq k,k'\in\mathcal{K}_r} \sqrt{p_{k'}}s_{k'}|^2\right\} \\ &= |\mathbf{w}_r^H\,\mathbf{h}_k|^2 \sum_{k'\neq k,k'\in\mathcal{K}_r} p_{k'}E\left\{|s_{k'}|^2\right\} \\ &= |\mathbf{w}_r^H\,\mathbf{h}_k|^2 \sum_{k'\neq k,k'\in\mathcal{K}_r} p_{k'}, \end{aligned} \tag{C.3}$$

where we have used the fact that the transmitted symbols are unit-power independent random variables. Lastly, for $k \in \mathcal{K}_r$, the inter-cluster interference power is given by

$$\begin{aligned} & E\left\{|\sum_{r'\neq r}^{R}\mathbf{w}_{r'}^H\,\mathbf{h}_k \sum_{k'\in\mathcal{K}_{r'}} \sqrt{p_{k'}}s_{k'}|^2\right\} \\ &= \sum_{r'=1}^{R} |\mathbf{w}_{r'}^H\,\mathbf{h}_k|^2 \sum_{k'\in\mathcal{K}_{r'}} \sqrt{p_{k'}}E\left\{|s_{k'}|^2\right\} \\ &= \sum_{r'\neq r} |\mathbf{w}_{r'}^H\,\mathbf{h}_k|^2 \sum_{k'\in\mathcal{K}_{r'}} p_{k'} \end{aligned} \tag{C.4}$$

As a result, the SINR expression in (5.5) can be obtained from (C.2), (C.3), and (C.4).

C.3 Derivation of (5.10)

Substituting (5.8) and (5.9) in (5.7), we obtain (C.5) as

$$\begin{aligned}
&|\mathbf{w}_r^H \mathbf{h}_k|^2 (1 + |\mathbf{w}_r^H \mathbf{h}_j|^2 \sum_{k' \neq k, k' \in \mathcal{K}_r} p_{k'} \\
&+ \sum_{r'=1}^{R} |\mathbf{w}_{r'}^H \mathbf{h}_j|^2 \sum_{k' \in \mathcal{K}_{r'}} p_{k'}) \geq \\
&|\mathbf{w}_r^H \mathbf{h}_j|^2 (1 + |\mathbf{w}_r^H \mathbf{h}_k|^2 \sum_{k' \neq k, k' \in \mathcal{K}_r} p_{k'} \\
&+ \sum_{r' \neq r} |\mathbf{w}_{r'}^H \mathbf{h}_k|^2 \sum_{k' \in \mathcal{K}_{r'}} p_{k'})
\end{aligned} \tag{C.5}$$

By expanding (C.5), the term $|\mathbf{w}_r^H \mathbf{h}_k|^2 |\mathbf{w}_r^H \mathbf{h}_j|^2 \sum_{k' \neq k, k' \in \mathcal{K}_r} p_{k'}$ can be canceled out from both side. For a given channel vector $\mathbf{h}$, we now define $a(\mathbf{p}_{-r}, \mathbf{h}) \triangleq 1 + \sum_{r' \neq r} |\mathbf{w}_{r'}^H \mathbf{h}|^2 \sum_{k \in \mathcal{K}_{r'}} p_k$ representing the inter-cluster interference plus noise value, and rewrite (C.5) as (5.10)

$$|\mathbf{w}_r^H \mathbf{h}_k|^2 a(\mathbf{p}_{-r}, \mathbf{h}_j) \geq |\mathbf{w}_r^H \mathbf{h}_j|^2 a(\mathbf{p}_{-r}, \mathbf{h}_k)$$

where we define $\mathbf{p}_{-r}$ as a sub-vector of the power allocation coefficients associated with those users which do not belong to cluster r.